PONTIFÍCIA UNIVERSIDADE CATÓLICA
DO RIO DE JANEIRO

Lucio Rossi de Souza

Greener Benzoxazine-Epoxy Coatings:
Investigating from Synthesis to Application

Tese de Doutorado

Thesis presented to the Programa de Pós-graduação em Engenharia Mecânica of PUC-Rio in partial fulfillment of the requirements for the degree of Doutor em Ciências – Engenharia Mecânica.

Advisor: Prof. José Roberto M. d'Almeida
Co-Advisor: Prof. Rigoberto C. Advincula

Rio de Janeiro
March 2021

PONTIFÍCIA UNIVERSIDADE CATÓLICA
DO RIO DE JANEIRO

Lucio Rossi de Souza

Greener Benzoxazine-Epoxy Coatings:
Investigating from Synthesis to Application

Thesis presented to the Programa de Pós-graduação em Engenharia Mecânica of PUC-Rio in partial fulfillment of the requirements for the degree of Doutor em Ciências – Engenharia Mecânica. Approved by the Examination Comittee:

Prof. José Roberto M. d'Almeida
Advisor
Departamento de Engenharia Química e de Materiais – PUC-Rio
Departamento de Engenharia Mecânica – PUC-Rio

Prof. Rigoberto C. Advincula
Co-Advisor
Department of Macromolecular Science and Engineering – CWRU

Prof. Gary Wnek
Department of Macromolecular Science and Engineering – CWRU

Prof. Laura Bruckman
Department of Materials Science and Engineering – CWRU

Prof. João Maia
Department of Macromolecular Science and Engineering – CWRU

Dr. Anna Akkus
Department of Macromolecular Science and Engineering – CWRU

Prof. Verônica Maria de Araújo Calado
Escola de Química – UFRJ

Rio de Janeiro, March 29, 2021

Lucio Rossi de Souza

Graduated in Mechanical Engineering at PUC-Rio (Pontifícia Universidade Católica do Rio de Janeiro) in 2006 and obtained his M.Sc. Degree in Materials Science and Engineering from PUC-Rio in 2015. Experienced engineer in the Oil & Gas Industry with great interest in research and development of products and characterization of materials.

. Bibliographic data

Souza, Lucio Rossi de

Greener Benzoxazine-Epoxy Coatings: Investigating from Synthesis to Application / Lucio Rossi de Souza; advisor: José Roberto M. d'Almeida ; co-advisor: Rigoberto C. Advincula. – 2021.

156 f. : il. color. ; 30 cm

Tese (doutorado)–Pontifícia Universidade Católica do Rio de Janeiro, Departamento de Engenharia Mecânica, 2021.

Inclui bibliografia

CDD: 621

To little Amanda

Acknowledgements

The completion of this dissertation would not be possible without the great support and contribution from the following people:

My advisors Dr. Rigoberto C. Advincula and Dr. José Roberto Moraes d'Almeida. Thank you for your mentorship and guidance throughout all of these years. Thank you for providing me all of the research and academic support that was needed for me to complete my PhD work. Thank you for taking me from Brazil to the world.

The committee members Professor Gary Wnek, Professor João Maia, Professor Laura Bruckman, Dr. Anna Akkus and Professor Verônica Maria de Araujo Calado, for the consideration in accepting being part of such an important event for me. For the time invested and individually, each on its own way, for helping me throughout my program.

To the program coordinators Professor Mônica Feijó Naccache and Professor João Maia for making this program possible.

To my all my friends and colleagues Italo Silva, Lihan Rong, Jin Ge, Yao Tang, Luiz Fernando Vieira, Lucivan Barros, Gustavo Schinazi, Claudio Souza, Felipe Leis, Erika Barcelos, Ana Maria Honorato, Gabriela Justino, Irlaine Machado, Thanyada Sukmanee, Bill Lenart, Dana Klein, Lu Han and so many others I certainly left out. Thank you for the talks, coffees, beers, for listening to me, for the advices and for being my friend.

To my family. My wife Renata Carvalho for leaving everything behind and following me to the unknown. My daughter Amanda, for…everything! To my parents Sonia and Célio for the infinite support. To my brother Guilherme for believing in me more than he believes in himself. To my brother Fábio for being proud of me and to my sister, who's not here but I'm sure would be proud as well.

This study was financed in part by the Coordenação de Aperfeiçoamento de Pessoal de Nível Superior - Brasil (CAPES) - Finance Code 001

This study was financed in part by the Macromolecular Science and Engineering Department at Case Western Reserve University

Abstract

Souza, Lucio Rossi de; d'Almeida, José Roberto M. (Advisor); Advincula, Rigoberto C. (Co-Advisor). **Greener Benzoxazine-Epoxy Coatings: Investigating from Synthesis to Application.** Rio de Janeiro, 2021. 156p. Tese de Doutorado – Departamento de Engenharia Mecânica, Pontifícia Universidade Católica do Rio de Janeiro.

Corrosion is a natural phenomenon that affects virtually every material, consumes billions of dollars annually worldwide and may result in catastrophic events. Coating is the most utilized technique to prevent corrosion. In this sense, epoxies are widely applied in all sectors of industry. Despite being high performance polymers, epoxies present issues, such as the use of toxic crosslinkers and long curing time. Benzoxazines are an emerging class of high performance self-curing thermosets. While typical monomers are based on mono- and difunctional derivatives, higher functional benzoxazines, prepared without using solvents, but purified with nontoxic solvents, are more desirable towards a greener synthesis of PBZ for high performance applications. Herein, we describe an environment-friendly approach to synthesizing a trifunctional benzoxazine from melamine, phenol, and paraformaldehyde. The chemical structure of the synthesized benzoxazine was confirmed by spectroscopic analyses, while the polymerization was monitored by thermal analysis. The synthesized benzoxazine monomer is, then, copolymerized with a commercial difunctional epoxy resin. We investigate the synergistic effect on improved thermal properties using differential scanning calorimetry (DSC) and thermogravimetric analysis (TGA). Results showed that a glass transition temperature of up to 268 °C was obtained. A higher thermal stability was also achieved with an onset degradation of nearly 400 °C and char yield of 22 wt% at 800 °C. Later, the copolymer was combined with silica to produce anticorrosion coatings. Results revealed superhydrophobic surfaces with great scratch resistance and adhesion to steel substrate. Electrochemical test proved high effectiveness of the coatings as anti-corrosion barrier, with increasing performance with the incorporation of silica.

Keywords

Trifunctional Benzoxazine; Epoxy; Anti-Corrosion Coating; Copolymer; Green Chemistry

Resumo

Souza, Lucio Rossi de; d'Almeida, José Roberto M. (Advisor); Advincula, Rigoberto C. (Co-Advisor). **Revestimentos mais Verdes de Benzoxazina e Epóxi: Investigando da Síntese à Aplicação.** Rio de Janeiro, 2021. 156p. Tese de Doutorado – Departamento de Engenharia Mecânica, Pontifícia Universidade Católica do Rio de Janeiro.

Corrosão é um fenômeno natural que afeta basicamente todo tipo de material, consome bilhões de dólares anualmente em todo o mundo e pode ter resultados catastróficos. Revestimentos são a técnica de prevenção de corrosão mais utilizada de todas. Nesse sentido, resinas epóxi são amplamente utilizadas em todos os setores da indústria. Apesar de serem polímeros de alta performance, resinas epóxi apresentam problemas, como a necessidade do uso de endurecedores normalmente tóxicos e longos tempos de cura. Benzoxazinas são uma classe emergente de monômeros termofixos de alta performance e auto-cura. Enquanto monômeros mono- e bifuncionais são tipicamente explorados, benzoxazinas de funcionalidade mais alta e sintetizados em procedimento sem solvente e purificados por solventes mais seguros, são um caminho mais desejável em direção à síntese de PBZ para aplicações de alta performance. Nesse trabalho nós descrevemos uma abordagem sustentável para a síntese de benzoxazina trifuncional a partir de melamina, fenol e paraformaldeído. A estrutura química do monômero sintetizado foi confirmada por análises espectroscópicas, enquanto o processo de polimerização foi monitorado por análise calorimétrica. O monômero de benzoxazina foi, então, copolimerizado com uma resina epóxi bifuncional comercial. Nós investimgamos o efeito sinergístico no aumento das propriedades térmicas por meio de DSC e TGA. Resultados revelaram temperatura de transição vítrea de até 268 °C. Alta estabilidade térmica também foi obtida, com início de degradação próximo a 400 °C e rendimento residual de 22 wt% a 800 °C. Posteriormente, o copolímero foi combinado com sílica para produzir revestimentos anti-corrosão. Resultados revelaram superfícies superhidrofóbicas com ótimas resistência a risco e adesão ao substrato de aço. Teste eletroquímico provou alta efetividade dos revestimentos como barreira anti-corrosão, com performance aumentada pela incorporação de sílica.

Palavras-chave

Benzoxazina Trifuncional; Epóxi; Revestimento anti-corrosão; Copolímero; Química Sustentável

Table of Contents

List of Tables

List of Figures

List of Figures – Supplementary Material

List of Abbreviations and Symbols

Symbol	Description
UV	Ultraviolet
DGEBA	Diglycidyl Ether of Bisphenol-A
O_2	Oxygen molecule
H_2S	Hydrogen sulfide
CO_2	Carbon Dioxide
FHWA	Federal Highway Administration
GDP	Gross Domestic Product
NACE	National Association for Corrosion Engineers
HVAC	Heat, Ventilation and Air Conditioning
PPS	Polyphenylene Sulfide
SiO_2	Silicon Dioxide - Silica
PP	Polypropylene
O&G	Oil and Gas
ZrO_2	Zirconium dioxide
TGA	Thermogravimetric Analysis
PBZ	Polybenzoxazine
PTFE	Polytetrafluoroethylene
[A]	Amine
[F]	Formaldehyde
[FAD]	Formaldehyde-Amine Derivative
[MB]	Mannich Base
[BOZ]	Benzoxazine monomer
THF	Tetrahydrofuran
DMF	Dimethylformamide
NaOH	Sodium Hydroxide
Tg	Glass Transition Temperature
^{1}H-NMR	Proton Nuclear Magnetic Resonance
PPS	Potentiodynamic Polarization Scan
i_{corr}	Corrosion Current Density

E_{corr}	Corrosion Potential
OCP	Open Circuit Potential
CR	Corrosion Rate
K	Constant in corrosion rate equation
EW	Equivalent weight
ρ	density
NaCl	Sodium Chloride
Al_2O_3	Aluminum Oxide - Alumina
FTIR	Fourier Transform Infra-Red Spectroscopy
DSC	Differential Scanning Calorimetry
MEK	Methyl Ethyl Ketone
SD	Supplementary Data
TBZ	Trifunctional Benzoxazine Monomer
P_B	Power at Baseline
P_O	Power at Onset
E_T	Total Energy
T_{d5}	Temperature of 5% weight loss
T_{d10}	Temperature of 10% weight loss
Py-GC/MS	Pyrolysis - Gas Chromatography / Mass Spectroscopy
DMSO	Dimethyl Sulfoxide
EGA	Evolved Gas Analysis
B-B	Benzoxazine Homopolymer
E-E	Epoxy Homopolymer
B-E	Benzoxazine-Epoxy Heteropolymer
RT	Room Temperature
B-E%	Percentual of composition B-E in the samples
T_{99}	Temperature of 1% weight loss
T_{95}	Temperature of 5% weight loss
SEM	Scanning Electron Microscope
CA	Contact Angle
S	Saturation Value

γ	Growth Rate
x_0	Controlling Variable for f=1/2 saturation
f_0	Initial value of contact angle
GU	Gloss Units

Work Organization

Chapter 1: *Introduction*

This chapter presents the thesis motivation, objectives and literature review on 1) Corrosion; 2) Coatings; 3) Epoxy; 4) Benzoxazines; 5) Conjugated Polymers; 6) G Chemistry; 7) Potentiodynamic Polarization Scan; 8) State of the Art. It presents information about corrosion and its consequences, mechanisms of preventing corrosion, polymers used as anti-corrosion coating materials, green chemistry towards production of such polymers and electrochemical testing of coatings.

Chapter 2: "A Greener Approach to Trifunctional Benzoxazine and High Temperature Polybenzoxazine Materials". This chapter presents the process of synthesis and proposed purification processes of a trifunctional benzoxazine monomer. Characterization of chemical structure, purity and thermal properties are discussed.

Chapter 3: "Highly Thermally Stable Copolymers of Polybenzoxazine and Epoxy: The Trifunctionality Advantage". This chapter shows an investigation about the copolymerization between the benzoxazine synthesized in chapter 2 and a commercial epoxy resin. The curing process is analyzed via a newly developed identification procedure by DSC. Thermal properties of the resulting copolymers are also discussed.

Chapter 4: "Superhydrophobic Benzoxazine-Epoxy Coatings: Electrochemical and Mechanical Performance". This chapter investigates the influence of different ratios of silica on the copolymer produced in chapter 3 regarding thermomechanical and anti-corrosion properties of coatings.

Chapter 5: General Conclusions. This chapter presents a general briefing on the issues and results discussed in the thesis.

Chapter 6: Future Works. This chapter proposes ideas for further development of the present work.

“**O pior naufrágio é não partir**”

- Amyr Klink -

1. Introduction

1.1. Motivation

From millimetric components in electronic devices, going through food containers and to intercontinental pipelines, most metallic parts are susceptible to the natural process of degradation known as corrosion[1]. Corrosion of metallic components is, therefore, of great concern to every sector of industry, as it can have catastrophic and costly effects by potentially causing shutdown of production, ruin of structures and environmental disaster. It is estimated that, worldwide, the annual cost of corrosion is US$2.5 trillion, and also that it is possible to realize savings of up to US$ 875 billion by applying only available corrosion control practices[2]. Several approaches are largely used to prevent corrosion, being coating the most widely applied technique[1].

Polymers are versatile materials used in numerous industrial applications, including coatings. Polyethylene, polyvinyl chloride, polyurethane, phenolic resins, acrylic resins, silicones and epoxies are examples of polymers used for coatings[3]. Each polymer can be applied as a single material, copolymerized, blended or layered with other polymers in order to meet the specific design requirements. A fundamental categorization can be made in terms of thermoplastics and thermosets. The latter being generally more thermally and chemically stable. Within this category, epoxies dominate an important share of the market due to their chemical resistance and versatility of application, in addition to the extensive history of use and reliability. Nevertheless, epoxies typically present unwanted characteristics, such as extended curing time, use of toxic and corrosive amines as hardener[4] and high water absorptivity[5].

Benzoxazines are high performance thermosetting resins which can be thermally cured, not requiring hardeners. Some outstanding properties include high resistance to water absorption, low surface energy[6], resistance to chemicals and UV, high thermal and mechanical properties and near-zero shrinkage upon curing[6,7]. On the other hand, benzoxazines may be of much more complex synthesis, higher cost, lower availability and far less history of use and research when compared to epoxies. Therefore, the combination of the two materials is a promising path towards obtaining remarkable physicochemical properties, while maintaining high reliability and low cost[8–10].

To be industrially applicable, some of the most important properties in a coating are adhesion, resistance to wear, permeability and thermal stability[11,12]. One interesting approach for these properties to be achieved is the production of a composite material by the incorporation of particles[13]. Silica is high hardness ceramic material, widely used in the industry as filler for composites[14], due to its improved interaction with polymeric matrixes, high mechanical properties, high availability and low cost.

Nowadays, green chemistry becomes increasingly a more important aspect of the coating industry as health and safety regulations get progressively stricter[15]. In this sense, from synthesis through storage, handling and application, it is vital that throughout the lifecycle of a coating, it represents minimal hazard without losing sight of performance[16].

Therefore, it is presented in this work a thorough investigation on all steps of the production and application of anticorrosion coatings. Composition is based on benzoxazine, epoxy and silica. From synthesis, purification and design of mixing procedure of the monomers, the greenest approach possible was always implemented. Highlight aspects of the investigation are time of reaction, reagents ratio for synthesis and composition of the coating, regarding ratio of monomers and volume fraction of filler.

1.2. Objective

The objective of this work was to develop a new coating for protection of metallic substrates against corrosion, based on a trifunctional benzoxazine and DGEBA epoxy copolymer. To achieve this goal three subsidiaries objectives were also envisaged, namely:

i. to synthesize a trifunctional benzoxazine monomer based on melamine, phenol and paraformaldehyde, using the greenest possible approach.
ii. to investigate the process of copolymerization between a trifunctional benzoxazine and DGEBA epoxy monomers and understanding the synergistic effects on thermal properties of the resulting copolymer.
iii. to investigate the influence of silica particles content on anticorrosion related and mechanical properties.

1.3. Literature Review

Corrosion is a natural chemical phenomenon between a material and its environment which damages the material, in most cases metals, degrading its properties[1,2]. It is estimated that the cost associated with corrosion globally amounts a total of US$ 2.5 trillion annually. Several approaches have been developed to protect materials from corrosion[2], such as controlling of the environment by means of inhibitors systems[3], cathodic protection by use of a sacrificial anodes[4], making use of corrosion resistant materials[2], application of plating or cladding by more noble materials[2] and organic coatings, which provide a continuous barrier to the substrate. In fact, organic coating systems are considered as one of the most widely used methods to protect metals against corrosion[2,5], and several application techniques are widely used. High solids[6,7], powder coating[8,9], UV curable[10,11] and water based[7,12] are examples of typical techniques applied in the industry[13,14]. Different aspects of the coating and its interaction with the substrate are highly influencing on the performance of the coating against corrosion. For example crosslinking density, hydrophobicity and adhesion are positively influencing to anticorrosion property [2,5,15,16]. Testing of coatings for anti-corrosion properties are typically performed by an accelerated test, such as salt spray or electrochemical experiment, which can shorten greatly the duration of the experiment[17]. Electrochemical tests, such as potentiodynamic polarization sweep, are able to provide a quantitative analysis by making use of modern instrumentation and measuring with much sensitivity[18]. Within the frame of organic coatings, epoxies have found a vast range of application due to their great combination of excellent adhesion, toughness, and chemical resistance[16,19,20], additionally to the long history of use and research, making it a highly cost effective material. Nevertheless, epoxies typically require toxic and hazardous chemicals such as amines or anhydrides as hardeners[21,22]. Additionally, water uptake may be an issue, especially considering the effect of degradation of the adhesion properties, which highly influences anticorrosion properties. In this sense, benzoxazines are thermosetting materials which exhibit outstanding performance, such as low surface energy [21], low water absorption, resistance to chemicals and UV, high thermal and mechanical properties and near-zero shrinkage upon curing [23,24]. Additionally, the flexibility of chemical structure design allows for the most diverse applications[25]. Nevertheless, polymerization of benzoxazines typically requires high

temeratures and the resulting polymer shows low crosslinking density[26–30]. An interesting, effective and largely applied solution for tuning properties while maintaining cost are the conjugated polymers, such as copolymers and polymer blends [31]. Copolymerization between benzoxazine and epoxy could lead to higher crosslink network density and, consequently, to improvement in properties[32–34]. The mechanism of copolymerization reaction between benzoxazine monomer (BZ) and epoxy is not well stablished to the moment, however it is reported to occur via the opening of the epoxide ring by the hydroxyl functionalities of the phenolic group present in the PBZ[35]. In the world of synthesis, development of new macromolecular structures and combination of polymers, one aspect sews all of these together and is progressively more approached and studied: Green chemistry. It covers several aspects related to the environment and is an area of chemistry and engineering concentrated on the design of products and processes that minimize the use and generation of hazardous substances[36]. Several works have been done towards this direction, especially regarding the use of renewable raw material. However, few work has been produced considering all or several aspects of green chemistry.

1.3.1. Corrosion

Corrosion is a natural chemical phenomenon between a material and its environment which damages the material, in most cases metals, degrading its properties[1,2]. This phenomenon is usually a heterogeneous redox reaction and occurs at the metal-environment interface, typically causing oxidation of the metal and reduction of the oxygen present in the environment[15] as represented in **Fig. 1.1**. Deterioration by corrosion is an important concern for mostly all metallic equipment, from industrial machinery and civil structures to vehicles and electronics. These materials are often exposed to aggressive environments, such as high temperature and pressure, chemically reactive substances such as O_2, H_2S, CO_2, water and salts. Similar to other natural phenomena such as earthquakes and floods, corrosion can cause catastrophic and costly damage to everything from civil engineering structures, machines, automobiles and pipelines. Interestingly enough, the U.S. Federal Highway Administration (FHWA) released study in 2002 in which it compares the cost of natural disasters and that directly associated with corrosion. It was estimated that direct cost associated with metallic corrosion in almost every U.S. industry sector sums a total of

staggering $276 billion annually. This amount is approximately 3.1% of the nation's Gross Domestic Product (GDP) and more than sixteen times higher than the cost U.S had annually with natural disasters in the same period[1]. The National Association for Corrosion Engineers (NACE) estimates a global cost of corrosion of US$2.5 trillion, and that it is possible to realize savings between 15 and 35% of that total by applying only available corrosion control practices[37].

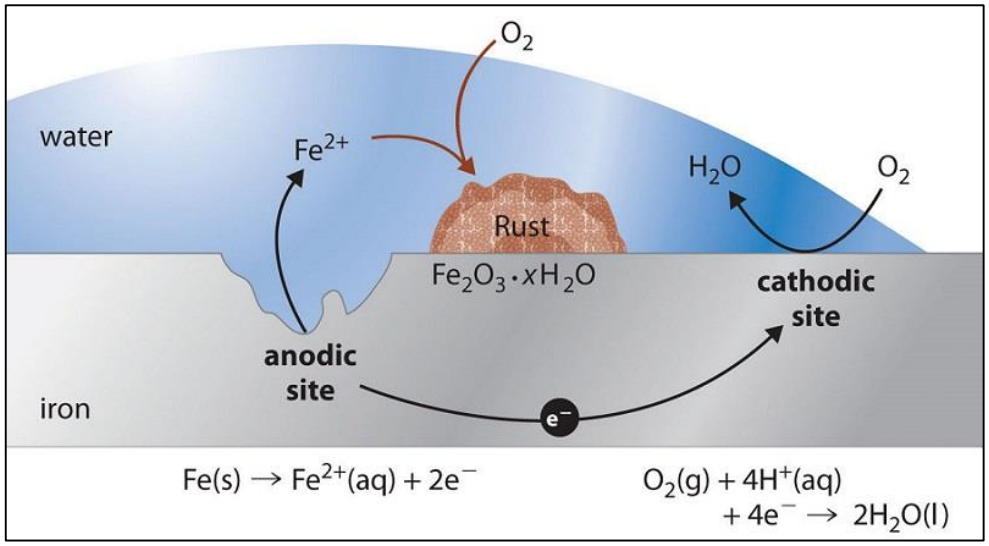

Fig. 1.1. Schematic representation of the oxidation of iron in water and oxygen-containing atmosphere.

Several approaches have been developed to protect materials from corrosion, such as:

- Control of the environment – Since corrosion of a material takes place in the interface between that material and the environment, in addition to the fact that chemical components of the environment are responsible for the corrosion process, it is coherent to control the environment in order to prevent corrosion. In this context corrosion inhibitors are widely used in several areas of industry. Two common operating mechanisms in inhibitors are i) the formation of a thin protective layer on the surface of the material, which prevents access of the corrosive media to the material and ii) the removal of corrosive agents from the environment by chemically reacting with them. This technique is used in closed systems such as automotive engine cooling systems, electronics cooling systems and HVAC systems[3].
- Cathodic protection – This is a technique used to prevent the corrosion of a metallic part by making it the cathode of an electrochemical cell. A largely employed system is the galvanic anode. In this system, a galvanic anode, a piece of sacrificial anode

made of a more negative potential material is attached to the metal to be protected on the surface where it is exposed to the electrolyte. The difference in electrode potential between the anode and the cathode provides the system with sufficient current to restore the electrical environment of the targeted metal[4].

- Corrosion Resistant Materials - Some metals are intrinsically more resistant to corrosion than others. The most resistant to corrosion are those for which corrosion is thermodynamically unfavorable. Alloys can be produced with metals less susceptible to corrosion, such as zinc, magnesium, chromium and nickel[2].
- Plating and Cladding – These are techniques in which a layer of a more noble metal or alloy is deposited on the surface of another metal in order to protect it against corrosion, for example. This allows for the use of a more cost effective base material and still obtain high resistance to corrosion. Materials used for deposition include zinc, nickel-chromium superalloys, gold and copper[2].

It is possible to observe that each technique has its specific application, where the system, cost, materials availability and manufacturing process must be taken in consideration. In this sense, organic coatings are protection system against corrosion that reveal to be applicable to very large parts, with high productivity, cost effective, that can be applied in the field and that can be combined with other techniques. In fact, organic coating systems are considered as one of the most widely used methods to protect metals against corrosion[5].

1.3.2. Coatings

Coatings are protective barriers that control corrosion by isolating, to a certain degree, the substrate from the corrosive environment. This anti-corrosion technique is widely applied in the most diverse fields of industry, including aviation, civil construction, industrial equipment, marine transportation and structures. Several materials and processes can be used in coating application, meeting the most distinct requirements of application[13,14].

- High Solids – Acrylics, Alkyds, Epoxy, Polyurethane, Saturated Polyesters. Used with reduced amounts of solvent and with the possibility of waterborne. Therefore, these coating materials present reduced volatile organic compounds (VOCs) and, consequently, controlled pollution and hazard. This technology solution has been

applied in several areas of industry, such as the automotive, aerospace, and marine. for utilization as primers and topcoats [7].

- Powder – Epoxy, Polyester, Polyurethane. Powder coatings can be made of either thermoset or thermoplastic. Characteristics such as zero use of solvents and low rate of waste make this technique the most economical environmentally friendly coating system for metals[8].
- UV Cured – acrylates (urethane, polyester, amino, epoxy). Monomers and oligomers mixed with photo initiators and additives are cured with UV radiation. This technique provides several advantages, such as quick curing, wide range of formulations, low energy consumption upon curing and coating of heat sensitive substrate[10,11].
- Water Based – latex, epoxy. Solution or suspension of monomers and oligomers in water based solvent. May use other solvents to improve performance. Have been widely applied in the aerospace, automotive and construction industries[7].

Effectiveness of barrier characteristic is influenced by intrinsic properties of the coating material and adhesion between coating and substrate[15,16]. Intrinsic material properties refer, for instance, to crosslink density and hydrophobicity [1,5]. Interestingly, the same features that improve barrier property may reduce adhesion of the coating to the substrate. Polar functional groups, for example, are positively influencers to adhesion and, at the same time, are likely to increase permeability to water due to their chemical affinity[20]. It is understood that adhesion plays such an important part in corrosion control, that several theories on the mechanism of failure of coatings suggest that the loss of adhesion precedes the onset of corrosion. Performance of coatings are commonly assessed by exposure of a substrate-coating system to an environment capable of simulating an accelerated corrosive condition, such as immersion in brine and salt spray. Evaluation of results are typically performed by evaluation of the type and extent of corrosion failure[15].

Several studies have evaluated the different aspects of adhesion and formulation of coatings in terms of their effective protection against corrosion. For example Shi et al.[38] produced PPS-PTFE/SiO_2 composites for coating. Results showed high wear resistance combined with hydrophobicity and good protection against corrosion.

The influence of SiO_2 particles was also analyzed by Conradi et al. [39], who observed improvement in mechanical and anti-corrosion properties with the

incorporation of silica nanoparticles. The results were attributed to improvement in hydrophobicity and to increase in diffusion path length for ions to travel.

Among the polymeric coatings, those based on epoxy have shown important practical results. Guidetti et al. [40] reported the use of PP layered with epoxy for O&G pipeline, resulting in high performance characterized by good adhesion, high cathodic disbonding protection, chemical resistance and low water absorption. Lazarević et al.[41] tested epoxy coatings applied by cathodic electrodeposition aluminum and pre-treated aluminum. Results revealed that depending on whether substrate was pre-treated or not and on the type of treatment, protective property against corrosion varied. Better protective performance was attributed to better wetting of the substrate surface by the epoxy and to lower porosity. Ramezanzadeh et al.[42] confirmed improvement in barrier properties of epoxy coatings with graphene oxide functionalized with primary amines when compared to coatings with neat graphene oxide. Result was partly attributed to greater hydrophobicity obtained with functionalization.

Photopolymerizable coating has also been studied. Sangermano et al.[43] investigated the influence of silica particles in the photopolymerization of epoxy coating and thermomechanical properties. Silica was able to improve degree of conversion, Tg and hardness of the coatings. A blend of epoxy and polyaniline was studied by Talo et al. [44] as coating material for the protection against corrosion of steel substrate. Results revealed a five orders of magnitude decrease in the corrosion current when compared to the bare metal. Behzadnasab et al. [45] investigated the influence of silane functionalized ZrO_2 content on epoxy coating as to anti-corrosion performance. Results showed best protections on samples with highest content of particles, i.e. 2 and 3 %.

From the works presented above, it can be inferred that epoxy resins are largely utilized as coating material due to its high thermal stability, chemical resistance, great adhesion, low shrinkage upon curing, high mechanical properties, and low cost [1,5,6].

1.3.3. Epoxy

Epoxy resins, since their introduction in 1939, have found important and steadily increasing use in the coatings field because of their incomparable combination of excellent adhesion, toughness, and chemical resistance[16,19]. Additionally, the long

history of use and research make it a highly cost effective material. Epoxies also find extensive use in structural and specialty composite applications, in addition to several other major areas of engineering, such as adhesive, casting and binders. Examples of such applications are [19]: i) epoxy-carbon fiber composites for the aerospace, automotive, construction and high performance sports equipment, due to its high strength to weight ratio. ii) Two-part high performance adhesives for the aerospace, automotive, boats, and other applications where high strength bonds are required. Important features of epoxy adhesives include high cohesion and adhesion strengths, solidification in high moisture environment and reduced or absence of solvents. iii) Two part coatings, highly resistant to environmental degradation applied in metallic structure for protection against corrosion and abrasion for application on floor of industrial plant and parking lots, industrial machinery, ships, subsea equipment and even in the food industry. Epoxies are used in compositions that can vary from a single epoxy resin with a hardener to multiple epoxy resins combined with modifiers, fillers, reinforcements and hardener package that drive specific reactions through time[46]. In fact, the term epoxy resin describes a broad class of thermosetting polymers in which the primary cross-linking occurs through the reaction of an epoxide group as highlighted in **Fig. 1.2**. While the presence of this group defines the molecule as an epoxy, the basic molecular structure to which the ring is attached can vary widely, from oligomers to telechelics, giving rise to various distinct properties. The chemical classes most commonly used as hardeners are the amines, amine derivatives and anhydrides[47]. The global epoxy resin market was valued at USD 6 billion in 2013, and is projected to grow more than USD 3 billion between 2017-2022[48]. Epoxy monomers are readily cross-linked with heat-reactive resins or polyfunctional primary amines to form highly resistant, thermoset polymers. The polar nature of the epoxy macromolecule, due to pendant hydroxyl groups derived from opening of the epoxide ring, accounts for its strong adhesion to a wide variety of surfaces. Polarity of epoxy monomers accounts for its solubility in oxygenated solvents such as ketones, esters, and ether-alcohols and in chlorinated hydrocarbons[16]. Diglycidyl ether of bisphenol-A (DGEBA), shown in **Fig. 1.2a** is one of the most common types of epoxy resin used in the industry[49], representing approximately 75% worldwide demand[32].

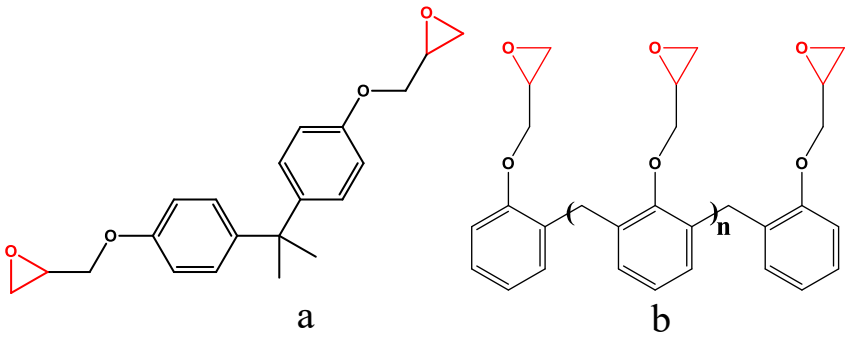

Fig. 1.2. a) Diglycidyl Ether of Bisphenol A (DGEBA). b) Epoxy Phenol Novolac Resin. Epoxide group highlighted in red.

Importantly, crosslinking of epoxies can occur through the epoxide or hydroxyl groups. It commonly takes place by two types of curing mechanism, i.e., direct reaction of resin molecules by a catalytic homopolymerization, or coupling through a reactive intermediate. The ability of the epoxy functional group to react by different paths and with several reactants gives epoxy resins great versatility. The most widely used curing agents are compounds containing active hydrogen such as polyamines, polyacids, polymercaptans and polyphenols[32].

A vast literature deals with many general aspects of the use of epoxy resins [19,50]. More recently, aspects related to the use of nanofillers, in order to increase thermal stability, and related to the safe use of certain chemical compounds as hardeners, have been researched. For example, Das and Karak[51] produced composites of epoxy and nano-clay and observed an improvement of 19 °C in the onset of degradation measured by TGA. Bourne et al.[52] reported health problems from amine-based hardeners used in epoxy. Both cured and uncured resins showed risks to health.

Several works are dedicated to a similar theme, being that, improvement of properties of epoxy. It is of great interest to produce thermally stable coatings, with simple and quick curing procedures which are safe and the least toxic possible. It is interesting to observe that Lascano [53] reveals that even though the molecular structure of the epoxy may be crafted in order to produce a less toxic polymer, amines are widely used as hardeners due to their high reactivity. As such, most of them tend to be corrosive and produce toxic fumes. Not only amines, but also other chemical compounds used for curing, such as anhydrides and organic-acid hydrazide, are hazardous and toxic [21,22]. Additionally, epoxies may require long time of cure and post curing procedures at temperatures higher than Tg in order to enable the full performance of the

polymer[54]. Furthermore, epoxy resins tend to allow for permeation of water due to the presence of the hydrophilic hydroxyl groups resulting from the opening of the epoxide ring upon polymerization. The result from the water uptake is deterioration of adhesion and consequent corrosion of the substrates[20]. In this sense, benzoxazines are self-curable, consequently eliminating side effects caused by hardeners. At the same time, benzoxazines tend to present a quick curing process at high temperatures, thus being a great option of chemical compound to be combined to epoxies.

1.3.4. Benzoxazine

Benzoxazines are molecules characterized by the presence of an aromatic benzene ring and an oxazine ring (a heterocyclic six-membered ring with one oxygen and one nitrogen atom) where two carbons are shared among the two rings, as represented schematically in **Fig. 1.3**. This class of molecules has been used as reducing agent [27], optoelectronic material precursor [28], antimicrobial material [29], therapeutic drug agent [30] and monomer. The use of benzoxazines as monomers is more recent and of great interest to both, industrial applications and scientific materials research [25]. Benzoxazine monomers, when polymerized, produce a high strength yet low surface energy polymer, the polybenzoxazine (PBZ). PBZs have shown lower surface energy than that of polytetrafluoroethylene (PTFE) [23]. In addition, PBZ shows low water absorption, resistance to chemicals and UV, high thermal and mechanical properties and near-zero shrinkage upon curing[23,24].

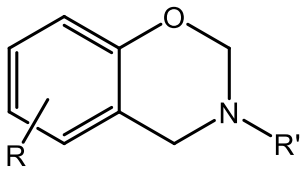

Fig. 1.3. Basic Structure of Benzoxazine Monomer

Benzoxazine molecules were first synthesized in 1944 by F. W. Holly and A. C. Cope by the condensation of aminobenzyl alcohol with a number of aldehydes and ketones followed by refluxing the reactants in benzene solution[55]. Currently, the most conventional route employed to prepare benzoxazines is condensation of a phenolic derivative, a primary amine and formaldehyde via solution synthesis using organic solvents, as represented in **Fig. 1.4** [56].

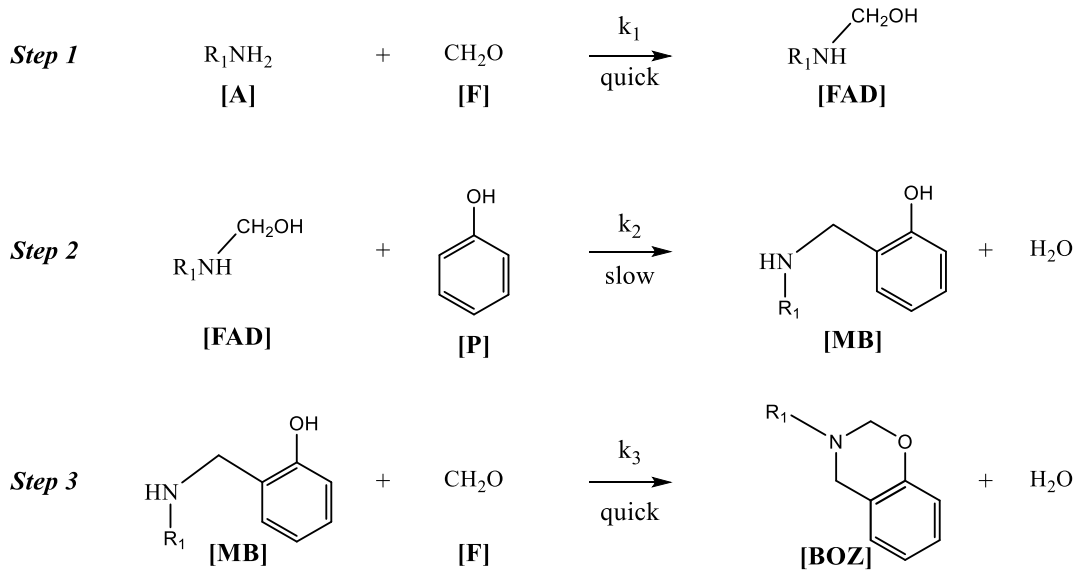

Fig. 1.4. Mechanism of synthesis of benzoxazine. Reactions steps in the benzoxazine synthesis. (adapted from Zhang et al. [56]).

Nomenclature in **Fig. 1.4** is as follows:

[A] – Amine

[F] – Formaldehyde

[FAD] – Formaldehyde-Amine Derivative

[MB] – Mannich Base

[BOZ] – Benzoxazine monomer

Ishida [24] confirms that multifunctional amines or phenolic derivatives can also be used to synthesize multifunctional benzoxazine. In addition, Ishida [57] indicates that several types of phenolic derivatives, aldehyde and primary amines may be used for the synthesis, specifically, phenol, melamine and paraformaldehyde are cited as possible reagents. Regarding ratio of reagents, Burke et al. [58] showed that reagents ratio influences the yield as well as the type of product, where higher yield was obtained when the ratio of phenol:amine was 2:1 regarding functional groups. It can be inferred, then, that synthesis of benzoxazine doesn't necessarily need to follow the stoichiometric ratio of reagents. Burke et al. [59] also showed that reaction time influences the formation of benzoxazine. When hydroquinone, formaldehyde, and benzylamine were reacted for 30 min they obtained six times lower yield when compared to a 2h reaction time. Furthermore, Burke et al. [60] obtained a higher yield in the formation of benzoxazine molecules at higher reaction temperatures.

With respect to reaction temperature, it is reported[57] that synthesis of benzoxazine can be performed at any temperature from 0 °C to 250 °C given sufficient

time. However, it is ideal that the reaction be conducted from 0 °C to 150 °C. Regarding pressure, most reactions may be conducted at atmospheric pressure or at a pressure up to about 100 psi (6.8 atm), although in some cases, reactions carried under higher pressure produce fewer byproducts, and when a polyfunctional benzoxazine is being prepared, higher yield is obtained. Time of reaction depends on the reaction conditions and on nature of reagents. Reaction times of around 15 to 30 minutes are commonly used, although, this time may vary depending on the conditions of reaction [57].

One of the most interesting properties of benzoxazines is the flexibility of chemical structure design, achieved by selection of different phenolic and amino compounds upon synthesis[25]. This molecular variability translates into specific physical, mechanical and thermal properties of the resulting polymer. Among the several aspects of molecular structure, benzoxazines with different functionalities have been reported, as exemplified in **Fig. 1.5**[23–25,61,62]. However, it is important to highlight that even among molecules with the same functionality, the chemical structure can assume distinct configurations, each one leading to its own particular set of properties[24].

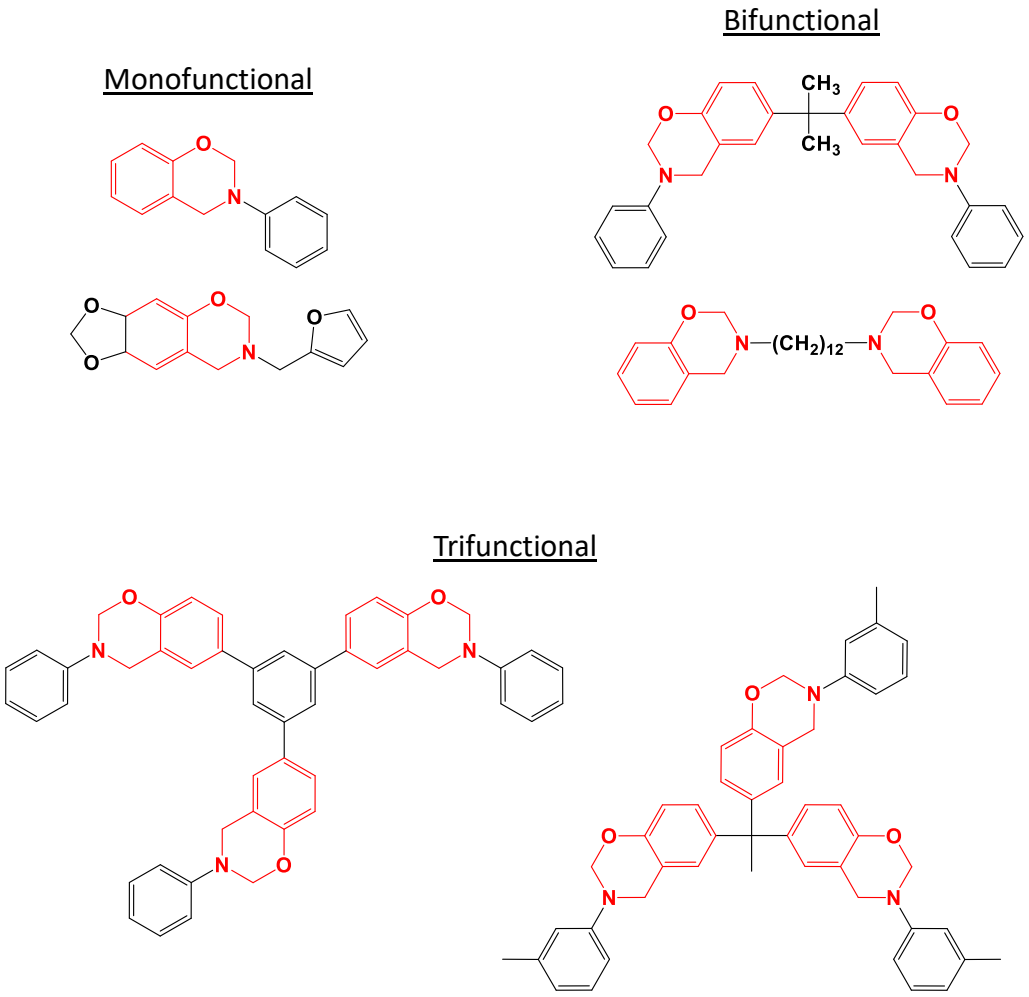

Fig. 1.5. Examples of benzoxazine monomers reported in literature [23–25,61,62]

Synthesis is typically accompanied by a purification procedure in order to remove unreacted reagents and, consequently, obtain high purity monomers. Commonly procedures used in research labs include i) rinsing with water and drying with anhydrous sodium sulfate, ii) column chromatographic separation, iii) recrystallization, iv) liquid-liquid extraction and combinations of any of these techniques [63,64]. From a practical standpoint, it is possible to notice that not all techniques are compatible with large scale or industrial applications, either due to the low yield rate intrinsically associated with the process or to the necessity of specialty equipment. Liquid-liquid extraction is one of the most appropriate techniques in such cases, where large batches can be treated and simple solvents are required. Nevertheless, it is important to highlight that due to the nature of reagents and of the benzoxazine monomers, it is common to see the use of very hazardous or toxic organic solvents, such as tetrahydrofuran (THF), dimethylformamide (DMF), chloroform and acetone.

Liquid-liquid extraction, also known as solvent extraction is a process in which two immiscible solvents are used to separate chemical compounds by solubility to those solvents. **Fig. 1.6** [65] shows a solvent miscibility chart used to select solvents for the liquid-liquid extraction. In the particular case of the product of synthesis of benzoxazine, firstly the mixture of unreacted reagents and monomers is dissolved in an organic solvent (solvent 1) known to be able to dissolve the benzoxazine monomers, typically chloroform or toluene [23,66–68]. A second solvent (solvent 2) is added to this solution. This second solvent must be immiscible with the first one in addition to being capable of dissolving the reagents. Typically, a solution of sodium hydroxide (NaOH) and water is used. The purpose of adding NaOH to the water is to increase solubility of the reagents in the water, as the NaOH ions attack the reagents and convert them to salts. It is through the interfaces of the solvents that the NaOH ions interact with the reagents, and it is also through these interfaces that the migration of the reagents from solvent 1 to solvent 2 take place[69]. Therefore, it is advantageous to maximize the interfacial area. For this reason, the mixture of solvents and products of reaction is then vigorously shaken in order to produce an emulsion of the two solvents, increasing the surface area of contact between the solvents though the formation of droplets. This emulsion is left to decant and the water phase is removed. Usually, this procedure is repeated several times and followed by rinsing with pure water to neutralize the pH[23,70].

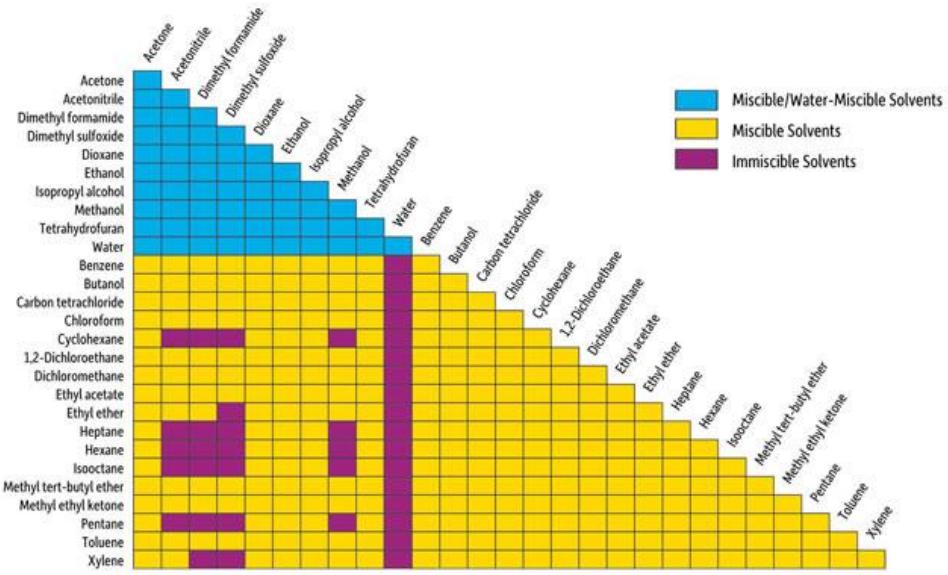

Fig. 1.6. Miscibility chart for solvents (adapted from Restek.com [65]).

Subsequent step of the purification procedure is drying of the resulting product. Typically, anhydrous sodium sulfate is added to the solvent-monomers solution to remove residual water. Mixture is then filtered, resulting in a “dry” monomer-solvent solution. Finally, solvent 1 is evaporated in a rotary evaporator apparatus, for example, resulting in the purified monomer.

Polymerization of benzoxazine monomers into polybenzoxazine is an addition process that takes place via ring opening polymerization by thermal activation/acceleration of the oxazine groups. It has been confirmed that the six-membered heterocycle with its irregular structure has stresses that provide the driving force for ring-opening polymerization. However, the ring stresses are usually not sufficient to promote curing at room temperature, requiring higher temperatures for the process to occur in comparison to epoxies, for example[24]. Opening of the ring allows for the extremity with the methyl group to react with the neighboring molecule on the ortho- or para- positions of the benzene ring[71], as shown in **Fig. 1.7**.

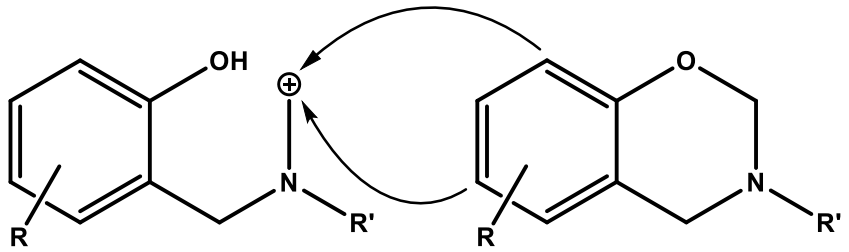

Fig. 1.7. Polymerization mechanism of generic benzoxazine monomer.

Nevertheless, it is important to mention that the effect of heating is to increase reaction rate. Polymerization of benzoxazines is a spontaneous process mainly because, after synthesis, the reaction medium frequently contains small amounts of residues even after purification, such as phenolic reagents and oligomers, and they act as initiators[24]. Typically, polymerization is performed at temperatures around 160-220°C[72]. Upon polymerization, polybenzoxazine exhibits amorphous structure as they are thermosets and, therefore, cross-linked[24].

Polybenzoxazines hold very interesting physicochemical and thermomechanical properties. Some of these properties have been reported as “unusual” when several aspects of the monomer chemical structure or the polymer conformation are taken in consideration. These properties are[24]:

a. Near-zero volume change upon polymerization – Shrinkage upon polymerization of most thermosets can be found at around 2-10%. This variation in dimension of

the polymeric material on a substrate generates interfacial residual stress, which decreases the mechanical interlocking of the polymer over the substrate. As a consequence, performance may be deteriorated for applications as coating, composites, adhesives and sealants.

b. Low water absorptivity – Some polybenzoxazines have shown water uptake at saturation of merely 1.9%, as opposed to polyesters, phenolic and polyimide, which may absorb up to 20% water. The low water absorption is advantageous in minimizing the difference between dry Tg and wet Tg.
c. High glass transition temperature - High glass transition temperatures ranging approximately from 160 to 400 °C. Importantly, Tg of polybenzoxazines can be higher than temperature of cure due to the abundant amount of active sites available and to the benzene rings to which the active sites react, which are also abundant. As such, further reactions or structural rearrangement of the polymer are possible, increasing Tg beyond the polymerization temperature.
d. High char yield - Char formation usually increases with increased content of benzene groups, as is the case of benzoxazines. Furthermore, according to Walter and Lyon's method[73], polybenzoxazines can be intrinsically good flame-retardants due to high molar group contribution of hydroxyl groups, tertiary amine, and benzene groups. High char yield is important in applications that require resistance to fire, as char reduces the diffusion rate of decomposed, flammable gases toward the flame front. In addition to thermally isolating the underlying unburned material from the flame. For example, Salum et al.[25] produced biobased monofunctional benzoxazine. When cured, resulting polybenzoxazine displayed high thermal stability, achieving char yield as high as 64%.

Several of the unique properties of polybenzoxazines can be explained by hydrogen bonds forming upon polymerization. Specifically, hydrogen bonds are responsible to the hydrophobicity, low dielectric constant, high char yield and high modulus. In fact, it has been reported that polybenzoxazines show higher modulus with lower crosslinking density when compared to other thermosets due to hydrogen bonds[26]. The reason for the higher mechanical properties with lower cross-linking density is attributed to the fact that polybenzoxazines generate huge density of hydrogen bonding, which may be simultaneously the cause of such low cross-linking density and the reason for the cited high properties, as these large amount of hydrogen bonds could be sufficient to hinder the chain mobility[26].

The use of fillers is also an alternative approach to improve certain properties of polybenzoxazines. Kajornchaiyakul et al. [74], for example, produced highly-filled polybenzoxazine-alumina composites. Results revealed improvements in storage modulus and Tg with up to 83 wt% alumina content. Pengdam and Rimdusit [75] also produced highly-filled polybenzoxazine-graphite composites with load ranging from 40 to 80 wt%. Results revealed improvement in Tg and storage modulus throughout the range of filler content. Caldona et al. [23] synthesized difunctional benzoxazine and produced coatings based on the monomer and silica. Resulting material revealed Superhydrophobicity and superior anticorrosion performance. Results were attributed to an increase in surface roughness caused by a densely packed arrangement of SiO_2 nanoparticles on the surface of the coating. Additionally, the presence of trapped air in the protrusions of the surface is responsible for minimizing the direct contact between the corrosive environment and the coating.

1.3.5. Conjugated Polymers

Combination of polymers is a traditional and effective technique to make materials viable to demands of industry with respect to properties such as, resistance to high temperature, light weight, toughness and cost. Several distinct techniques are employed industrially in large scale in order to combine two or more polymeric materials [31]:

- Polymer blends - combination of two or more polymeric materials, where the mixing is obtained by the fusing of each polymer component and subsequent amalgamation by means of a mechanical system, such as an extruder. Polymer blends can be divided into three groups:
    - Immiscible polymer blends: materials used in the blend are not compatible, producing clearly distinct phases in the microstructure. The lack of compatibility tends to result in a loss of some mechanical properties. Glass transition temperature is characterized by multiple regions, where each region corresponds to the respective polymeric component.
    - compatible polymer blends: There is sufficiently strong interactions between the component polymers, however they are still Immiscible. Such characteristic provides more uniform physical macroscopic properties.

    - miscible polymer blends: Polymer blends composed of highly compatible polymers that, when mixed, produce a single-phase structure. In this case, great synergistic effect is expected and one single glass transition temperature can be observed.

- Copolymers - combination of two or more polymers in which the polymerization occurs with the monomers of all materials involved mixed, generating macromolecules composed of all the monomers involved. Therefore, different from a polymer blend that is produced by mixing polymerized materials, a copolymer is characterized by the polymerization occurring subsequently or during the mixing of monomers. Copolymers can be divided into four major categories:
    - Random: macromolecules are composed of different monomers disposed in a random sequence.
    - Alternating: macromolecules are composed of the monomers organized in a sequentially pattern of a single monomer of each type at a time.
    - Block: blocks of monomers of one type alternate with blocks of monomers of the types sequentially arranged.
    - Graft: the backbone of the macromolecule is composed of a single type of monomer, while another type of monomer is grafted as smaller macromolecules.

It important to highlight that for the production of polymer blends, polymers must be thermoplastics. As such, they are susceptible to melting and consequent mixing. On the other hand, copolymers can be produced from both thermoplastic and thermosetting monomers. In this regard, it has been reported that it is possible to copolymerize benzoxazines with other monomers such as epoxy and urethane[26,33].

It has been reported that the cross-linking density of PBZ is rather lower than that of other thermosetting polymers, and yet PBZ possesses high Tg and Young's modulus. The reason is attributed to the fact that PBZ generates huge density of hydrogen bonding, which may be simultaneously the cause of such low cross-linking density and the reason for the cited high properties, as these large amount of hydrogen bonds could be sufficient to hinder the chain mobility and induce the rigidity observed in the glassy state[26]. Copolymerization between PBZ and DGEBA, the most commonly used epoxy resin in the copolymer, could lead to higher crosslink network density and, consequently, to improvement in properties[32,33], as indicated by Ishida and Allen[34].

The mechanism of copolymerization reaction between benzoxazine monomer (BZ) and epoxy is reported in literature to occur via the opening of the epoxide ring by the hydroxyl functionalities of the phenolic group present in the PBZ[35]. This concept means that the reaction between benzoxazine and epoxy is constituted of two steps as represented in **Fig. 1.8** [76]. The first step is the homopolymerization reaction among the monomers of benzoxazine, the second step is the reaction between the hydroxyl group generated upon opening of the oxazine ring in the first step and the epoxide group of the epoxy. Relevance of this model of copolymerization is in anticipating that the first reaction to occur is always benzoxazine homopolymerization.

One interesting observation from **Fig. 1.8** is that number of hydroxyl groups formed during copolymerization of benzoxazine and epoxy is the same as that produced from the homopolymerization of either monomers. As a consequence, the resulting copolymer should possess a good interaction with the substrate it is applied to[20]. As stated previously, adhesion is vital to the performance of a coating.

Other aspects of the benzoxazine/DGEBA copolymer have also been analyzed. For example, Rimdusit et al.[76] confirmed a synergistic behavior on glass transition temperature of the benzoxazine/epoxy copolymer at the stoichiometric ratio. However, compositions with excess epoxy revealed decrease in Tg. Kumar and Nair [35][32] describe that copolymerization of benzoxazine with epoxy reduces char yield compared with pure polybenzoxazine.

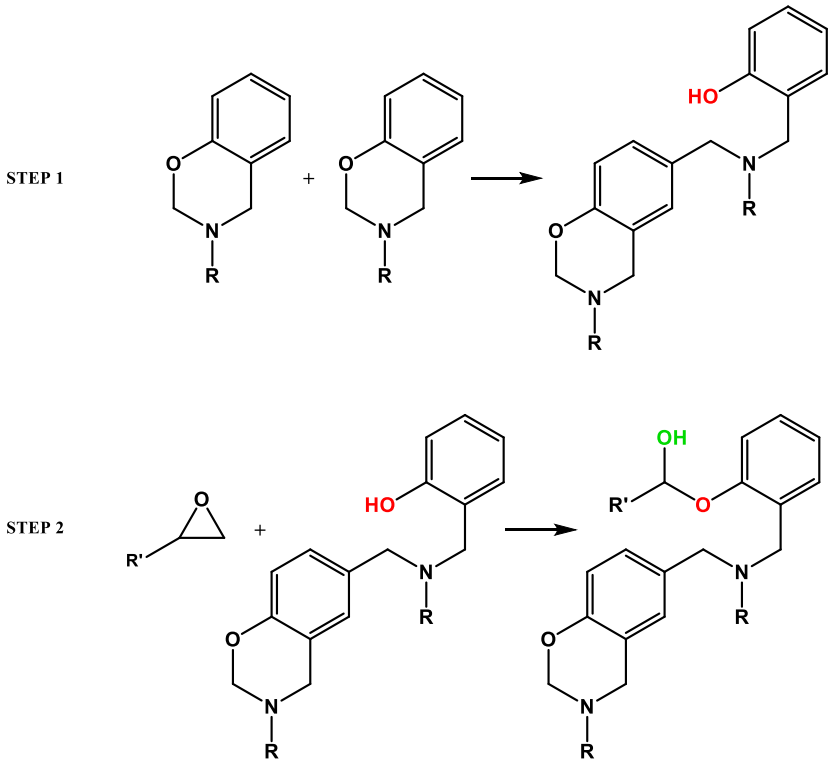

Fig. 1.8. Schematic representation of benzoxazine-epoxy copolymerization reaction [76]

1.3.6. Green Chemistry

The concept of green chemistry covers several aspects related to the environment, such as sustainability, hazards, wastes, toxicity and disposal. Essentially, green chemistry is an area of chemistry and engineering concentrated on the design of products and processes that minimize the use and generation of hazardous substances[36]. When new chemical products or reaction routes are developed, it is appropriate that a green approach is implemented with the purpose of leading a more sustainable process. Literature[25] indicates, however, that there is a conceptual misinterpretation, where the common sense of simply using natural renewable raw material is taken as a synonym of carrying out green chemistry. According to Anastas and Eghbali[36] the foundation of green chemistry is to improve safety of processes and products throughout all stages of chemical life-cycle. The authors propose the "twelve principles of green chemistry", which are guidelines to provide sustainable design. Here, all twelve principles are presented.

1) **Prevention of Waste** – "It is better to prevent the formation of waste rather than to clean it up after the fact". Reduction of Environmental Impact Factor (E-Factor) is

the goal for this principle. E-Factor is calculated as the mass of waste per mass of product of a chemical reaction;

2) **Atom Economy** – "The concept of synthetic efficiency: Atom Economy (AE) also called Atom Efficiency". It refers to the concept of optimizing the use of raw materials so that the final product consumes the maximum amount of the reagents.
3) **Less Hazardous Chemical Synthesis** – "synthetic methodologies should be designed to use and generate substances that pose little or no toxicity to human health and the environment"
4) **Designing Safer Chemicals** – "Chemical products should be designed to preserve efficacy of the function while reducing toxicity";
5) **Safer Solvents and Auxiliaries –** "The use of auxiliary substances should be made unnecessary whenever possible and, when used, innocuous";
6) **Design for Energy Efficiency** – "Energy requirements should be recognized for their environmental and economic impacts" – incorporation of renewable energy sources is also desirable.
7) **Use of Renewable Feedstock** – "A raw material or feedstock should be renewable rather than depleting whenever technically and economically practicable";
8) **Reduce Derivatives** – "Unnecessary derivatization […] should be minimized or avoided if possible";
9) **Catalysis** – "Catalytic reagents are superior to stoichiometric reagents" – "Catalysis can improve the efficiency of a reaction by lowering the energy input required, by avoiding the use of stoichiometric amount of reagents, and by greater product selectivity";
10) **Design for Degradation** – "Chemical products should be designed so that at the end of their function they break down into innocuous degradation products and do not persist in the environment";
11) **Real-Time Analysis for Pollution Prevention –** most methodologies require pretreatment of samples in order to enable analysis, which generates waste;
12) **Inherently Safer Chemistry for Accident Prevention** – "Substances and the form of a substance used in a chemical process should be chosen to minimize the potential for chemical accidents".

Therefore, it can be observed that throughout a synthesis development process, whenever technically and economically possible, green chemistry must be

implemented. Moreover, observing simultaneously principles 3 and 5, it is evident that the use of less toxic and less hazardous solvents is a direct approach towards green chemistry. Most benzoxazine synthesis pathways employed on literature involve the use of some solvent such as dioxane, methanol, hydrochloric acid, toluene, dimethyl sulfoxide, tetrahydrofuran or chloroform[23,25,56,77,78]. However, it is known that most of these solvents are highly toxic, corrosive, expensive and require special handling. Prat et al.[79] discuss safety, health and environmental issues of several solvents and rank them into four categories. **Table 1.1** is an adaptation from their work. This itself may be reason enough to impair industrial application of the process. In this sense, previous attempts have been made to produce benzoxazine monomers in more sustainable media. Rattanopas et al. [21] performed synthesis under a mixture of ethanol and water as solvent. Purification process employed only covers removal of solvents and additive. Characterization was performed only by FTIR. Shi et al. [22] performed synthesis under a mixture of methanol and water as solvent and no purification process is mentioned. Characterization by ^{1}H-NMR revealed peaks assigned to formation of oxazine to be broad, short and too distant from one another, diverging from references in the literature [23]. In fact, the synthesis of benzoxazine forms two molecules of water for every oxazine produced as explained by Zhang et al. [18] (**Fig. 1.4**, page 34). In addition, the polarity of the solvents influences the yield of the reaction. Results in literature show much lower yields for synthesis performed under more polar solvents [24], which is the case of ethanol, methanol and water. Therefore, reaction in the presence of water tends to be pushed back in the direction of the reagents. It can be established, then, that water is not the ideal solvent to be used in the synthesis of benzoxazine, despite the fact that water is the most abundant and safe solvent.

Table 1.1. Ranking of solvents as Recommended, Problematic, Hazardous and Highly Hazardous, regarding safety, health and environment. (adapted from Prat et al. [79])

Family	Solvent	BP (°C)	FP (°C)	Worst H3xx[a]	H4xx	Safety score	Health score	Env. score	Ranking by default	Ranking after discussion[b]
Water	Water	100	na	None	None	1	1	1	Recommended	Recommended
Alcohols	MeOH	65	11	H301	None	4	7	5	Problematic	Recommended
	EtOH	78	13	H319	None	4	3	3	Recommended	Recommended
	i-PrOH	82	12	H319	None	4	3	3	Recommended	Recommended
	n-BuOH	118	29	H318	None	3	4	3	Recommended	Recommended
	t-BuOH[c]	82	11	H319	None	4	3	3	Recommended	Recommended
	Benzyl alcohol	206	101	H302	None	1	2	7	Problematic	Problematic
	Ethylene glycol	198	116	H302	None	1	2	5	Recommended	Recommended
Ketones	Acetone	56	−18	H319	None	5	3	5	Problematic	Recommended
	MEK	80	−6	H319	None	5	3	3	Recommended	Recommended
	MIBK	117	13	H319	None	4	2	3	Recommended	Recommended
	Cyclohexanone	156	43	H332	None	3	2	5	Recommended	Problematic
Esters	Methyl acetate	57	−10	H302	None	5	3	5	Problematic	Problematic
	Ethyl acetate	77	−4	H319	None	5	3	3	Recommended	Recommended
	i-PrOAc	89	2	H319	None	4	2	3	Recommended	Recommended
	n-BuOAc	126	22	H336	None	4	2	3	Recommended	Recommended
Ethers	Diethyl ether	34	−45	H302	None	10	3	7	Hazardous	HH
	Diisopropyl ether	69	−28	H336	None	9	3	5	Hazardous	Hazardous
	MTBE	55	−28	H315	None	8	3	5	Hazardous	Hazardous
	THF	66	−14	H351	None	6	7	5	Problematic	Problematic
	Me-THF	80	−11	H318	None	6	5	3	Problematic	Problematic
	1,4-Dioxane	101	12	H351	None	7	6	3	Problematic	Hazardous
	Anisole	154	52	None	None	4	1	5	Problematic	Recommended
	DME	85	−6	H360	None	7	10	3	Hazardous	Hazardous
Hydrocarbons	Pentane	36	−40	H304	H411	8	3	7	Hazardous	Hazardous
	Hexane	69	−22	H361	H411	8	7	7	Hazardous	Hazardous
	Heptane	98	−4	H304	H410	6	2	7	Problematic	Problematic
	Cyclohexane	81	−17	H304	H410	6	3	7	Problematic	Problematic
	Me-cyclohexane	101	−4	H304	H411	6	2	7	Problematic	Problematic
	Benzene	80	−11	H350	None	6	10	3	Hazardous	HH
	Toluene	111	4	H351	None	5	6	3	Problematic	Problematic
	Xylenes	140	27	H312	None	4	2	5	Problematic	Problematic
Halogenated	DCM	40	na	H351	None	1	7	7	Hazardous	Hazardous
	Chloroform	61	na	H351	None	2	7	5	Problematic	HH
	CCl_4	77	na	H351	H420	2	7	10	Hazardous	HH
	DCE	84	13	H350	None	4	10	3	Hazardous	HH
	Chlorobenzene	132	29	H332	H411	3	2	7	Problematic	Problematic
Aprotic polar	Acetonitrile	82	2	H319	None	4	3	3	Recommended	Problematic
	DMF	153	58	H360	None	3	9	5	Hazardous	Hazardous
	DMAc	166	70	H360	None	1	9	5	Hazardous	Hazardous
	NMP	202	96	H360	None	1	9	7	Hazardous	Hazardous
	DMPU	246	121	H361	None	1	6	7	Problematic	Problematic
	DMSO[c]	189	95	None	None	1	1	5	Recommended	Problematic
	Sulfolane[c]	287	177	H360	None	1	9	7	Hazardous	Hazardous
	HMPA	>200	144	H350	None	1	9	7	Hazardous	HH
	Nitromethane	101	35	H302	None	10	2	3	Hazardous	HH
Miscellaneous	Methoxy-ethanol	125	42	H360	None	3	9	3	Hazardous	Hazardous
	Carbon disulfide	46	−30	H361	H412	9	7	7	Hazardous	HH
Acids	Formic acid	101	49	H314	None	3	7	3	Problematic	Problematic
	Acetic acid	118	39	H314	None	3	7	3	Problematic	Problematic
	Ac_2O	139	49	H314	None	3	7	3	Problematic	Problematic
Amines	Pyridine	115	23	H302	None	4	2	3	Recommended	Hazardous
	TEA	89	−6	H314	None	6	7	3	Problematic	Hazardous

One of the most promising approaches to synthesis of benzoxazine regarding solvents in green chemistry is the solventless process[36]. Ishida[57] stated that in cases where one or more of the reagents is a liquid, they may simply be mixed and heated so they homogenize, either through melting, or by dissolving in one or more of the liquid components. To proceed with reaction, the mixture is held at a temperature and for enough time to enable the synthesis reaction for the specific benzoxazine monomer being synthesized. This process assumes that at least one of the reagents is liquid at room temperature. However, it limits the variety of reagents that can be used, narrowing, then, the possibilities of molecular structures to be produced as explained previously (section 1.3.4, page 33). An interesting alternative is to promote the mixture and consequent dissolution of reagents at high enough temperature to allow for at least

one of the reagents to melt and, being a liquid, enable the process just described. With this approach, the variety of reagents possible to be used is widened. In fact, this procedure is described in literature [57].

1.3.7. Electrochemical Corrosion Test.

Testing of coatings requires extensive time of exposure to real life environment to allow for the differentiation of the corrosion protection of each system. Tests may reach the order of years. Accelerated tests such as salt spray may shorten this time to the order of thousands of hours. Long times of testing result in a hindered development of coatings. Additionally, both cases provide qualitative results that can vary as a function of testing site and conditions, testing chamber and individual analysis of the results[17].

Electrochemical techniques come to fill this necessity by making use of modern instrumentation and measure very small electrical currents. These techniques allow for measurements which are much more sensitive than most non-electrochemical techniques based on weight loss or visual inspection, for example[18]. Electrochemical experiments are typically performed by means of an electrochemical cell in a three-electrode setup as depicted in **Fig. 1.9**. The working electrode is the sample to be studied. The current is measured via the counter electrode. The potential of the working electrode is measured by the reference electrode. The chamber is filled with the electrolyte of interest to allow for the current to flow. Potentiodynamic polarization scan (PPS) is a widely applied electrochemical technique which provides critical information of the performance of a coating. Corrosion current density (i_{corr}), corrosion potential (E_{corr}) and Tafel lines are directly obtained from the experimental curves. This data can be used to calculate corrosion rate and polarization resistance[18]. In this technique, the potential is scanned at a fixed rate between two set values and the current is measured at periodic intervals[18].

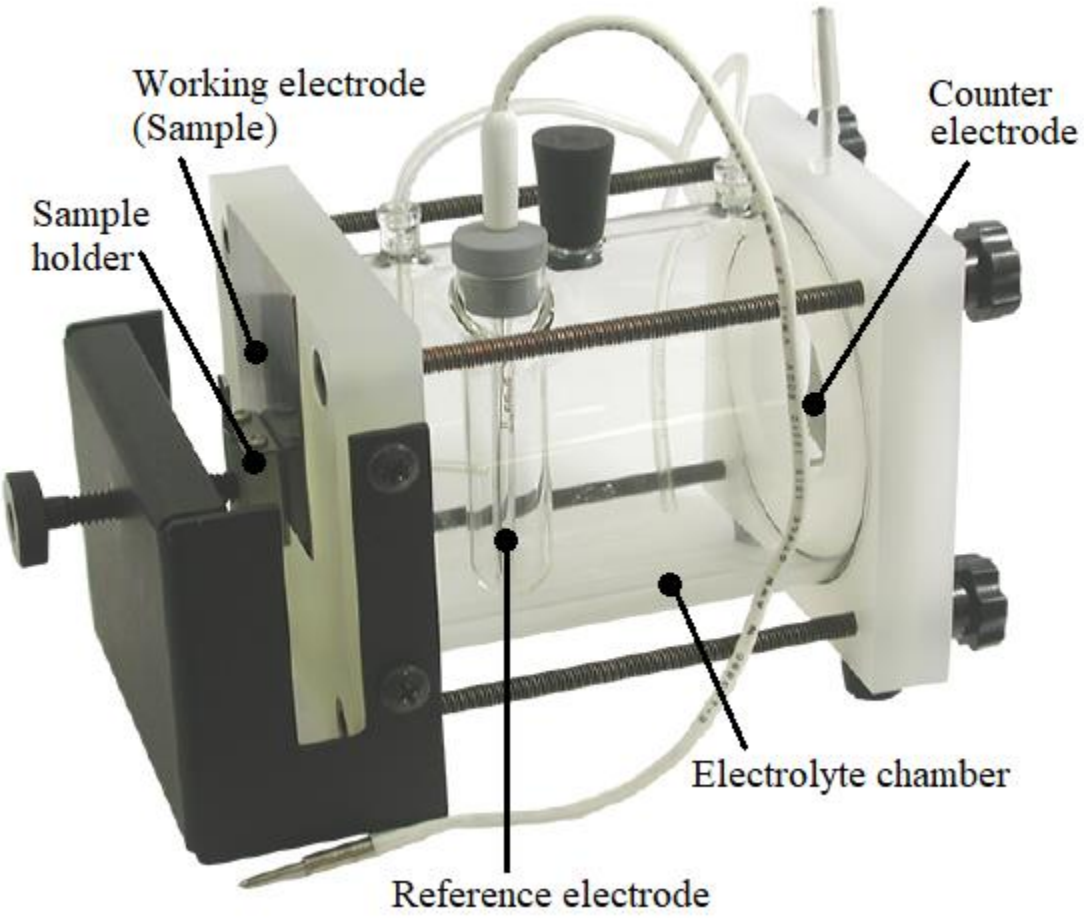

Fig. 1.9. Example of electrochemical testing cell

A typical PPS curve is presented in **Fig. 1.10**. The anodic polarization scan starts at point 1 and progresses towards point 2. The most relevant features on the curve are[82]:

A. The open circuit potential (OCP)- At this potential the sum of the anodic and cathodic reaction rates on the electrode surface is zero, meaning that the measured current will be close to zero.

B. The active region - In this region, the main reaction occurring is oxidation of the sample.

C. The passivation potential – at this point passivation starts to occur.

D. As the applied potential increases, the current density decreases.

E. Passive region – low current density.

F. Breakaway potential – increase in potential results in rapid increases in current

G. Increase in current - several reasons are associated with this increase in current, such as pitting and transpassive dissolution.

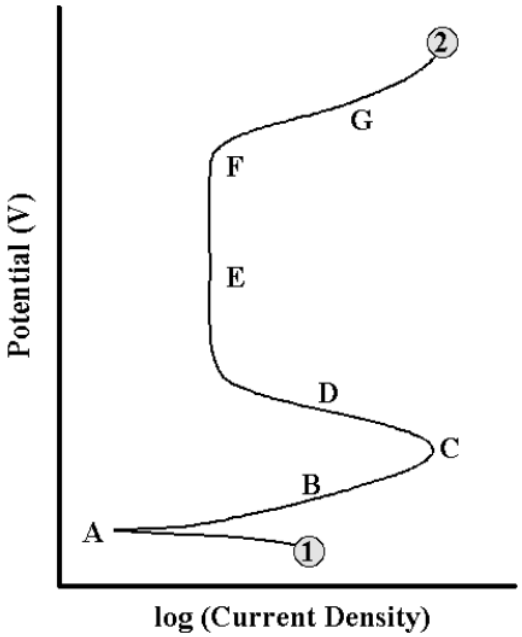

Fig. 1.10. Schematic anodic polarization scan (adapted from Enos and Scribner [82])

The region of interest for obtaining i_{corr}, E_{corr}, and Tafel lines is the near-open circuit potential. A ±250 mV range of potential around OCP is sufficient to allow the observation of a Tafel region[18]. **Fig. 1.11** shows a typical PPS plot in the OCP region, where it is possible to see the two dashed straight lines (Tafel lines) constructed tangent to the cathodic and anodic regions. The extrapolation of the Tafel line of the cathodic side to E_{corr} provides a measure of i_{corr}, used to calculate corrosion rate. The extrapolation of the line of the anodic side may not coincide with the intersection of the cathodic line with E_{corr}. This is a common phenomenon typically associated with roughening of the electrode (sample) surface or the formation of an oxide layer. Corrosion rate can be calculated by equation 1[83]

$$\boldsymbol{CR = \frac{i_{corr}.K.EW}{\rho}} \quad (1)$$

where,

CR - Corrosion rate (mm/year)

i_{corr} - Corrosion current (A)

K - Constant that defines the units for the corrosion rate (mm/A.cm.year)

EW - Equivalent weight - mass of sample that will react with one faraday of charge (g)

ρ - density (g/cm^3)

One interesting observation is that the calculation of corrosion rate is based on the current (flow of electrons) and equivalent weight (mass of sample that react with a unit of electron charge). Therefore, it must be pointed that this calculation is theoretical and is not an absolutely accurate representation of what is expected from a field service, but rather, a standardized approximation. In fact, all laboratory experiments are simulations of real life and this must be taken in consideration. A great effort has been done to correlate the results from different types of corrosion test to performance of coatings in real life service [84–86]. Nevertheless, it is important to highlight that accelerated tests are highly reliable and serve as a standardized means of comparison between samples and provides and approximate estimation for a real life environmental degradation.

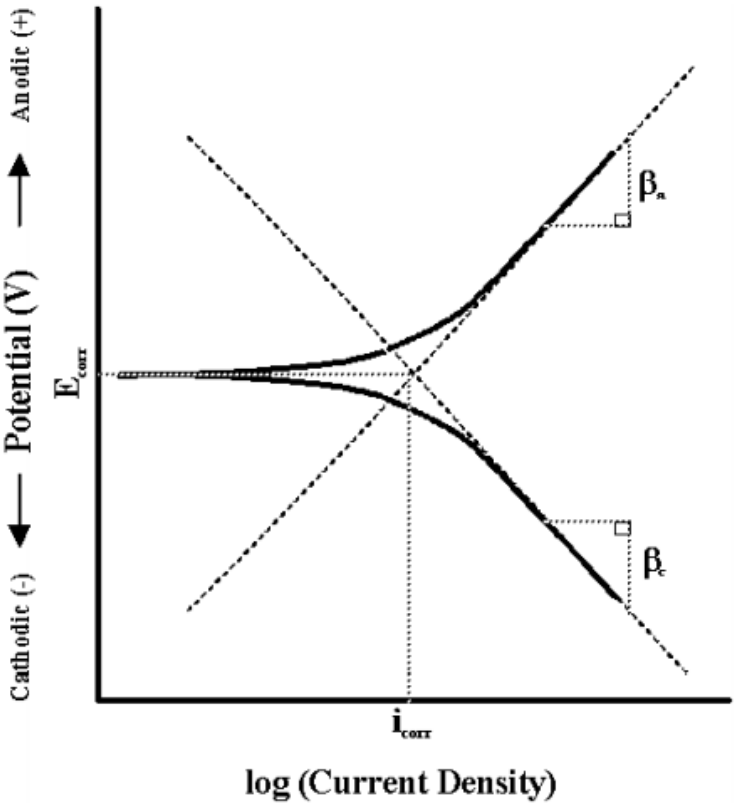

Fig. 1.11. Plot of potentiodynamic polarization scan with Tafel lines (adapted from [82])

Electrochemical experiments are, in fact, being largely used to evaluate the performance of the most varied types of coatings. For example, Al-Sabagh et al.[87] used PPS to study the electrochemical behavior of epoxy coatings with different thicknesses and also with varying concentration of ilmenite particles. Results revealed decrease in corrosion current with increasing concentration of particles. Caldona et al. [23] investigated the anti-corrosion performance of benzoxazine coatings on steel substrate after one day and seven days of immersion in NaCl solution. Results revealed improvement in performance with addition of silica particles, characterized by decrease in measured corrosion current. Gallegos-Melgar et al. [88] used PPS plots to investigate the anti-corrosion performance of an inorganic-organic film coating consisting on Al_2O_3/chitosan-sodium alginate. Qiu et al.[89] analyzed by PPS the influence of self-doped sulfonated polyaniline nanofibers on the anti-corrosion property of waterborne epoxy. Results revealed improvement in performance with incorporation of the fibers up to 1 wt%.

Other materials, such as metal alloys and ceramics, have also been investigated to their anticorrosion properties. Qiu et al. [90] investigated the influence of graphene oxide as a pore blocking agent for plasma electrolytic oxidation coating on magnesium substrates. Results indicate significant improvement in performance with the incorporation of the particles. Česánek and Schubert [91] categorize six metallic alloy based and cermet based coatings as to their corrosion resistance by PPS analysis. Wang and Frankel[92] used PPS to investigate the effect of trivalent chromium passivation treatment on aluminum rich coating as a means to prevent self-corrosion.

1.3.8. State of the art

Great effort has been invested in the direction of producing high performance, benzoxazine with a greener approach while maintaining high productivity. However, it is clear that not all properties have been fully achieved. Manoj et al., for example, synthesized a pyrazolidine-based benzoxazine, less hazardous than the Bisphenol-F derivatives, for anticorrosion coating purpose. Thermal stability was improved, corrosion rate was reduced and hydrophobicity increased with the latter property being assigned to increase in surface roughness. Synthesis was performed under ethanol, acetic acid and dioxane reflux. Purification was performed by recrystallization[93]. It

is evident that although the final product is indeed a safer material, the production process is not fully environmentally sustainable and the purification procedure does not achieve a high production rate. Caldona et al. produced high performance anticorrosion, anti-ice and superhydrophobic benzoxazine coatings. Monomers were synthesized under chloroform reflux and purified by NaOH solution and anhydrous sodium sulfate[23]. Zhang et al. produced a high performance biobased trifunctional benzoxazine with 64% char yield, T_{d10} of 403 °C and high fire resistance. Synthesis was performed under toluene reflux and product was purified by NaOH solution and recrystallization[94]. Salum et al. [25] produced biobased benzoxazine under solution in either ethyl acetate or ethanol. Purification was performed by recrystallization under ethyl acetate and ethanol. Zhang et al. [80] produced biobased benzoxazine under solution in toluene. Purification was performed by recrystallization under ethyl acetate and hexane. Resulting polymer presented interesting thermos-mechanical properties. However, toluene does not fulfill the requirements for green chemistry[81]. It is clear, then, that a comprehensive approach towards green chemistry of benzoxazine synthesis is lacking and only very punctual sections of the process have been considered. Although improvements in this sense have been achieved, further development is still possible and necessary to produce monomers safer to health and environment.

Furthermore, benzoxazine-epoxy blends have been widely studied with the objective of attaining higher thermomechanical properties through crosslinking and combination of the two monomers and their respective properties. Vaithilingam et al., for instance, produced biobased eugenol benzoxazine, the resulting material was then blended with epoxy and varying amounts of amine-functionalized carbon powder to produce anticorrosion coatings. Incorporation of epoxy and functionalized carbon increased glass transition temperature from 104°C to 203°C, where results were associated with higher crosslinking density. Contact angle also increased from 80° to 106°. Corrosion rate decreased by 100 times. Purification of benzoxazine monomers was performed by solvent extraction using chloroform and water-sodium hydroxide solution and dried over anhydrous sodium sulphate [95]. Zhou et al. incorporated benzoxazine to an epoxy resin to allow for thermal curing of the epoxy, where hydrophobicity and anticorrosion properties were improved. Contact angle shifted from 85° to 100°. Corrosion rate decreased by half. Synthesis of benzoxazine monomers was performed under chloroform reflux with no purification process mentioned[96]. Liu et al. produced a series of benzoxazine-epoxy thermosets with a bifunctional benzoxazine

monomer with high thermal conductivity phase separation caused by curing procedure and presence of imidazole. Additionally, T_g and T_{d10} of up to 216 and 334°C respectively were obtained. Synthesis of benzoxazine monomers was performed under dioxane reflux in the presence of trimethylamine. Purification by solvent extraction made use of dichloromethane and water followed by recrystallization under a mixture of ethanol and toluene[97].

References

[1] K. Gerhardus, N.G. Thompson, Y.P. Virmani, J.H. Payer, CORROSION COSTS AND PREVENTIVE STRATEGIES IN THE UNITED STATES, 2010.

[2] K. Gerhardus, V. Jeff, N. Thopson, O. Moghissi, M. Gould, J. Payer, International Measures of Prevention , Application , and Economics of Corrosion Technologies Study, (2006) 1–216.

[3] A.G. Roberts, Organic Coatings - Properties, Selection and Use, United States Department of Commerce, 1968.

[4] A. Verma, P. Negi, V.K. Singh, Experimental Analysis on Carbon Residuum Transformed Epoxy Resin: Chicken Feather Fiber Hybrid Composite, Polym. Compos. 40 (2019) 2690–2699. https://doi.org/10.1002/pc.25067.

[5] G.Z. Xiao, M.E.R. Shanahan, Water absorption and desorption in an epoxy resin with degradation, J. Polym. Sci. Part B Polym. Phys. 35 (1997) 2659–2670. https://doi.org/10.1002/(SICI)1099-0488(19971130)35:16<2659::AID-POLB9>3.0.CO;2-K.

[6] E.B. Caldona, A.C.C. De Leon, P.G. Thomas, D.F. Naylor, B.B. Pajarito, R.C. Advincula, Superhydrophobic Rubber-Modified Polybenzoxazine/SiO2Nanocomposite Coating with Anticorrosion, Anti-Ice, and Superoleophilicity Properties, Ind. Eng. Chem. Res. 56 (2017) 1485–1497. https://doi.org/10.1021/acs.iecr.6b04382.

[7] H. Ishida, Handbook of Benzoxazine Resins, 1st ed., Elsevier B.V., 2011. https://doi.org/10.1016/B978-0-444-53790-4.00046-1.

[8] H. Ishida, H.Y. Low, A study on the volumetric expansion of benzoxazine-based phenolic resin, Macromolecules. 30 (1997) 1099–1106. https://doi.org/10.1021/ma960539a.

[9] S. Rimdusit, W. Bangsen, P. Kasemsiri, Chemorheology and Thermomechanical Characteristics of Benzoxazine-Urethane Copolymers, J. Appl. Polym. Sci. 121 (2011) 3669–3678. https://doi.org/10.1002/app.34170.

[10] S. Rimdusit, P. Kunopast, I. Dueramae, Thermomechanical Properties of Arylamine-Based Benzoxazine Resins Alloyed With Epoxy Resin, Polym. Eng. Sci. 51 (2011) 1797–1807. https://doi.org/10.1002/pen.

[11] A. Overview, R.A. Dickie, F.L. Floyd, Polymeric Materials for Corrosion Control, (1986).

[12] R. Nixon, Coating selection and important properties of coatings for concrete, J. Prot. Coatings Linings. 19 (2002) 38–42.

[13] W.D. Callister Jr., Materials Science and Engineering - An Introduction, 7th ed., John Wiley & Sons, Inc., 1991. https://doi.org/10.1007/BF01184995.

[14] Michelin, An unknown object: the tire - materials, Thetiredigest. (n.d.). https://thetiredigest.michelin.com/an-unknown-object-the-tire-materials (accessed November 30, 2020).

[15] OSHA, OSHA Celebrates 40 years of accomplishments in the Workplace, (n.d.) 1–17. http://www.osha.gov/cranes-der...ks/index.html%0Ahttp://www.osha.gov/oilspills/index.html (accessed December 1, 2020).

[16] P. Anastas, N. Eghbali, Green Chemistry : Principles and Practice, R. Soc. Chem. 39 (2010) 301–312. https://doi.org/10.1039/b918763b.

[17] P.R. Roberge, Handbook of Corrosion Engineering, McGraw-Hill, 1999. https://linkinghub.elsevier.com/retrieve/pii/S0026057600834455.

[18] S.F. Bosen, W.A. Bowles, E.A. Ford, B.D. Perlson, Ullmann's Encyclopedia of Insudtrial Chemistry - Antifreezes, Weinheim: Wiley-VCH, 2000. https://doi.org/10.1002/14356007.a03.

[19] A.W. Peaboy, Control of Pipeline Corrosion, Anti-Corrosion Methods and Materials, 2001.

[20] D.E. Tallman, Æ.G. Spinks, Æ.A. Dominis, G.G. Wallace, Electroactive conducting polymers for corrosion control, (2002) 73–84. https://doi.org/10.1007/s100080100212.

[21] J.M. Sanchez-Amaya, R.M. Osuna, M. Bethencourt, F.J. Botana, Monitoring the degradation of a high solids epoxy coating by means of EIS and EN, Prog. Org. Coatings. 60 (2007) 248–254. https://doi.org/10.1016/j.porgcoat.2007.07.020.

[22] R.J. Gray, G. Incorporated, Paint and Coatings : a Mature Transition Industry, Science (80-.). 22 (1997) 203–245.

[23] T.A. Misev, R. Van Der Linde, Powder coatings technology: New developments at the turn of the century, Prog. Org. Coatings. 34 (1997) 160–168. https://doi.org/10.1016/S0300-9440(98)00029-0.

[24] A.G. Bailey, The science and technology of electrostatic powder spraying, transport and coating, J. Electrostat. 45 (1998) 85–120. https://doi.org/10.1016/S0304-3886(98)00049-7.

[25] F. Wang, J.Q. Hu, W.P. Tu, Study on microstructure of UV-curable polyurethane acrylate films, Prog. Org. Coatings. 62 (2008) 245–250. https://doi.org/10.1016/j.porgcoat.2007.12.005.

[26] J.H. Moon, Y.G. Shul, H.S. Han, S.Y. Hong, Y.S. Choi, H.T. Kim, A study on UV-curable adhesives for optical pick-up: I. Photo-initiator effects, Int. J. Adhes. Adhes. 25 (2005) 301–312. https://doi.org/10.1016/j.ijadhadh.2004.09.003.

[27] P.T. Elliott, J.E. Glass, WATER-BORN COATINGS, (n.d.). https://doi.org/10.1016/B978-008043417-9/50032-5.

[28] Allnex, allnex energy (UV/EB) curable resins technologies, (n.d.). https://allnex.com/en/technologies/energy-curable-resins?gclid=CjwKCAiAtej9BRAvEiwA0UAWXpfekpHnjR8eshpZqMm_Hn9F717NYok7oIWw8vi5rtl8u6ec2CcLYhoCedgQAvD_BwE.

[29] J. Parker, Organic Coatings for Industrial Projects, (2018). https://www.performance-painting.com/blog/organic-coatings-for-industrial-projects.

[30] F. Contu, S.R. Taylor, The Prediction of Long-term Coating Performance from Short-term Electrochemical Data, Part II. Comparison of Electrochemical Data to Field Exposure Results for Coatings on Steel, ECS Trans. 24 (2010) 197–209.

[31] G.S. Frankel, M. Rohwerder, Encyclopedia of Electrochemistry vol. 4 - Corrosion and Oxide Films, 2007. https://doi.org/10.1002/9783527610426.bard040007.

[32] C. Augustsson, Nm Epoxy Handbook, Third Edit, 2004.

[33] W.G. Ji, J.M. Hu, J.Q. Zhang, C.N. Cao, Reducing the water absorption in epoxy coatings by silane monomer incorporation, Corros. Sci. 48 (2006) 3731–3739. https://doi.org/10.1016/j.corsci.2006.02.005.

[34] Avantor, 5-Phenylisoxazole-3-carboxylic acid hydrazide Safety Data Sheet, 2019. https://us.vwr.com/assetsvc/asset/en_US/id/16490607/contents.

[35] S. Wattanasin, Succinic Anhydride Safety Data Sheet, 2020. https://doi.org/10.1002/047084289x.rs125.

[36] M.L. Salum, D. Iguchi, C.R. Arza, L. Han, H. Ishida, P. Froimowicz, Making Benzoxazines Greener: Design, Synthesis, and Polymerization of a Biobased Benzoxazine Fulfilling Two Principles of Green Chemistry, ACS Sustain. Chem. Eng. 6 (2018) 13096–13106. https://doi.org/10.1021/acssuschemeng.8b02641.

[37] H. Ishida, D.J. Allen, Physical and mechanical characterization of near-zero shrinkage polybenzoxazines, J. Polym. Sci. Part B Polym. Phys. 34 (1996) 1019–1030. https://doi.org/10.1002/(SICI)1099-0488(19960430)34:6<1019::AID-POLB1>3.0.CO;2-T.

[38] A. Kaewvilai, A.; Wattanathana, W.; Jongrungruangchok, S.; Veranitisagul, C.; Koonsaeng, N.; Laobuthee, 3,4-Dihydro-1,3− 2H-benzoxazines: Novel reducing agents through one electron donation mechanism and their application as the formation of nano-metallic silver coating., Mater. Chem. Phys. 167 (2015) 9−13.

[39] A. Vaithilingam, S.; Jayanthi, K. P.; Muthukaruppan, Synthesis and characterization of cardanol based fluorescent composite for optoelectronic and antimicrobial applications., Polym. J. 108 (2017) 449−461.

[40] N. Alper-Hayta, S.; Aki-Sener, E.; Tekiner-Gulbas, B.; Yildiz, I.; Temiz-Arpaci, O.; Yalcin, I.; Altanlar, Synthesis, antimicrobial activity and QSARs of new benzoxazine-3-ones., Eur. J. Med. Chem. 41 (2006) 1398−1404.

[41] P.L. Gupta, N.; Sharma, S.; Raina, A.; Dangroo, N. A.; Bhushan, S.; Sangwan, Synthesis and anti-proliferative evaluation of novel 3,4dihydro-2H-1,3-oxazine derivatives of bakuchiol., RSC Adv. 6 (2016) 106150−106159.

[42] P. Saini, Fundamentals of Conjugated Polymer Blends, Copolymers and Composites, Wiley, 2015. http://library1.nida.ac.th/termpaper6/sd/2554/19755.pdf.

[43] S. Kumar, C.P.R. Nair, Polybenzoxazines: Chemistry and Properties, Smithers Rapra Technology, 2010.

[44] S. Rimdusit, C. Jubsilp, S. Tiptipakorn, Alloys and Composites of Polybenzoxazines:Properties and Applications, Springer. (2013).

https://doi.org/10.1007/978-981-4451-76-5.

[45] Santhosh Kumar K. S., C.P.R. Nair, Polybenzoxazines: Chemistry and Properties, iSmithers Rapra Publishing, 2010.

[46] L.M. Schmidt, International Measures of Prevention, Application, and Economics of Corrosion Technologies Study, NACE Int. (2016) 1–216. http://impact.nace.org/documents/Nace-International-Report.pdf%0Apapers3://publication/uuid/9784056A-47E3-4988-8D70-B6763CF35EBF.

[47] L. Shi, J. Hu, X.D. Lin, L. Fang, F. Wu, J. Xie, F.M. Meng, A robust superhydrophobic PPS-PTFE/SiO2 composite coating on AZ31 Mg alloy with excellent wear and corrosion resistance properties, J. Alloys Compd. 721 (2017) 157–163. https://doi.org/10.1016/j.jallcom.2017.05.333.

[48] M. Conradi, A. Kocijan, D. Kek-Merl, M. Zorko, I. Verpoest, Mechanical and anticorrosion properties of nanosilica-filled epoxy-resin composite coatings, Appl. Surf. Sci. 292 (2014) 432–437. https://doi.org/10.1016/j.apsusc.2013.11.155.

[49] G.P. Guidetti, G.L. Rigosi, R. Marzola, The use of polypropylene in pipeline coatings, Prog. Org. Coatings. 27 (1996) 79–85. https://doi.org/10.1016/0300-9440(95)00523-4.

[50] Z.Ž. Lazarević, V.B. Mišković-Stanković, Z. Kačarević-Popović, D.M. Dražić, The study of corrosion stability of organic epoxy protective coatings on aluminium and modified aluminium surfaces, J. Braz. Chem. Soc. 16 (2005) 98–102. https://doi.org/10.1590/S0103-50532005000100015.

[51] B. Ramezanzadeh, S. Niroumandrad, A. Ahmadi, M. Mahdavian, M.H. Mohamadzadeh Moghadam, Enhancement of barrier and corrosion protection performance of an epoxy coating through wet transfer of amino functionalized graphene oxide, Corros. Sci. 103 (2016) 283–304. https://doi.org/10.1016/j.corsci.2015.11.033.

[52] M. Sangermano, G. Malucelli, E. Amerio, A. Priola, E. Billi, G. Rizza, Photopolymerization of epoxy coatings containing silica nanoparticles, Prog. Org. Coatings. 54 (2005) 134–138. https://doi.org/10.1016/j.porgcoat.2005.05.004.

[53] A. Talo, P. Passiniemi, S. Ylasaari, Polyaniline/Epoxy Coatings with Good Anti-Corrosion Properties, Synth. Met. 85 (1997) 1333–1334.

[54] M. Behzadnasab, S.M. Mirabedini, K. Kabiri, S. Jamali, Corrosion performance of epoxy coatings containing silane treated ZrO2 nanoparticles on mild steel in 3.5% NaCl solution, Corros. Sci. 53 (2011) 89–98. https://doi.org/10.1016/j.corsci.2010.09.026.

[55] A.P.O. Costa, A.E. Gerbase, C.L. Petzhold, Investigação da Cinética de Cura por Calorimetria Diferencial Exploratória (DSC) de Resinas Epóxi Preparadas a partir de Óleo de Soja Epoxidado com Diferentes Anidridos e Aminas Terciárias, Polímeros. 21 (2011) 146–150. https://doi.org/10.1590/s0104-14282011005000022.

[56] M.A. Boyle, C.J. Martin, J.D. Neuner, ASM HANDBOOK - Composites, ASM International, 2001.

[57] Research and Markets: Epoxy Resin Market - Trends & forecasts to 2019: Paints & Coating, Wind Turbine, Composites, Construction, Electrical & Electronics, Adhesives, (2014). https://www.businesswire.com/news/home/20140909005440/en/Research-Markets-Epoxy-Resin-Market---Trends.

[58] S. Kumar, S.K. Samal, S. Mohanty, S.K. Nayak, Toughening of Petroleum based (DGEBA) Epoxy Resins with various Renewable Resources based Flexible Chains for high performance Applications : A Review Toughening of Petroleum based (DGEBA) Epoxy Resins with various Renewable Resources based Flexible C, (2018). https://doi.org/10.1021/acs.iecr.7b04495.

[59] L.S. Penn, T.T. Chiao, Handbook of Composites, Van Nostrand Reinhold Company Inc, 1982. https://doi.org/10.1007/978-1-4615-7139-1.

[60] G. Das, N. Karak, Thermostable and flame retardant Mesua ferrea L. seed oil based non-halogenated epoxy resin/clay nanocomposites, Prog. Org. Coatings. 69 (2010) 495–503. https://doi.org/10.1016/j.porgcoat.2010.09.004.

[61] L.B. BOURNE, F.J. MILNER, K.B. ALBERMAN, Health problems of epoxy resins and amine-curing agents., Br. J. Ind. Med. 16 (1959) 81–97. https://doi.org/10.1136/oem.16.2.81.

[62] D. Lascano, L. Quiles-Carrillo, S. Torres-Giner, T. Boronat, N. Montanes, Optimization of the curing and post-curing conditions for the manufacturing of partially bio-based epoxy resins with improved toughness, Polymers (Basel). 11 (2019). https://doi.org/10.3390/polym11081354.

[63] A. Nagai, A. Takahashi, M. Wajima, K. Tsukanishi, The curing reaction and glass transition temperature of maleimide resin containing epoxy groups, Polym. J. 20 (1988) 125–130. https://doi.org/10.1295/polymj.20.125.

[64] W. Holly, C. Cope, Amines 1875, 2987 (1944).

[65] Q. Zhang, P. Yang, Y. Deng, C. Zhang, R. Zhu, Y. Gu, Effect of phenol on the synthesis of benzoxazine, RSC Adv. 5 (2015) 103203–103209. https://doi.org/10.1039/c5ra17395g.

[66] H. Ishida, PROCESS FOR PREPARATION OF BENZOXAZINE COMPOUNDS IN SOLVENTLESS SYSTEMS, 5,543,516, 1996.

[67] C. Burke, W. J.; Smith, R. P.; Weatherbee, N,N−Bis-(hydroxybenzyl)-amines: synthesis from phenols,formaldehyde and primary amines, J. Am. Chem. Soc. 74 (1952) 602–605.

[68] C.R.. W. Burke, W. J.; Hammer, Bis-m-oxazines from Hydroquinone, 26 (1961) 4403−4407.

[69] C.W.C. Burke, W. J.; Kolbenze, A. J.; Stephens, Condensation of Naphthols with Formaldehyde and Primary Amines, 74 (1952) 3601–3605.

[70] S. Nalakathu Kolanadiyil, M. Azechi, T. Endo, Synthesis of novel tri-benzoxazine and effect of phenolic nucleophiles on its ring-opening

polymerization, J. Polym. Sci. Part A Polym. Chem. 54 (2016) 2811–2819. https://doi.org/10.1002/pola.28167.

[71] C. Incorvia, (12) United States Patent, 2 (2015).

[72] S. Ohashi, K. Zhang, Q. Ran, C.R. Arza, P. Froimowicz, H. Ishida, Preparation of High Purity Samples , Effect of Purity on Properties , and FT-IR , Raman , 1 H and 13 C NMR , and DSC Data of Highly Purified Benzoxazine Monomers, Elsevier Inc., 2017. https://doi.org/10.1016/B978-0-12-804170-3.00049-4.

[73] Making Benzoxazines Greener - Ethanol-unlocked.pdf, (n.d.).

[74] Restek, Solvent Miscibility and Solubility, (2020). https://www.restek.com/techtips/Solvent-Miscibility-and-Solubility.

[75] S. Kirschbaum, K. Landfester, A. Taden, Synthesis and Thermal Curing of Benzoxazine Functionalized Polyurethanes, Macromolecules. 48 (2015) 3811–3816. https://doi.org/10.1021/acs.macromol.5b00954.

[76] M. Soto, M. Hiller, H. Oschkinat, K. Koschek, Multifunctional benzoxazines feature low polymerization temperature and diverse polymer structures, Polymers (Basel). 8 (2016) 1–14. https://doi.org/10.3390/polym8080278.

[77] C.X. Viet, Synthesis of Benzoxazine Monomer With Low Curing Temperature From Renewable Diphenolic Acid, Benzylamine and Paraformaldehyde, Vietnam J. Sci. Technol. 55 (2018) 63. https://doi.org/10.15625/2525-2518/55/1b/12092.

[78] C.J. Geankoplis, Transport Processes and Unit Operation, third, Prentice-Hall International, Inc., 2003.

[79] C. Lou, R. Zhang, X. Lu, C. Zhou, Z. Xin, Facile fabrication of epoxy/polybenzoxazine based superhydrophobic coating with enhanced corrosion resistance and high thermal stability, Colloids Surfaces A Physicochem. Eng. Asp. 562 (2019) 8–15. https://doi.org/10.1016/j.colsurfa.2018.10.066.

[80] L. Han, M.L. Salum, K. Zhang, P. Froimowicz, H. Ishida, Intrinsic self-initiating thermal ring-opening polymerization of 1,3-benzoxazines without the influence of impurities using very high purity crystals, J. Polym. Sci. Part A Polym. Chem. 55 (2017) 3434–3445. https://doi.org/10.1002/pola.28723.

[81] X. Ning, H. Ishida, Phenolic Materials via Ring- Opening Polymerization of Benzoxazines : Effect of Molecular Structure on Mechanical and Dynamic Mechanical Properties, J. Polym. Sci. Phys. 32 (1994) 1121–1129.

[82] R.N. Walters, R.E. Lyon, Molar group contributions to polymer flammability, J. Appl. Polym. Sci. 87 (2003) 548–563. https://doi.org/10.1002/app.11466.

[83] J. Kajornchaiyakul, C. Jubsilp, S. Rimdusit, Thermal and mechanical properties of highly-filled polybenzoxazine-alumina composites, Key Eng. Mater. 545 (2013) 211–215. https://doi.org/10.4028/www.scientific.net/KEM.545.211.

[84] A. Pengdam, S. Rimdusit, Preparation and Characterization of Highly Filled Graphite-Based Polybenzoxazine Composites, 22 (2012) 83–87.

[85] L.M. Parks, C. Mitter, P.K. Bose, , 1949 609, 9 (1949) 609–612.

[86] S.N. Kolanadiyil, M. Minami, T. Endo, Synthesis and Thermal Properties of Difunctional Benzoxazines with Attached Oxazine Ring at the Para -, Meta -, and Ortho -Position, (2017). https://doi.org/10.1021/acs.macromol.7b00487.

[87] D. Prat, A. Wells, J. Hayler, H. Sneddon, C.R. Mcelroy, S. Abou-shehada, P.J. Dunn, CHEM21 selection guide of classical- and less classical-solvents, Green Chem. (2016) 288–296. https://doi.org/10.1039/c5gc01008j.

[88] D.G. Enos, L.L. Scribner, The Potentiodynamic Polarization Scan, 1997.

[89] Gamry, Calculation of Corrosion Rate, (n.d.). https://www.gamry.com/Framework Help/HTML5 - Tripane - Audience A/framework_help.htm#EFM/Introduction/Calculation of Corrosion Rate.htm%3FTocPath%3DElectrochemical%2520Frequency%2520Modulation%7CIntroduction%2520to%2520Electrochemical%2520Frequency%2520Mo (accessed October 19, 2020).

[90] D. Ward, Ward, D. (2008, January 1). Correlation Of Accelerated Corrosion Testing With Natural Exposure After 6+ Years In A Coastal Environment. NACE International, in: NACE International, 2008: pp. 16–20.

[91] O. Knudsen, U. Steinsmo, M. Bjordal, S. Nijjer, Accelerated testing: Correlation between four accelerated tests and five years of offshore field testing, J. Prot. Coatings Linings. (2001) 52–56.

[92] E.L. Montgomery, L.M. Calle, J.C. Curran, M.R. Kolody, Timescale correlation between marine atmospheric exposure and accelerated corrosion testing, in: Corros. Conf., 2011.

[93] A.M. Al-Sabagh, M.I. Abdou, M.A. Migahed, S. Abd-Elwanees, A.M. Fadl, A. Deiab, Investigations using potentiodynamic polarization measurements, cure durability, ultra violet immovability and abrasion resistance of polyamine cured ilmenite epoxy coating for oil and gas storage steel tanks in petroleum sector, Egypt. J. Pet. 27 (2018) 415–425. https://doi.org/10.1016/j.ejpe.2017.07.006.

[94] A. Gallegos-Melgar, S.A. Serna, I. Lázaro, E.-J. Gutiérrez-Castañeda, V.H. Mercado-Lemus, H. Arcos-Gutierrez, M. Hernández-Hernández, J. Porcayo-Calderón, J. Mayen, M.D.A. Monroy, Potentiodynamic Polarization Performance of a Novel Composite Coating System of Al2O3/Chitosan-Sodium Alginate, Applied on an Aluminum AA6063 Alloy for Protection in a Chloride Ions Environment, Coatings. 10 (2019). https://doi.org/10.3390/coatings10010045.

[95] S. Qiu, C. Chen, M. Cui, W. Li, H. Zhao, L. Wang, Corrosion protection performance of waterborne epoxy coatings containing self-doped polyaniline nanofiber, Appl. Surf. Sci. 407 (2017) 213–222. https://doi.org/10.1016/j.apsusc.2017.02.142.

[96] Z. Qiu, R. Wang, J. Wu, Y. Zhang, Y. Qu, X. Wu, Graphene oxide as a corrosion-inhibitive coating on magnesium alloys, RSC Adv. 5 (2015) 44149–44159. https://doi.org/10.1039/c5ra05974g.

[97] Z. Česánek, J. Schubert, Potentiodynamic evaluation of corrosion resistant

coatings, Met. 2014 - 23rd Int. Conf. Metall. Mater. Conf. Proc. (2014) 940–945.

[98] X. Wang, G.S. Frankel, Protection mechanism of Al-rich epoxy primer on aluminum alloy 2024-T3, Corrosion. 73 (2017) 1192–1195. https://doi.org/10.5006/2526.

[99] M. Manoj, A. Kumaravel, R. Mangalam, P. Prabunathan, A. Hariharan, M. Alagar, Exploration of high corrosion resistance property of less hazardous pyrazolidine-based benzoxazines in comparison with bisphenol-F derivatives, J. Coatings Technol. Res. 17 (2020) 921–935. https://doi.org/10.1007/s11998-019-00312-4.

[100] K. Zhang, M. Han, Y. Liu, P. Froimowicz, Design and Synthesis of Bio-Based High-Performance Trioxazine Benzoxazine Resin via Natural Renewable Resources, ACS Sustain. Chem. Eng. 7 (2019) 9399–9407. https://doi.org/10.1021/acssuschemeng.9b00603.

[101] K. Zhang, Y. Liu, M. Han, P. Froimowicz, Smart and sustainable design of latent catalyst-containing benzoxazine-bio-resins and application studies, Green Chem. 22 (2020) 1209–1219. https://doi.org/10.1039/c9gc03504d.

[102] D. Prat, J. Hayler, A. Wells, A survey of solvent selection guides, Green Chem. 16 (2014) 4546–4551. https://doi.org/10.1039/c4gc01149j.

[103] S. Vaithilingam, R. ThangavelRavivarman, A. Muthukaruppan, Development of cashew nut shell carbon reinforced thiourea based biophenolic benzoxazine-epoxy composites: High performance biobased coating materials, Polym. Compos. 41 (2020) 1950–1961. https://doi.org/10.1002/pc.25510.

[104] C. Zhou, X. Lu, Z. Xin, J. Liu, Y. Zhang, Hydrophobic benzoxazine-cured epoxy coatings for corrosion protection, Prog. Org. Coatings. 76 (2013) 1178–1183. https://doi.org/10.1016/j.porgcoat.2013.03.013.

[105] Y. Liu, S. Gao, X. Gong, Q. Xue, Z. Lu, Benzoxazine-epoxy thermosets with smectic phase structures for high thermal conductive materials, Liq. Cryst. 46 (2019) 1686–1695. https://doi.org/10.1080/02678292.2019.1595755.

2. A Greener Approach to Trifunctional Benzoxazine and High Temperature Polybenzoxazine Materials

(Paper submitted to Reactive and Functional Polymers – Elsevier on Feb 25, 2021)

Abstract

Polybenzoxazines (PBZ), prepared from thermal ring-opening polymerization of benzoxazine monomers, are an important class of high temperature thermosets, which display a wide array of interesting and attractive properties. While typical monomers are based on mono- and difunctional derivatives, higher functional benzoxazines, prepared without using solvents, but purified with nontoxic solvents, are more desirable towards a greener synthesis of PBZ for high performance applications. In this work, we describe an environment-friendly approach to synthesizing a trifunctional benzoxazine from melamine, phenol, and paraformaldehyde via a solventless reaction and purifying the resulting monomer with benign and preferred solvents. The chemical structure of the synthesized benzoxazine was confirmed by spectroscopic analyses, while the polymerization was monitored by thermal analysis. Compared to its typical mono- and difunctional alternatives, the resulting trifunctional PBZ exhibited higher thermal stability and char yield. Combined with the importance of a trifunctional monomer, both the solventless synthesis and eco-friendly purification route will enable an environmentally-sound approach towards PBZ and its many useful applications.

Keywords: trifunctional benzoxazine; polybenzoxazine; green chemistry; thermosets; polymer synthesis; high temperature

2.1. Introduction

Polybenzoxazines (PBZ) are a relatively new class of phenolic polymeric materials derived from thermally-activated ring-opening polymerization of heterocyclic benzoxazine monomers without inclusion of any catalysts or initiators [1,2]. They have been used as high-performance thermosetting materials for a wide range of composite, dielectric, and coating applications [1,3–8] due to their high tensile strength, high thermal stability, electrical insulation, resistance to chemicals and UV, dimensional stability during curing, and even lower surface energy than polytetrafluoroethylene (PTFE) [1,2,9,10], while their monomeric precursor, benzoxazines, have been employed as reducing agents [11], optoelectronic material precursors [12], antimicrobial materials [13], therapeutic drug agents [14], and modifiers for other thermosetting resins [15]. The six-membered heterocyclic oxazine is molecularly distorted and possesses ring strain that provides some driving force for the ring-opening process. However, this strain is marginal and compared to other thermosetting resins [2], higher temperatures are required for benzoxazine polymerization to proceed. It is noteworthy that heating simply speeds up the polymerization rate as synthesized benzoxazine monomers usually contain low cationic phenolic and oligomeric impurities that serve as initiators during the curing process [2].

The earliest reports on benzoxazine monomer preparation date back to the 1940s by Holly and Cope [16] and 1950s by Burke *et al.* [17–19], involving the condensation reaction between three primary precursors–phenolic derivative, amine, and formaldehyde, all of which have become the foundation for the current syntheses of cost-effective benzoxazines with varying molecular geometries and network architectures. Indeed, molecular design flexibility [2] is one of the most interesting features of benzoxazines, which results from the utility of a wide range of different phenolic and amine precursors. This structural flexibility affords a tailor-made PBZ exhibiting, not only physically and chemically tuned properties, but also multifunctionality. Ning and Ishida [20] used bisphenols to synthesize a series of benzoxazines, the polymerization of which resulted in crosslinked difunctional PBZs with mechanical strength, thermal stability, and molecular weights higher than any typical monofunctional alternatives. Thereafter, numerous amines and phenolic compounds of varying degrees of functionality have been used to synthesize multifunctional benzoxazines (i.e. with ≥ 2 oxazine rings) [21–25]. Kolanadiyil *et al.*

[21] used a triphenol to synthesize a trifunctional benzoxazine with lower curing temperature and PBZ with higher thermal stability. Zhang et al. [22] synthesized a series of trifunctional benzoxazines from resveratrol and different amines resulting in PBZs with high thermal stability and flame retardancy. Feng et al. [23] prepared a series of tetrafunctional benzoxazines using a tetraphenol fluorene and mixed amines, and the resulting PBZs showed higher glass transition temperature and crosslinking density compared to their difunctional analogues. Wang et al. [24] also prepared a highly thermally stable tetrafunctional PBZ from a fluorene-based, furan-containing benzoxazine synthesized using a bisphenol- and diamine-containing precursor. Furthermore, Sini et al. [25] synthesized a series of multifunctional benzoxazines and found that lower curing temperatures, minimal weight losses during curing, and higher PBZ thermal stability can be achieved with increasing number of oxazine rings.

Development of high performance materials via green approaches has also been the subject of many current scientific researches [26–28]. While PBZs have been acknowledged as viable alternatives to other popularly-known thermosetting resins, achieving high performance alongside Green Chemistry preparation for benzoxazines still remains a challenge. Many benzoxazines commonly reported in the literature were synthesized and/or purified using solvents [27] classified as toxic and undesirable based on the Principles of Green Chemistry. According to Anastas and Warner [29], to the extent possible, Green Chemistry should be taken seriously throughout the entire process of development and fabrication. It is interesting to note that benzoxazine monomers can be readily prepared in solventless systems when at least one of the precursors is liquid at room temperature [2,30]. Ishida [30] pointed out that in the event where all the three precursors are solid, they may be combined and heated until they melt and become liquid, or one of the reactants may be first melted and then combined with the other two. While these solventless syntheses eliminate the use of extra or undesirable reagents, the purification step should still be performed using less toxic and less hazardous solvents.

Herein, we report the solventless synthesis of a trifunctional benzoxazine from melamine, phenol, and paraformaldehyde, and highlight the greener purification approach involved. To the best of our knowledge, there are only a few studies emphasizing the greener approach towards melamine-based trifunctional benzoxazines. Likewise, not much have been reported overall on the greener synthetic and purification routes for benzoxazine monomers. In this work, we highlight, not only the

trifunctionality advantage of our synthesized PBZ, but also demonstrate that our benzoxazine preparation has fulfilled some Principles of Green Chemistry. Furthermore, these PBZs are expected to have high temperature stability as a thermoset.

2.2. Materials and methods

2.2.1. Materials

Phenol (99%), melamine (99%), and paraformaldehyde (purity ≥ 95%) were purchased from Merck KGaA, Alfa Aesar, and J. T. Baker, respectively. Chloroform (HPLC Grade) and sodium hydroxide (NaOH) pellets were obtained from Fisher Scientific. Methyl ethyl ketone (MEK, ACS grade) was purchased from Sigma-Aldrich. All chemicals were used as received.

2.2.2. Synthesis of benzoxazine monomer

The trifunctional benzoxazine (TBZ) monomer was prepared by reacting phenol, paraformaldehyde, and melamine using a solventless method. Two distinct molar ratios, 3:6:1 (stoichiometric) and 6:6:1, were also used to study the reactant consumption and optimization. The reactant mixture from each ratio was magnetically stirred at 50-60 °C for 1 h in order to allow for a complete melting and dissolution of the solid reagents. Subsequently, the mixture was heated to 95-100 °C at different reaction times (i.e. 1, 2, 4.5, 9.5, 19.5, and 44 h) to evaluate the effect on the product yield, followed by cooling naturally to room temperature. Steps of reaction time were selected in such way to allow for a reasonably power law distribution as the chemical reactions rates tend to follow such function with time due to reagent consumption and increase in product concentration and viscosity, as is the case, for example, of bulk polymerization. The resultant crude TBZ monomer was then purified using two different liquid-liquid extraction procedures to investigate, not only the efficiency, but also the utility of safer solvents and simple purification steps: dissolution of the monomer in (1) procedure #1 - chloroform, washing with 1 N NaOH solution for several times, and rinsing with deionized water until neutral; (2) procedure #2 - methyl ethyl ketone (MEK) and washing with deionized water for several times. Finally, the

samples were dried in a rotatory evaporator to remove the solvents used during the purification process.

2.2.3. Characterization

Fourier transform infrared (ATR-FTIR) spectroscopy was done with a Cary 600 Series FTIR spectrometer (Agilent Technologies), with each spectrum recorded at an average of 128 scans at a nominal spectral resolution of 2 cm^{-1}. Proton nuclear magnetic resonance (^{1}H-NMR) spectra were acquired using a Varian Oxford AS600 at a proton frequency of 600 MHz. The average number of transients for ^{1}H measurement was 64, while a relaxation time of 10 s was used for the integrated intensity determination of the spectra. Differential scanning calorimetry (DSC) and thermogravimetric analysis (TGA) were performed using a DSC 2920 differential scanning calorimeter and TGA Q500 thermogravimetric analyzer (TA Instruments), respectively, both on a N_2 gas purge at 50 mL min^{-1} and ramp rate of 10 °C min^{-1}.

2.3. Results and discussion

2.3.1. Reaction times and ratios

The reaction involving the synthesis of benzoxazine monomers can be generally summarized in three steps (**Fig. 2.1**) [2]: (1) amine quickly reacts with formaldehyde resulting in an amine-formaldehyde intermediate, (2) which reacts with phenol at its *ortho* position forming a Mannich base; (3) oxazine ring is then formed between the Mannich base and formaldehyde through a dehydration reaction.

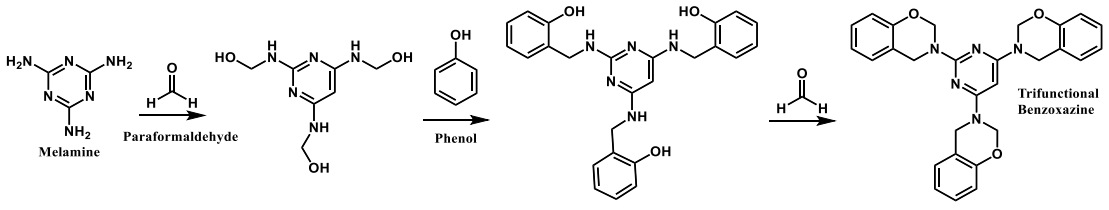

Fig. 2.1. Synthesis of the trifunctional benzoxazine (TBZ) from melamine, paraformaldehyde, and phenol.

Two different reaction ratios were used in the synthesis of TBZ and compared to investigate the extent of reaction between the three precursors (i.e. phenol,

paraformaldehyde, and melamine). For the stoichiometric ratio 3:6:1, rapid formation of a white, but infusible solid product was observed (**Fig. S 1**) possibly containing unreacted melamine and formaldehyde, which cannot be further dissolved by the given amount of phenol. This result suggests that such reaction is unlikely to continue and further go to completion. On the other hand, an increased amount of phenol, as in the case of the 6:6:1 ratio, resulted in a homogeneous mixing with lower viscosity reaction mixture, furthering reaction steps 2 and 3 outlined in **Fig. 2.1**. The progress of the dissolution process is given in **Fig. S 2**, where the initially solid reactant mixture was observed to gradually transform into a white and fairly transparent liquid as the reaction was allowed to proceed correspondingly from 0 to 70 min at 50-60 °C. Further, the temperature was increased to 95-100 °C and samples were qualitatively examined after 1, 2, 4.5, 9.5, 19.5 and 44 h of continuous reaction to evaluate the progress. As shown in **Fig. S 3**, the reaction mixture changed from a low-viscosity clear liquid after 1 h to a high-viscosity white paste after 9.5 and 19.5 h. On the other hand, hard and brittle products are obtained for extended reaction times (e.g. 44 h). This transformation indicates that a reaction is indeed occurring and highlights the influence of reaction duration on yield. Finally, two procedures for purification, procedure #1 and procedure #2, were used to compare the effectiveness of a commonly applied procedure with a proposed process, which makes use of greener solvents.

2.3.2. ^{1}H-NMR experiments

Characterization by ^{1}H-NMR was used to differentiate the results of the various reaction times and purification procedures, confirm the chemical structure of the desired product, and ascertain the presence of impurities or by-products. To begin with, **Fig. 2.2** shows the ^{1}H-NMR of TBZ sample reacted for 9.5 h and purified by procedure #1. The peak at 5.71 ppm is assigned to O-CH_2-N and the shift at 5.00 ppm is assigned to Ar-CH_2-N, indicating the formation of the oxazine ring [31]. By peak integration, the peak at 4.58 was assigned to the bridging methylene groups from oligomerization. Overlapping peaks at around 7.0 ppm represented by “c, d, e, f” are assigned to protons in the aromatic ring of the benzoxazine group and melamine ring [31].

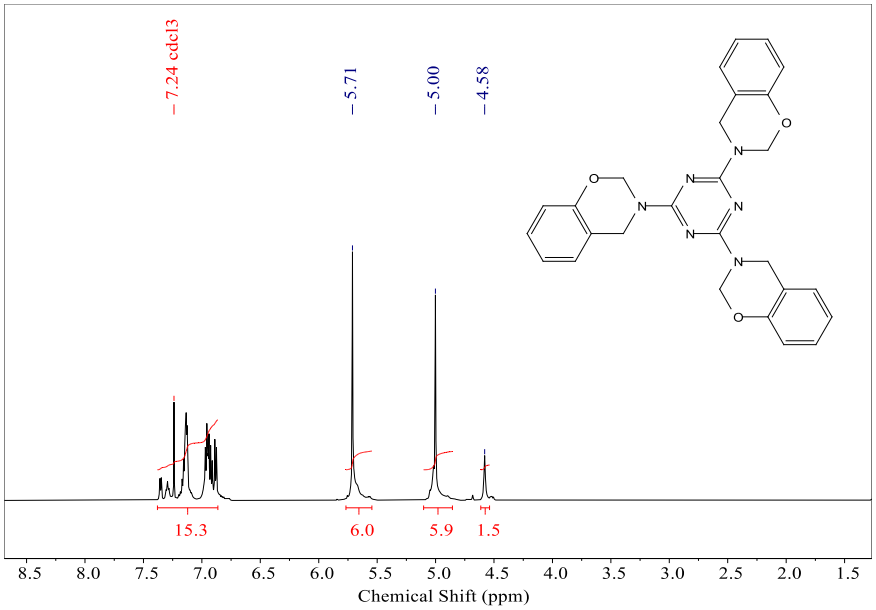

Fig. 2.2. ^{1}H-NMR of TBZ (purified by procedure #1) obtained after 9.5 h reaction time.

In comparison, **Fig. S 4** shows ^{1}H-NMR spectrum of TBZ sample of 9.5 h synthesis time purified using procedure #2. The presence of benzoxazine monomers was verified by the peaks at 5.68 and 4.98 ppm. Additionally, the peaks at 7.0 ppm represent the aromatic rings of the benzoxazine monomer. Similar to procedure #1, (**Fig. 2.2**), it is possible to observe the presence of oligomers, identified by the peak at 4.71 ppm. Additional peaks can be observed and are associated with residual reagents, pre-monomers or monomers that have started the process of polymerization, as described in **Table S 1**. One of the synthesis' steps is the initial reaction between formaldehyde and amine, which creates a sub-product as observed at 3.47 ppm. As previously explained, polymerization of benzoxazine occurs by opening of the oxazine ring. In this process, a methyl group is formed, giving rise to the 2.99 ppm shift.

From these data, it can be inferred that procedure #2, was less effective in removing impurities from the product than procedure #1. This may be confirmed by the low solubility of such chemical products in water as previously cited [32]. Phenol could not be identified in the spectrum due to overlap with the aromatic rings present in the monomer structure. In addition, solubility of phenol in water is significantly higher than that of the other reagents and is affected by the basic media. It is interesting to observe that procedure #2 was not capable of eliminating pre-monomers, compared to procedure #1.

Fig. S 5 shows ^{1}H-NMR spectrum of sample at 44 h synthesis time purified using procedure #2. Once again, it is possible to confirm the presence of benzoxazine monomers by the peaks at 5.68 and 4.98 ppm. Interestingly, the chemical shift and integration are highly similar when compared to all previous results (other polymerization times). This indicates consistency on the process of formation of oxazine for all reaction times.

2.3.3. FTIR spectroscopy

Fig. 2.3a shows the FTIR spectra of the (1) benzoxazine monomer product obtained after 44 h of reaction time and purified by procedure #1 and starting materials (2) phenol, (3) melamine and (4) paraformaldehyde. The spectrum for paraformaldehyde shows peaks at 2924 cm^{-1} and 904 cm^{-1}, which are assigned to the CH_2 asymmetric stretch and C-O stretch of the aliphatic ether [33], respectively. The spectrum for melamine shows peaks at 3467, 3417, 3323, and 3120 cm^{-1}, all of which can be assigned to $–NH_2$ [34]. The phenol spectrum shows a characteristic broad peak at 3344 cm^{-1}, assigned to OH stretch, and band at 1365 cm^{-1}, assigned to OH in-plane bend [35]. It can be observed that none of the peaks from the reactant spectra are present in the benzoxazine spectrum. This result suggests that a reaction has occurred after 44 h and the purification procedure #1 was effective. In addition, a likely side product of this reaction, melamine-formaldehyde resin containing OH and secondary amine groups [34], is not observed in the benzoxazine spectrum.

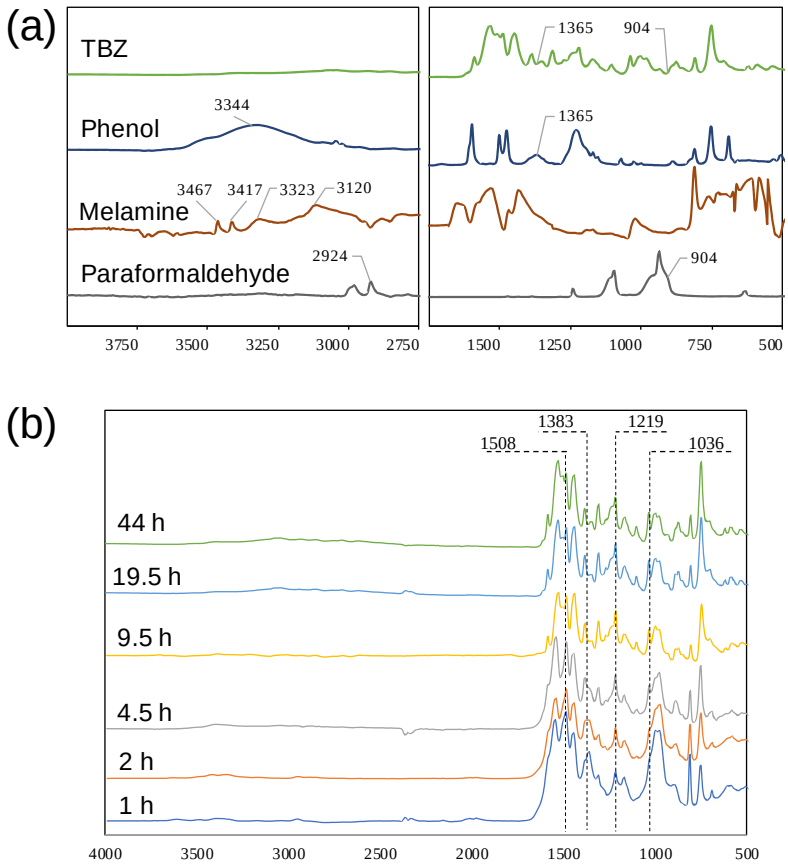

Fig. 2.3. FTIR spectra of (a) TBZ (44 h reaction time and purified by procedure #1), phenol, melamine, and paraformaldehyde, and (b) TBZ obtained at different reaction times (purified by procedure #1).

Furthermore, the reaction was also monitored as function of time. **Fig. 2.3b** shows the FTIR spectra of the monomer products obtained at different reaction times. All spectra were normalized per peak at 1219 cm^{-1} as a reference of completion of the oxazine ring. In all these spectra, the following benzoxazine peaks were found [36]: 1036 cm^{-1} (Ar-O-C symmetric stretch), 1000-1300 cm^{-1} (C-O stretch), 1219 cm^{-1} (C-O-C asymmetric stretching), 1383 cm^{-1}(oxazine ring), and 1508 cm^{-1} (*ortho*-substituted benzene ring). It is interesting to note that the peak at 1508 cm^{-1} is less intense in the spectra taken after 1, 2, and 4.5 h of reaction times. This result indicates that the formation of benzoxazine is still occurring at these early reaction times. But by 9.5 h and higher they begin to diminish indicating the conversion to polymer – crosslinking to form the PBZ thermoset.

2.3.4. Reaction yield

Fig. 2.4a shows the yield versus reaction time plot for the benzoxazine product purified by procedure #1 based on gravimetric determination. It can be seen that the data points for the yield obtained experimentally fit well to a power law equation (R^2 = 0.92). The experimental data corresponding to **Fig. 2.4a** are tabulated in **Table S 3**.

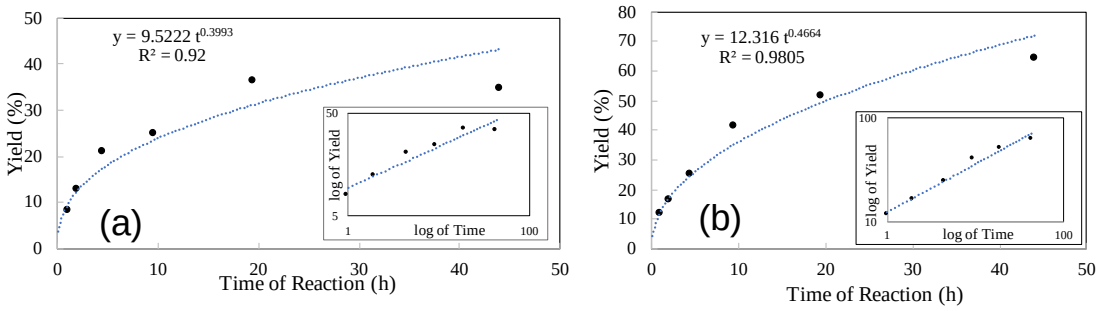

Fig. 2.4 Yield vs. reaction time graphs for TBZ purified by (a) procedure #1 and (b) procedure #2.

Clearly, the yield increases as a power law function of time, with high and low derivatives at short and longer times, respectively. The determination of optimum reaction time is based on the yield rate (i.e. yield/time). Lower reaction time is practical for any large scale production as it should indicate lower energy cost according to the sixth Principle of Green Chemistry (see section 1.3.6, page 43). Higher yield is directly associated with production efficiency, while longer reaction times result in a small yield rate increase. Thus, in **Table S 3**, 4.5 h is considered as the optimum reaction time as the corresponding relative yield (yield at a specific temperature divided by maximum yield) was nearly 60% and longer reaction times further result in lower yield rates. Hence, reaction times longer than 4.5 h can be identified as less efficient as it results in small yield improvement.

Fig. 2.4b shows the yield versus reaction time plot for the benzoxazine product purified by procedure #2, which seems to promote higher yield when compared to those for procedure #1.

Table S 4 reveals yield > 60% for 44 h reaction time. However, this result may be misleading as ^{1}H-NMR analysis showed considerable amounts of impurities in the product. These impurities (incomplete benzoxazine formation and pre-polymerization products) are hard to isolate and separate from the pure benzoxazine unlike in procedure #1. Consequently, this yield does not totally refer to the pure benzoxazine yield. In addition, 9.5 h is considered as the optimum reaction time as the corresponding relative yield was above 60%. Interestingly, both optimum reaction times in **Table S 3** and

Table S 4 had approximately the same relative yield, implying that the reaction rate for the benzoxazine synthesis decreases rapidly after around 60% yield has been

achieved. Overall, we considered 9.5 h as the optimum reaction time, while procedure #1 as the preferred purification process.

2.3.5. DSC study

The polymerization of TBZ was monitored by DSC and the resulting thermogram, shown in **Fig. 2.5a,** exhibits an exothermic peak with onset and maximum power release at 314 and 342 °C, respectively, which is associated with the crosslinking or curing process. For the definition of the curing procedure, the onset was designated as the temperature for cure with the purpose of promoting polymerization at the lowest temperature possible. The curing time is calculated based on the total energy released by the system during the whole process and the power released at the onset. The total energy is obtained by integrating the area below the curve, which is found to be 750 mJ, while the power is the difference between the measured power values at the onset (0.843 mW) and baseline (0 mW). Upon calculation, the curing time at 314 °C was found to be roughly 15 min.

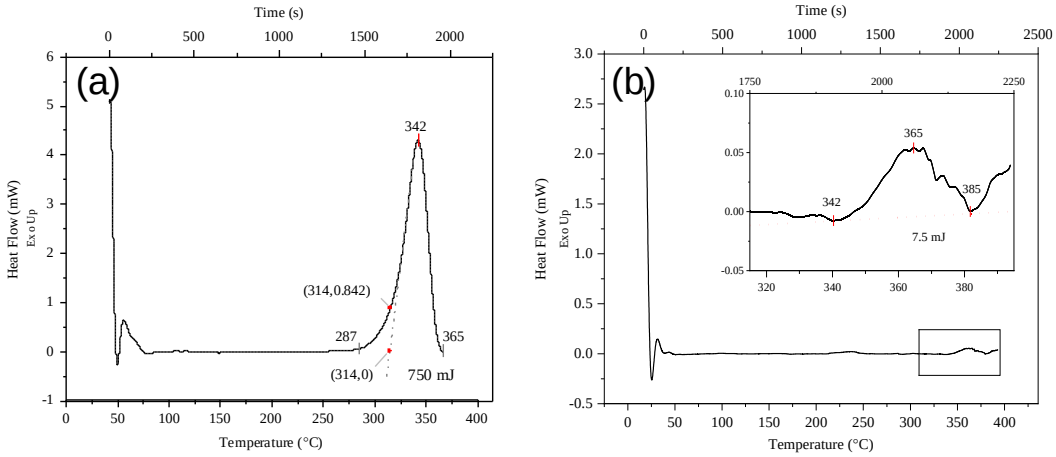

Fig. 2.5. DSC thermograms of (a) TBZ from room temperature to 370 °C, where the exothermic peak at 342 °C indicates the curing process and (b) cured TBZ from room temperature to 400 °C, where the peak at 365 °C is attributed to residual polymerization.

The DSC thermogram in **Fig. 2.5b** also indicates that the obtained TBZ monomer exhibits high purity. According to the literature [2], higher benzoxazine purity requires higher curing temperature. This phenomenon is associated with the presence of impurities (i.e. phenols and oligomers), which act as catalysts for oxazine ring opening [37,38]. Additionally, it is interesting to note that the melting peak is absent in the thermogram, which indicates the amorphous structure of the synthesized TBZ

monomers. Such phenomenon is possibly caused by the presence of marginal amounts of impurity, which hinder the formation of highly organized crystalline structures, as confirmed by the ^{1}H-NMR results (**Fig. 2.2**). Ohashi *et al.* [38] showed the formation of benzoxazine crystals and presence of melting peak for products purified by column chromatography. Ishida *et al.* [2] confirmed that increasing purification effectiveness shifts the curing peak to higher temperatures.

A second DSC run (**Fig. 2.5b**) was performed from room temperature to 370 °C at 10 °C min^{-1} ramp rate to determine the presence of any possible residual curing event. A small onset peak can be observed at 342 °C, while the maximum at 365 °C. Peak integration shows a 7.5 mJ of energy released, which represents 1% of the total energy released upon complete curing in **Fig. 2.5a**. This result indicates that the proposed curing process is highly effective and that crosslinking is complete.

2.3.6. Thermal stability study

Fig. 2.6a displays the DSC thermogram of the cured TBZ between room temperature and 300°C. A slight depression indicating an endothermic reaction centered at 95 °C can be observed. This peak indicates the glass transition temperature (T_g) and is a typical signature for thermosets like PBZ as it broadly runs from 70 and 130 °C.

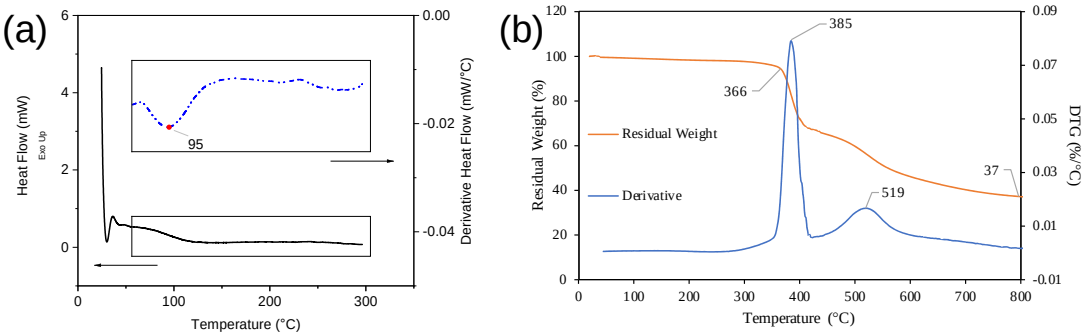

Fig. 2.6. (a) DSC thermogram of poly-TBZ with T_g = 95 °C. (b) TGA curve of poly-TBZ.

The thermal degradation of PBZs, in general, is a multi-step process [39]. **Fig. 2.6b** shows the TGA curve for poly-TBZ, which can be divided into a number of regions or steps [40,41]. The first major onset temperature at 366 °C is associated with amine degradation products resulting from the breakdown of the Mannich bridge and some weight loss related to some small and side chains [42]. The second and succeeding

higher onset temperatures at 400 and peak at 519 °C are associated with weight losses due to the scission of phenolic (free hydroxyl species) and aliphatic C-C bonds. Overall, poly-TBZ is more thermally stable compared to its mono- and difunctional analogues [20,25,42], owing to its trifunctionality and many hydrogen bonding networks.

2.4. Conclusions

A TBZ monomer was successfully synthesized from melamine, paraformaldehyde, and phenol in a one-pot, solventless process, with the reaction performed at various times to maximize the product yield. The resulting monomer product was purified using two different purification procedures and results showed that impurities were indeed present on both procedures, but much less with procedure #1. Procedure #2 showed to be highly promising with interesting results upon investigation of yield. The chemical structure of the synthesized TBZ was characterized by ^{1}H-NMR, which revealed small amounts of oligomers and impurities, and FTIR spectroscopy, which confirmed the presence of signature functional groups of the monomer in all reaction times. The DSC and TGA experiments, on the other hand, revealed a thermosetting PBZ product with a T_g of 95 °C, high thermal stability of up to 366 °C, and a high char yield of 37% at 800 °C. Finally, we were able to demonstrate that our TBZ preparation has satisfied a few Principles of Green Chemistry by (1) using safer solid starting materials for easy handling, (2) using solventless synthetic method, which reduces the use of solvents and thus, minimizes waste, (3) using more benign solvents in the purification process, (4) tuning the reactant ratio and reaction times to optimize the product yield, and (5) realizing that the monomer product itself is intrinsically stable, as it requires high temperatures for polymerization.

Acknowledgements

This work was supported by Coordenação de Aperfeiçoamento de Pessoal de Nível Superior - Brasil (CAPES) - Finance Code 001. Work (or Part of this work) was conducted by ORNL's Center for Nanophase Materials Sciences, which is a US Department of Energy Office of Science User Facility. The funding sources had no involvement in the design, production or decision to submit this article for publication.

References

[1] N. Ghosh, B. Kiskan, Y. Yagci, Polybenzoxazines—new high performance thermosetting resins: synthesis and properties, Prog. Polym. Sci. 32 (2007) 1344–1391.

[2] H. Ishida, T. Agag, Handbook of benzoxazine resins, Elsevier, 2011.

[3] S. Rimdusit, C. Jubsilp, S. Tiptipakorn, Alloys and composites of polybenzoxazines, Springer, 2013.

[4] B. Kiskan, N.N. Ghosh, Y. Yagci, Polybenzoxazine-based composites as high-performance materials, Polym. Int. 60 (2011) 167–177.

[5] E.B. Caldona, A.C.C. De Leon, P.G. Thomas, D.F. Naylor III, B.B. Pajarito, R.C. Advincula, Superhydrophobic Rubber-Modified Polybenzoxazine/SiO2 Nanocomposite Coating with Anticorrosion, Anti-Ice, and Superoleophilicity Properties, Ind. Eng. Chem. Res. 56 (2017) 1485–1497.

[6] E.B. Caldona, C. Al Christopher, J.D. Mangadlao, K.J.A. Lim, B.B. Pajarito, R.C. Advincula, On the enhanced corrosion resistance of elastomer-modified polybenzoxazine/graphene oxide nanocomposite coatings, React. Funct. Polym. 123 (2018) 10–19.

[7] E.B. Caldona, C. Al Christopher, B.B. Pajarito, R.C. Advincula, Novel anti-corrosion coatings from rubber-modified polybenzoxazine-based polyaniline composites, Appl. Surf. Sci. 422 (2017) 162–171.

[8] E.B. Caldona, A.C.C. De Leon, B.B. Pajarito, R.C. Advincula, A Review on Rubber-Enhanced Polymeric Materials, Polym. Rev. 57 (2017) 311–338.

[9] H. Ishida, H.Y. Low, A study on the volumetric expansion of benzoxazine-based phenolic resin, Macromolecules. 30 (1997) 1099–1106.

[10] H. Ishida, D.J. Allen, Physical and mechanical characterization of near-zero shrinkage polybenzoxazines, J. Polym. Sci. Part B Polym. Phys. 34 (1996) 1019–1030.

[11] A. Kaewvilai, W. Wattanathana, S. Jongrungruangchok, C. Veranitisagul, N. Koonsaeng, A. Laobuthee, 3, 4-Dihydro-1, 3-2H-benzoxazines: Novel reducing agents through one electron donation mechanism and their application as the formation of nano-metallic silver coating, Mater. Chem. Phys. 167 (2015) 9–13.

[12] S. Vaithilingam, K. Jayanthi, A. Muthukaruppan, Synthesis and characterization of cardanol based fluorescent composite for optoelectronic and antimicrobial applications, Polymer. 108 (2017) 449–461.

[13] S. Alper-Hayta, E. Akı-Sener, B. Tekiner-Gulbas, I. Yıldız, O. Temiz-Arpacı, I. Yalcın, N. Altanlar, Synthesis, antimicrobial activity and QSARs of new benzoxazine-3-ones, Eur. J. Med. Chem. 41 (2006) 1398–1404.

[14] N. Gupta, S. Sharma, A. Raina, N.A. Dangroo, S. Bhushan, P.L. Sangwan, Synthesis and anti-proliferative evaluation of novel 3, 4-dihydro-2 H-1, 3-oxazine derivatives of bakuchiol, RSC Adv. 6 (2016) 106150–106159.

[15] T. Chaisuwan, H. Ishida, High-performance maleimide and nitrile-functionalized benzoxazines with good processibility for advanced composites applications, J. Appl. Polym. Sci. 101 (2006) 548–558.

[16] F.W. Holly, A.C. Cope, Condensation products of aldehydes and ketones with o-aminobenzyl alcohol and o-hydroxybenzylamine, J. Am. Chem. Soc. 66 (1944) 1875–1879.

[17] W. Burke, R.P. Smith, C. Weatherbee, N, N-bis-(hydroxybenzyl)-amines: synthesis from phenols, formaldehyde and primary amines1, J. Am. Chem. Soc. 74 (1952) 602–605.
[18] W. Burke, M.J. Kolbezen, C.W. Stephens, Condensation of naphthols with formaldehyde and primary amines1, J. Am. Chem. Soc. 74 (1952) 3601–3605.
[19] W. Burke, C.R. HAMMER, C. WEATHERBEE, Bis-m-oxazines from Hydroquinone1, J. Org. Chem. 26 (1961) 4403–4407.
[20] X. Ning, H. Ishida, Phenolic materials via ring-opening polymerization: Synthesis and characterization of bisphenol-A based benzoxazines and their polymers, J. Polym. Sci. Part Polym. Chem. 32 (1994) 1121–1129.
[21] S.N. Kolanadiyil, M. Minami, T. Endo, Synthesis and thermal properties of difunctional benzoxazines with attached oxazine ring at the para-, meta-, and ortho-position, Macromolecules. 50 (2017) 3476–3488.
[22] K. Zhang, M. Han, L. Han, H. Ishida, Resveratrol-based tri-functional benzoxazines: Synthesis, characterization, polymerization, and thermal and flame retardant properties, Eur. Polym. J. 116 (2019) 526–533.
[23] T. Feng, J. Wang, L. Pan, M. Derradji, N. Ramdani, W. Liu, H. Zhou, Tunable properties of novel tetra-functional fluorene-based benzoxazines from mixed amines: Synthesis, characterization and curing kinetics, Thermochim. Acta. 633 (2016) 1–11.
[24] H. Wang, J. Wang, X. He, T. Feng, N. Ramdani, M. Luan, W. Liu, X. Xu, Synthesis of novel furan-containing tetrafunctional fluorene-based benzoxazine monomer and its high performance thermoset, RSC Adv. 4 (2014) 64798–64801.
[25] N. Sini, T. Endo, Toward elucidating the role of number of oxazine rings and intermediates in the benzoxazine backbone on their thermal characteristics, Macromolecules. 49 (2016) 8466–8478.
[26] N. Teng, S. Yang, J. Dai, S. Wang, J. Zhao, J. Zhu, X. Liu, Making benzoxazine greener and stronger: renewable resource, microwave irradiation, green solvent, and excellent thermal properties, ACS Sustain. Chem. Eng. 7 (2019) 8715–8723.
[27] M.L. Salum, D. Iguchi, C.R. Arza, L. Han, H. Ishida, P. Froimowicz, Making benzoxazines greener: design, synthesis, and polymerization of a biobased benzoxazine fulfilling two principles of green chemistry, ACS Sustain. Chem. Eng. 6 (2018) 13096–13106.
[28] X.-L. Sha, L. Yuan, G. Liang, A. Gu, Development and Mechanism of High-Performance Fully Biobased Shape Memory Benzoxazine Resins with a Green Strategy, ACS Sustain. Chem. Eng. (2020).
[29] P.T. Anastas, J.C. Warner, Principles of green chemistry, Green Chem. Theory Pract. (1998) 29–56.
[30] H. Ishida, Process for preparation of benzoxazine compounds in solventless systems, (1996).
[31] L. Han, D. Iguchi, P. Gil, T.R. Heyl, V.M. Sedwick, C.R. Arza, S. Ohashi, D.J. Lacks, H. Ishida, Oxazine ring-related vibrational modes of benzoxazine monomers using fully aromatically substituted, deuterated, 15N isotope exchanged, and oxazine-ring-substituted compounds and theoretical calculations, J. Phys. Chem. A. 121 (2017) 6269–6282.

[32] S.H. Yalkowsky, Y. He, P. Jain, Handbook of aqueous solubility data, CRC press, 2016.
[33] A. Novak, E. Whalley, Infra-red spectra and structure of polyaldehydes. Part 1.—Polyformaldehyde, Trans. Faraday Soc. 55 (1959) 1484–1489.
[34] D.J. Merline, S. Vukusic, A.A. Abdala, Melamine formaldehyde: curing studies and reaction mechanism, Polym. J. 45 (2013) 413–419.
[35] B.C. Smith, IR Spectral Interpretation Workshop Alcohols The Rest of the Story, Spectroscopy. 32 (2017) 19–23.
[36] C.W. Chang, C.H. Lin, H.T. Lin, H.J. Huang, K.Y. Hwang, A.P. Tu, Development of an aromatic triamine-based flame-retardant benzoxazine and its high-performance copolybenzoxazines, Eur. Polym. J. 45 (2009) 680–689.
[37] L. Han, M.L. Salum, K. Zhang, P. Froimowicz, H. Ishida, Intrinsic self-initiating thermal ring-opening polymerization of 1, 3-benzoxazines without the influence of impurities using very high purity crystals, J. Polym. Sci. Part Polym. Chem. 55 (2017) 3434–3445.
[38] S. Ohashi, K. Zhang, Q. Ran, C. Arza, P. Froimowicz, H. Ishida, Preparation of High Purity Samples, Effect of Purity on Properties, and FT-IR, Raman, 1H and 13C NMR, and DSC Data of Highly Purified Benzoxazine Monomers, in: Adv. Emerg. Polybenzoxazine Sci. Technol., Elsevier, 2017: pp. 1053–1082.
[39] J. Liu, H. Ishida, Anomalous isomeric effect on the properties of bisphenol f-based benzoxazines: Toward the molecular design for higher performance, Macromolecules. 47 (2014) 5682–5690.
[40] J. Chen, M. Zeng, Z. Feng, T. Pang, Y. Huang, Q. Xu, Design and preparation of benzoxazine resin with high-frequency low dielectric constants and ultralow dielectric losses, ACS Appl. Polym. Mater. 1 (2019) 625–630.
[41] D.J. Das, R. Rajeev, R. Rajeev, K.S. Kumar, Synthesis, characterization, curing and thermal decomposition kinetics of bisphenol-A based polybenzoxazine, Int J Sci Technol Res. 2 (2013) 146–155.
[42] X. Ning, H. Ishida, Phenolic materials via ring-opening polymerization of benzoxazines: Effect of molecular structure on mechanical and dynamic mechanical properties, J. Polym. Sci. Part B Polym. Phys. 32 (1994) 921–927.

3. Highly Thermally Stable Copolymers of Polybenzoxazine and Epoxy: The Trifunctionality Advantage

(Paper submitted to Polymer Degradation and Stability – Elsevier on Feb 16, 2021)

Abstract

Synergistic composition of copolymer thermosets depends on their miscibility and similar reactivity that can lead to higher performance. In this work, we report the copolymerization of a triamine-based benzoxazine and a commercial difunctional epoxy resin, and investigate their synergistic effect on improved thermal properties using differential scanning calorimetry (DSC) and thermogravimetric analysis (TGA). Results showed that a glass transition temperature increase of up to 268 °C was obtained for the copolymer with as low as 25 wt% epoxy. A higher thermal performance was also achieved with an onset degradation of nearly 400 °C and char yield of 22 wt% at 800 °C for the copolymer with 52 wt% epoxy. The behavior was compared to previously reported benzoxazine/epoxy combinations and was found to be advantageous. Overall, the prepared PBZ/epoxy copolymers displayed higher thermal stability than their individual components, indicating suitability for a number of potential extended uses including utility in higher temperature applications.

3.1. Introduction

Epoxy resins are a widely known group of prepolymers characterized by an aliphatic and/or aromatic backbone containing two or more reactive oxirane rings (or epoxides), where primary crosslinking occurs to form thermosets [1,2]. This reaction can take place via catalytic homopolymerization or coupling with hardeners (or curing agents), both of which lead to oxirane ring opening and subsequent hydroxyl formation and chain extension [3,4]. The use of hardeners (e.g. amines, carboxylic acids, anhydrides, and phenols) is the most common polymerization technique as it promotes epoxy crosslinking into a thermosetting three-dimensional network [3]. The functionality (i.e. number of epoxide moieties) of epoxy resins and their reaction affinity towards a wide range of chemical reagents offer versatility and tailorable

chemical, mechanical, and thermal properties for a wide range of applications [3,5–7]. Diglycidyl ether of bisphenol A (DGEBA), a difunctional epoxy representing roughly 75% of the total epoxy demand worldwide, is the most widely used [3].

Benzoxazine monomers, on the other hand, are traditionally prepared from a phenolic compound, formaldehyde, and amine by condensation reaction in the presence or absence of organic solvents [8,9]. Known for their molecular design flexibility, they are characterized by one or more groups of six-membered aromatic ring fused to an oxazine ring, which, upon thermal curing, opens to form thermosetting polybenzoxazine (PBZ) without needing any initiators or catalysts [8,9]. PBZ is a unique class of phenolic materials having an array of interestingly important properties such as minimal shrinkage upon curing, low dielectric constant, low water absorption, low surface energy, chemical and UV resistance, mechanical strength, thermal stability, high char yield, and flame retardancy [8–11]. Although these characteristics make PBZ an attractive material for the fabrication of high performance composites and corrosion-resistant coatings [9,12–17], its higher curing temperature and lower crosslinking density [18], compared to other thermosetting polymers, need to be resolved. Introduction of functional groups that serve as additional crosslinking sites and/or copolymerization with other resins are among the most commonly employed approaches to overcome these issues [18–24]. Copolymerization is more practical as it permits the preparation of a wide range of polymeric products with the best balance and combination of properties that may not be achievable with each component alone. In addition, its utility in modifying the properties of polymers has become a viable means to meet specific needs and end-use requirements. Copolymerization of benzoxazines with epoxy resin monomers has been shown to be effective in improving, not only mechanical, but also thermal properties of the resulting copolymers [18,21–24]. Ishida and Allen [18] reported that the inclusion of epoxy into the PBZ structure produces copolymers with higher glass transition temperature (Tg) and crosslinking density compared to the PBZ homopolymer. Several studies on PBZ/epoxy copolymers have, thus, been reported [21–24]. Jubsilp et al. [21] studied the curing kinetics of a benzoxazine monomer copolymerized with an epoxy novolac resin. Rimdusit et al. [22] investigated the thermomechanical properties of a series of difunctional benzoxazine resins copolymerized with a diglycidyl-ether-based epoxy. Rao and co-workers [23] copolymerized a difunctional benzoxazine with chain-extended epoxies and examined the effects of molecular weight on the viscoelastic and thermal properties of the

crosslinked copolymers. Xu et al. [24] studied the thermal stability and processability of copolymers of cyano-containing difunctional benzoxazine and difunctional epoxy and evaluated their potential applications for glass fiber composites.

In this work, we prepared PBZ/epoxy systems with varying weight ratios by copolymerizing a trifunctional benzoxazine (Fig. 1a) with DGEBA-based epoxy resin (Fig. 1b), and investigated the improvement in thermal stability caused by increase in crosslinking density. To the best of our knowledge, few studies on copolymers of trifunctional benzoxazines and epoxy resins have been reported. Since both the curing reactions of benzoxazine and epoxy resin monomers are based on ring-opening polymerization, it is thought that the phenolic hydroxyl groups resulting from the oxazine ring opening (Fig. 1c) can react with the oxirane ring of the epoxy via nucleophilic attack, forming an ether linkage (Fig. 1d) and leading to a chain extension [18,21–24]. Therefore, these thermosetting PBZ/epoxy copolymers of varying compositions not only show hybrid network formations, but they can also be achieved without any phase separation issue [25]. It also highlights the potential advantage of a trifunctionality vs difunctional benzoxazine groups in a copolymer combination.

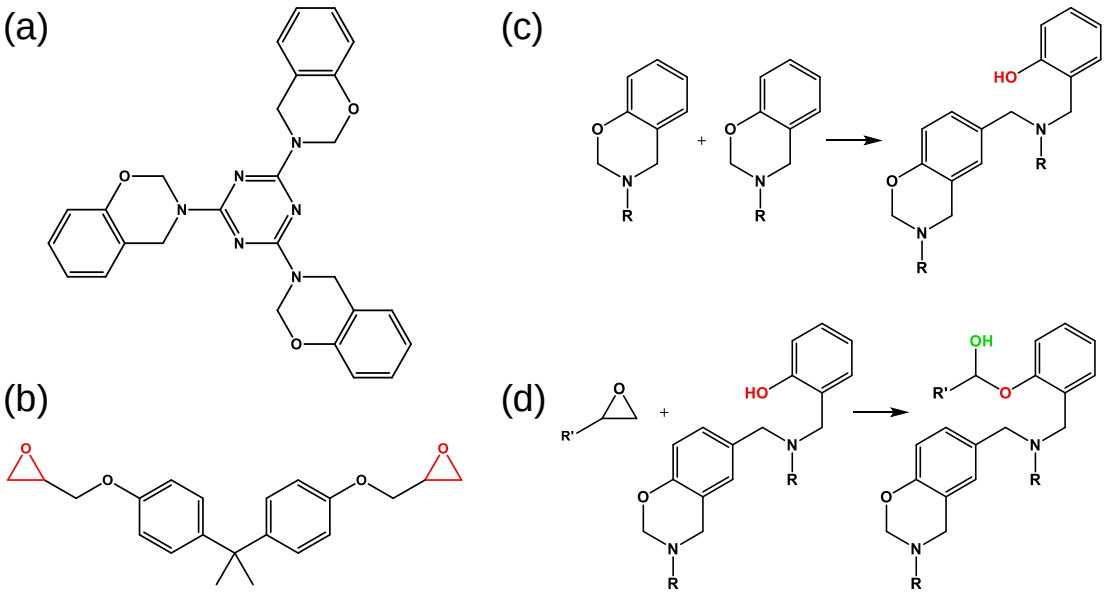

Fig. 3.1. Chemical structures of the (a) synthesized trifunctional BZ monomer and (b) DGEBA EP resin used in this study. Copolymerization reaction showing (c) the homopolymerization toward PBZ, followed by (d) the reaction of the EP's oxirane ring with the hydroxyl of the PBZ.

3.2. Experimental

3.2.1. Materials

Beckopox® EP385w/56WA, a DGEBA-based epoxy (EP) resin, was supplied by Allnex Belgium SA. 99.9%-purity grade dimethyl sulfoxide (DMSO) was purchased from Sigma-Aldrich, while 200-proof ethanol was obtained from Decon Laboratories, Inc. Ethyl acetate (certified ACS grade) and sodium hydroxide (NaOH) pellets (certified ACS grade), used to prepare the NaOH solution, were acquired from Fisher Scientific. All chemicals were used as received.

The trifunctional benzoxazine (BZ) monomer was synthesized by Mannich reaction between phenol, paraformaldehyde, and melamine in a solventless environment and stoichiometric ratio of 6:6:1. The reactant mixture was magnetically stirred at 50-60 °C for 1 h and heated to 95-100 °C for 9.5 h, followed by cooling to room temperature. The resulting crude BZ monomer was then dissolved in chloroform, washed with 1N NaOH solution for several times, and rinsed with deionized water until neutral. This preparation method is considered an example of green chemistry, with the minimum use of organic solvents and simple purification methods.

The copolymers were prepared by first dissolving each monomer separately in a suitable solvent; BZ monomer in DMSO at a concentration of 1 $mg.\mu L^{-1}$ and EP resin in a 50:50 mixture of ethyl acetate and ethanol at 0.32 $mg.\mu L^{-1}$. The two monomer solutions were then combined and mixed to form a single homogeneous solution, which was subsequently heated to evaporate the solvents. The BZ to EP weight ratios were varied as follows: 5/95, 25/75, 31/69, 48/52, 55/45, 75/25 and 100/0. The synthesized BZ monomer displays a 200 g/mol equivalent weight, while the EP resin an average of 500 g/mol epoxy-equivalent (solids). Calculations based on these parameters gives a stoichiometric 29/71 ratio, characterized by much lower amounts of BZ. This characteristic may be interesting in the perspective of application, as small quantities of BZ can lead to a higher crosslinked copolymer material and possibly improved mechanical and thermal properties [26]. In addition, the low-cost, ready availability, and popularity of Eps relative to BZ monomers can result in BZ/EP copolymers with high benefit-cost ratios.

3.2.2. Instrumentation

Fourier transform infrared (FTIR) spectroscopy was performed using a Cary 600 Series FTIR spectrometer (Agilent Technologies). Each spectrum was recorded at an average of 128 scans with a nominal spectral resolution of 2 cm^{-1}. To investigate the thermal stability and degradation of the copolymers, differential scanning calorimetry (DSC) and thermogravimetric analysis (TGA) were done with a DSC 2920 differential scanning calorimeter and TGA Q500 thermogravimetric analyzer (TA Instruments), respectively, both on a N2 gas purge at 50 mL min^{-1} and ramp rate of 10 °C.min^{-1}. Evolved gas analysis (EGA) was conducted on a gas chromatography-mass spectrometry (GC-MS) system (Agilent 5973, Quantum Analytics) equipped with a multi-shot pyrolyzer (EGA/PY-3030D, Frontier Laboratories) containing a 2.5-m long metal column (Ultra alloy DTM, 0.15 and 0.25 mm inner- and outer- diameter, respectively). A 100 °C preheated sample cup containing 0.2 mL sample was heated to 800 °C at 20 °C.min^{-1} and the evolved gas was directly injected into the column maintained at 300 °C, while the interface between the GC-MS and pyrolyzer was kept at 200 °C.

3.3. Results and discussion

3.3.1. Epoxy resin characterization

EP resin Beckopox® EP385w/56WA was selected for its flexibility, wet film adhesion, and good adhesion to metallic substrates. However, the molecular structure of the EP has not been identified. The EP structure is important as it helps predict its reactivity and properties and determine suitable BZ/EP ratios for copolymerization. Therefore, EGA/GC-MS was performed in order to confirm the composition and investigate the chemical structure of the EP. The EGA curve of the EP resin is shown in **Fig. 3.2a**, while the results from GC-MS are displayed in **Fig. S5.2-S5.4** in the Supplementary Information (SI).

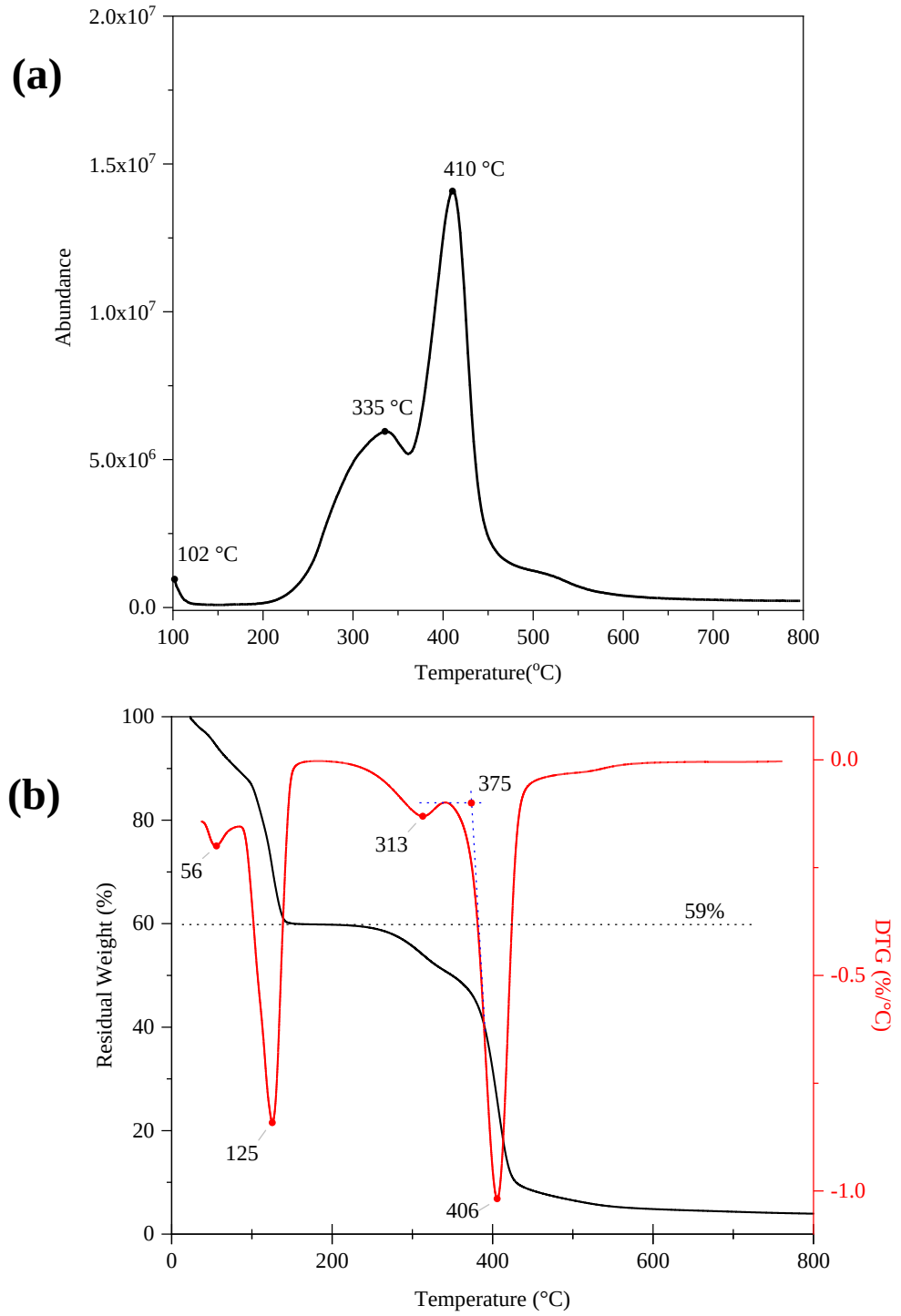

Fig. 3.2. (a) EGA curve as a function of temperature and (b) thermogram of the EP resin used in this study.

Three peaks were observed in **Fig. 3.2a**, each representing a component or fragment of the original EP resin. As evidenced by the mass spectra in **Fig. S 7**, the first peak in the EGA curve at 102 °C is assigned to isopropyl alcohol and the corresponding abundance reflects its total volume in the product (equivalent to 2.5% according to the manufacturer). The second peak, at 335 °C, is attributed to DGEBA according to the

mass spectra in **Fig. S 8**, which confirms the molecular structure of the EP. Furthermore, this peak indicates the evaporation of DGEBA monomers rather than degradation, as evidenced by the detection of the whole molecule. The third peak, at 410 °C, is attributed to bisphenol-A, as observed from **Fig. S 9**. These bisphenol-A molecules likely originated from stable radical fragmentation of DGEBA due to degradation upon heating during the measurement. Additionally, this fragment can come from residues during the synthesis of DGEBA, which can function as plasticizer, curing rate controllers, etc., providing specific effects on the thermomechanical properties of a cured resin. Again, it is important that EGA and MS techniques were used to qualitatively confirm the molecular structure and composition of the commercial EP resin used in this study and the presence of isopropyl alcohol, which is stated by the manufacturer as one of the solvents used.

Fig. S 7b shows the TGA and derivative thermogram (DTG) of the uncured EP resin. The DTG peaks at 56 °C and 125 °C are assigned to the solvents used in the formulation of the commercial EP product (i.e. isopropanol and water, respectively). Data obtained experimentally from TGA indicate 59% residual mass after evaporation of these solvents. This result is consistent with the manufacturer's information stating a 56% solids content. Interestingly, the peaks for these solvents are slightly shifted from their respective boiling points. It is important to highlight two mechanisms that clarify such shift. First, the solvents involved are composed of more volatile small molecules and what is observed is evaporation, rather than degradation followed by volatilization as would be expected for larger molecules such as polymers. On the other hand, a competing mechanism that may be present is the reaction of these small molecules to other compounds within the sample. It has been reported that water may present two distinct peaks of evaporation depending on whether the molecules are free or bound to other molecules [27]. As a result, depending on the combination of these mechanisms, evaporation peaks may be shifted to a higher or lower temperature. Furthermore, a minor peak can be observed at 313 °C, which, according to the EGA result, is associated with the volatilization of DGEBA monomers. Combining the TGA and EGA results, it is clear that the degradation of EP monomers exhibited onset and peak of degradation at 375 °C and 406 °C, respectively. These results are consistent from the literature data [28,29] and show the stability of the EP resin to copolymerize BZ at temperatures up to 375 °C.

3.3.2. DSC and identification of peaks of curing

Prior to curing, the solvents were removed by drying the samples in an inert atmosphere at a heating rate of 1 °C min^{-1} and holding the temperature at the boiling points of each solvent for 1 min. Samples were then cooled at 5 °C min^{-1}, weighed, and run in DSC. Several curing peaks were observed for each sample in Fig. 3, which may be due to the polymerization or thermosetting processes from three different routes [18,21–24]: (1) BZ reacts with itself, generating a PBZ homopolymer; (2) EP reacts with itself, generating an EP homopolymer; and (3) BZ reacts with EP, producing a BZ/EP copolymer. From here on, these reactions will be referred to as B-B, E-E and B-E, respectively. It is clear that the relative mass of the monomers consumed in each peak cannot be predicted and is not equal to the total mass of the sample. Therefore, the DSC curve was also plotted as power vs. time to obtain energy (mJ) via curve integration, which allows identification of the peaks.

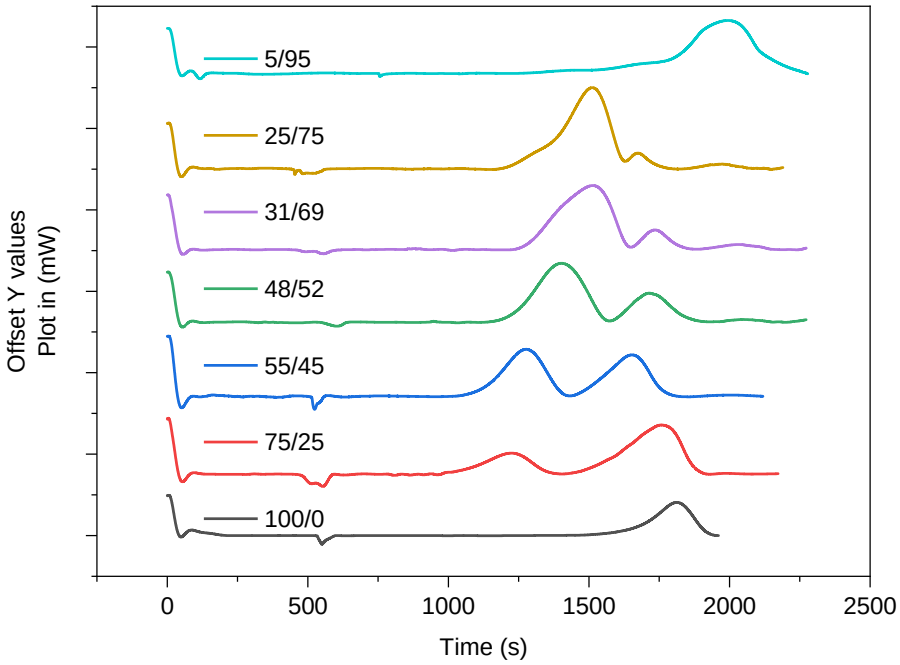

Fig. 3.3. DSC curves of BZ/EP samples with different weight ratios for copolymerization analysis.

To distinguish the reaction type, the intrinsic energy for each reaction and the mass for each sample were compared to the released energy associated with the peak obtained experimentally. Curves were deconvoluted and every resulting peak was integrated to obtain the amount of energy released (mJ) in each peak (see **Fig. S 11** for example). This energy was then compared to two distinct information: (1) energy data from the literature for the homopolymerization of EP, that is 90.7 kJ/mol of epoxide

[30], equivalent to 181.4 mJ/mg EP in the case of Beckopox® EP 385w/56WA; and (2) energy data for the homopolymerization of BZ obtained experimentally from its pure sample (i.e. 100/0), where a total energy release of 746 mJ upon BZ polymerization was calculated via peak integration. This amount of energy was due to the complete polymerization of a 6.24 mg sample, equivalent to 120 mJ/mg. A detailed procedure for this process can be found in the SI.

The peak around 350 °C is due to the latent homopolymerization of EP (E-E), which was defined based on two observations: (1) sample 5/95 revealed a broad peak near this temperature, corresponding to only this type of reaction due to the marginal amount of BZ; and (2) samples with high BZ concentration revealed the absence of such peak, in which it is likely that excess BZ completely consumed the EP monomers, thus, no residual E-E polymerization observed. It is also interesting to notice the presence of melting peaks at ~120°C in all DSC curves, which are assigned to the melting of BZ [31], confirming their high purity. It is important to highlight that these peaks were not observed previously in chapter 2. Samples from previous chapter were polymerized directly after purification. Different from those samples, benzoxazine and epoxy were mixed by solvent solution and prior to the curing process, they were dried at high temperatures with subsequent slow cooling. It is likely that the drying procedure allowed for crystallization of the benzoxazine monomers. The small size of the peaks suggests that not all BZ is crystalline in the samples, indicating the possibility of crystalline domains within an amorphous matrix. These peak identities are summarized in **Table 3.1**.

Table 3.1. Summary of peak identities analysis from DSC experiments.

Sample	Peak 1	Peak 2	Peak 3	Peak 4
5/95	E-E	B-E	B-B	E-E
25/75	E-E	B-E	B-B	E-E
31/69	B-E	E-E	B-B	E-E
48/52	B-E	B-B	E-E	-
55/45	B-B	E-E	B-E	-
75/25	B-B	B-E	E-E	-
100/0	B-B	-	-	-

Polymerization of sample 5/95 starts with E-E reaction at around 250 °C, followed by B-E and B-B at 280 and 330 °C, respectively. This sample shows residual

E-E reaction close to 350 °C. Excess EP is likely to favor E-E reaction over other possible reactions. Likewise, sample 25/75 begins polymerization with E-E reaction near 250 °C, followed by B-E and B-B reactions at around 280 and 315 °C, respectively, and further showing residual E-E reaction close to 350 °C. Sample 25/75 also shows attenuation of the 3rd peak (B-B) when compared to 5/95. It is likely that the higher concentration of BZ increased the probability of greater interaction between these monomers, facilitating more B-E reactions. In addition, sample 25/75 exhibits a considerable decrease in the energy released from the residual E-E reaction. This result indicates less EP left from the previous reactions, given there is more BZ available to consume the EP compared to sample 5/95.

Sample 31/69 starts polymerization with B-E reaction at around 250 °C, followed by E-E at 270 °C and B-B reaction at 310°C. This sample presents residual E-E reaction close to 360 °C. Clearly, B-E reaction was more favored for this ratio of monomers. This phenomenon anticipates greater lessening of the E-E reaction when compared to samples 5/95 and 25/75. At this ratio, EP is no longer in excess and is very close to 1:1 reaction stoichiometry. Therefore, it is consistent that the B-E is dominant and E-E is not the most favored reaction. Interestingly, B-B continues to be the last among the three possible reactions due to the high temperature of PBZ curing. This sample also displayed high reduction in energy released from the residual E-E reaction. Again, higher BZ concentration allows for greater EP consumption, resulting in less residue.

Sample 48/52, on the other hand, begins polymerization with B-E reaction at around 240 °C, followed by B-B reaction at around 250 °C and E-E at around 310 °C. This sample also shows no residual E-E reaction. B-B reaction was anticipated in relation to E-E reaction when compared to samples 5/95, 25/75 and 31/69. This observation is consistent as the composition of the sample is shifted towards excess BZ and intensely influences the favorability of B-B reaction. Similarly, sample 55/45 starts polymerization with B-B reaction at around 240 °C, followed by E-E reaction at around 250 °C and B-E at around 310 °C. This sample does not present any residual E-E reaction, but B-B reaction was more dominant in the polymerization process. Higher concentration of BZ increases the likelihood of interaction and, consequently, facilitates the reaction.

Sample 75/25 starts polymerization with B-B reaction at around 240 °C, followed by B-E reaction close to 300 °C and completes at 325 °C. This sample does not present any residual E-E reaction. B-B reaction is maintained as the dominant reaction, likely

due to the very high concentration of BZ monomers. In addition, E-E reaction is the least favorable due to the very low EP concentration and its likelihood of encountering a BZ molecule. Furthermore, sample 100/0 shows a single peak of cure at around 340 °C representing the single monomer B-B cure only. Interestingly, the temperature for B-B reaction in this sample is higher than that of all the other samples. This phenomenon is predicted in the literature [31,32], where the 100/0 is due to the reaction between BZ monomers only via ring-opening, forming hydroxyl groups and eventually thermosetting PBZ.

In summary, with excess EP (i.e. 5/95 and 25/75), E-E reaction is shown as most favorable, whereas, samples with excess BZ (i.e. 55/45, 75/25 and 100/0) show B-B reaction as most favorable. Samples with composition close to stoichiometric (i.e. 31/69 and 48/52) show favored B-E reactions. The compatibility, good solvent mixing, and near quantitative shift of the EP and trifunctional BZ is highlighted.

3.3.3. Characterization of cured samples

A second cycle of DSC was performed from room temperature to 400 °C in order to validate the accomplishment of cure of the samples (**Fig. 3.4a**). It is observed that the temperature range between 200 and 350 °C, where curing peaks were previously present, did not show any peaks and a good baseline. The fact that the peaks are completely gone in the second cycle indicates a very successful polymerization/crosslinking process. This phenomenon was observed for all the compositions, again indicating good compatibility and the absence of any unreacted residues after the first run when carried to above 400 °C, where complete BZ reactivity is expected.

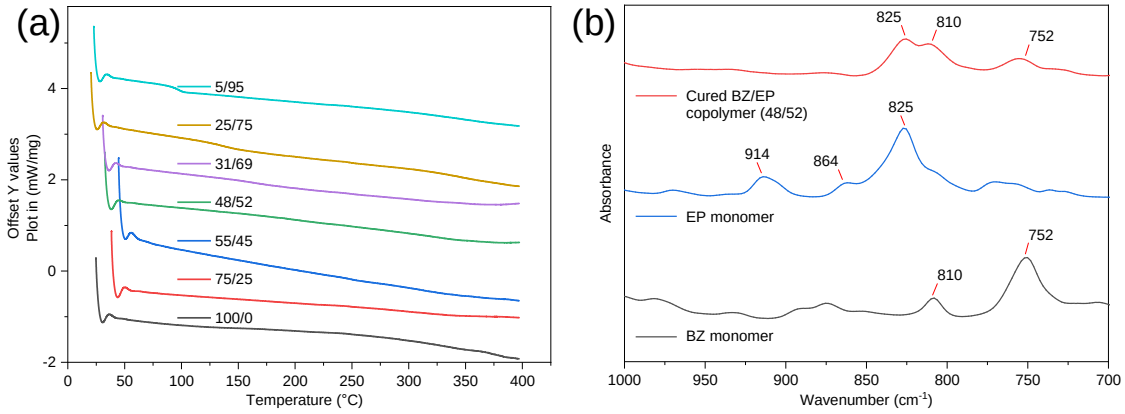

Fig. 3.4. (a) DSC curves (second run) of cured BZ/EP samples. (b) FTIR spectra of BZ, EP resin, and cured BZ/EP (48/52).

Prior to investigating the properties of the bulk copolymers, a qualitative FTIR analysis confirmed that both monomeric species participated in the reaction. **Fig. 3.4b** shows the IR spectra within the wavenumber range of interest for BZ monomer, EP monomer and BZ/EP copolymer (sample 48/52). EP consumption can be evidenced by the peaks at 914 cm^{-1} and 864 cm^{-1}, corresponding to epoxide ring vibration modes, which disappeared due to ring-opening [18] in the BZ/EP spectrum. In addition, the peak at 825 cm^{-1}, assigned to p-disubstituted aromatic ring of DGEBA [33], can be observed both in the EP and copolymer spectra. This result suggests that the backbone structure of the EP was not altered after polymerization. On the other hand, BZ spectrum shows a peak at 752 cm^{-1}, corresponding to o-disubstituted aromatic ring [33], which converts into a trisubstituted aromatic ring upon polymerization and, therefore, should be expected to become less intense, as evidenced in the BZ/EP spectrum. Furthermore, the peak at 810 cm^{-1} spotted in the BZ/EP spectrum is assigned to the trisubstituted aromatic ring [33] of PBZ. Interestingly, it can be seen that the BZ spectrum also contains such peak, indicating the presence of oligomers in the BZ sample. Overall, these results confirm that epoxies are readily crosslinked with heat reactive BZ resins.

3.3.4. Glass transition temperature

Fig. 3.5a shows the derivative of the second DSC run from room temperature to 300°C. Samples 5/95 and 100/0 display a clear valley at 94 °C, in which the former is dominated by the EP material while the latter is completely composed of BZ. However, this valley is broader in sample 100/0 than in sample 5/95, which implies a higher

uniformity in molecular structure of the latter sample despite its 5 wt% BZ content. Differences in crosslinking density throughout the sample, for instance, may generate a wider temperature range in Tg due to differences in mobility for varying compositions. In the same material, regions with lower crosslinking density show lower Tg [34]. The functionality of the BZ monomers with higher concentration may favor intermolecular hydrogen bonds in PBZ as reported in the literature [11].

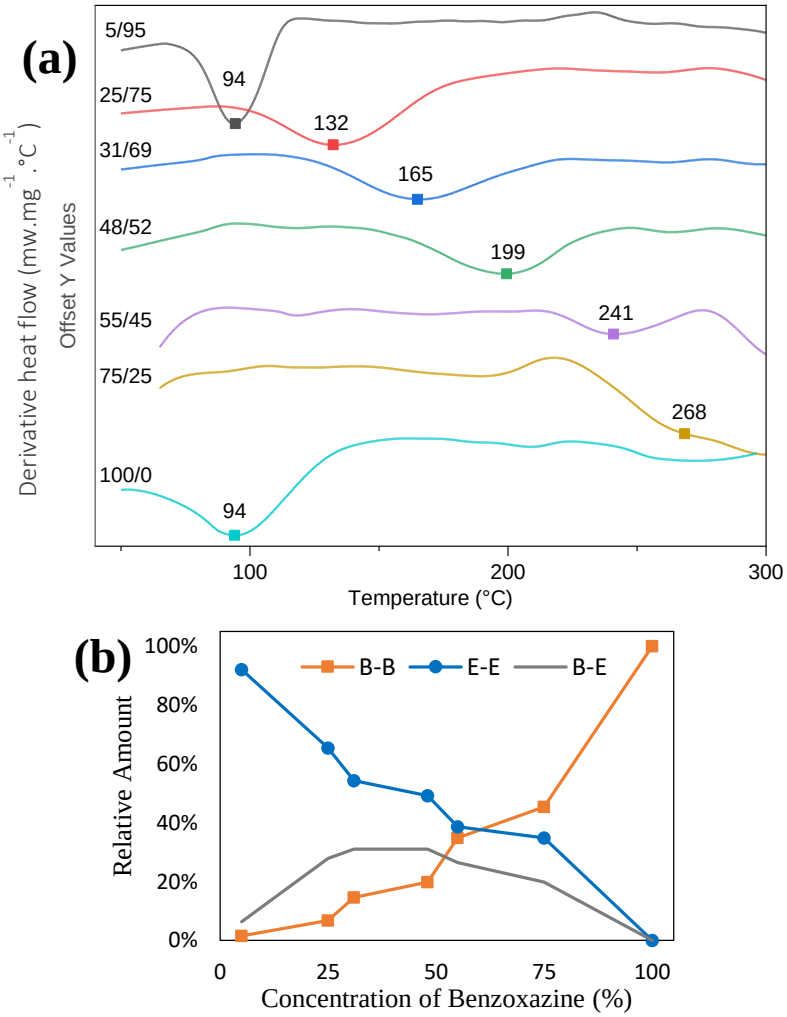

Fig. 3.5. (a) DSC derivative thermograms (DTG, second run) of cured BZ/EP samples. (b) Amount of each polymerized component in cured BZ/EP copolymer samples.

It is clear that increasing BZ concentration shifts Tg to a higher value, as indicated by the valleys at progressively higher temperatures in **Fig. 3.5a**. Samples 25/75, 31/69, 48/52, and 55/45 display very evident valleys at 132, 165, 199, and 241 °C, respectively. A synergistic effect is, thus, obtained from the copolymerization, where Tg is higher for samples with compositions closer to the stoichiometric. This result can be explained by the combination of high rigidity of the trifunctional BZ, with improved crosslink density, thanks to the presence of EP [20]. Additionally, the shapes of the

valleys for the copolymer samples are similar to that for sample 100/0, which imply that these samples possess higher level of hydrogen bonding and a less uniform molecular structure compared to a majority EP sample 5/95. In these four compositions, the presence of three main polymeric domains (i.e. B-B, E-E, and B-E) favor the higher chemical heterogeneity. Furthermore, the possible heterogeneity in crosslink density, as previously discussed, can influence the shape of the Tg region. Although sample 75/25 displays an indistinct Tg valley at 268 °C, the trend in Tg increase is still consistent with composition. Additionally, a clear step towards the endothermic direction can be observed in the respective DSC curve presented in **Fig. S 13** in the SI.

DSC of cure (**Fig. 3.3**) was further used for the analysis of relative amounts of each polymeric domain (i.e. B-B, E-E and B-E). Energy of cure from the respective peaks were considered for the calculation of the percentage amount of each domain. The results are plotted in **Fig. 3.5b**. It is evident that the percentage of B-B reaction increases with increasing BZ concentration. Such a trend is anticipated as larger amounts of BZ increases the likelihood of B-B reaction to occur. Conversely, E-E reaction displayed a decreasing trend with increasing BZ concentration and such result is anticipated due to a reduction in the probability of EP molecule interaction. For the B-E reaction, percentage increases with increasing BZ concentration until becoming plateau at 31-48 wt%. This result indicates that samples 31/69 and 48/52 displayed the highest degree of B-E reaction occurrence since their composition was very close to the theoretical stoichiometric ratio. The percentage for B-E then drops due to: (1) increased likelihood of interaction between each of the same kind of molecules (i.e. B-B and E-E); (2) intrinsic thermodynamic favorability for each reaction type; and (3) catalyzing effect of the same monomers on each another [28,29]. Excess of one of the monomers promoted decrease in B-E reaction due to a disequilibrium in the number of functional groups and subsequent reduction in hybrid interactions. It is important to note that these results can be corroborated by the DSC peaks determined in Section 3.3.2.

3.3.5. Thermal stability study

Fig. 3.6 shows both TGA and DTG curves for samples 100/0, 48/52 and 5/95, while the important extracted thermal parameters are summarized in **Table 3.2**. Sample 100/0 shows the highest char yield (37% at 800 °C) and presents two major decomposition regions at 384 and 525 °C. The onset degradation at 384 °C is due to the

bond scission of C-N, while the degradation at 525 °C is due to the scission of C-C and C-H bonds [8]. Sample 5/95, having the lowest char yield (11% at 800 °C), displays a sharp, symmetric single peak at 397 °C, which suggests homogeneity of the polymeric structure. This observation is in agreement with results described in Section 3.4. Meanwhile, sample 48/52 shows a wide, but less symmetric degradation peak centered at 434 °C, which indicates structural heterogeneity of the polymeric material (in agreement with the results discussed in Section 3.2) due to the ability of the three polymeric domains to promote a wider degradation temperature range. A small shoulder can also be observed for sample 48/52 near 525 °C, the same temperature as the second step of degradation for sample 100/0, showing characteristics of the PBZ homopolymer.

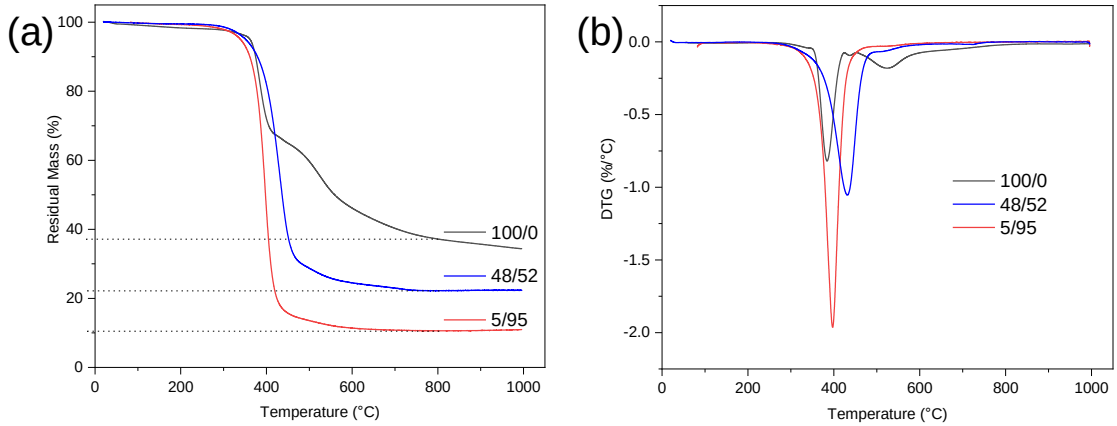

Fig. 3.6. (a) TGA and the corresponding (b) DTG curves of 5/95, 48/52, and 100/0 samples.

It is very important to note the improvement in thermal stability obtained by combining both BZ and EP. Almost every thermal parameter was improved for sample 48/52, compared to the other two samples. The onset degradation increased by nearly 20 °C and degradation peak shifted by around 40 °C, while char yield was found to be almost an average of the other two compositions. Although the intrinsic characteristics of both components are still noticeable, the improvement in degradation temperature was indeed achieved by copolymerization.

Table 3.2. Data from TGA and DTG thermograms of samples 100/0, 5/95 and 48/52

	100/0	**5/95**	**48/52**
Onset (°C)	365	368	382
Peak (°C)	384; 525	397	434
T_{99} (°C)	116	247	285
T_{95} (°C)	362	339	351
Char @ 800°C	37%	11%	22%
Offset (°C)	570	422	473

In general, the use of a trifunctional BZ in a BZ/EP copolymerization is more beneficial compared to its typical difunctional substitute. For instance, a copolymer prepared from difunctional BZ and DGEBA-based EP (with composition close to stoichiometric ratio) reported in the literature [22,23] exhibits an onset degradation of ~350 °C, Tg near 220 °C, and a curing temperature of ~240 °C. Conversely, our copolymers based on trifunctional BZ displayed higher onset degradation and Tg of ~400 °C and 268 °C, respectively, with comparable char yield at 800 °C and curing temperature. This synergistic effect on enhanced thermal properties is all attributed, not only to the contribution of the EP, which lowers the overall copolymer curing temperature, but also to the trifunctionality of the BZ, leading to a higher crosslinking density and higher thermal stability for the resulting copolymers.

3.4. Conclusions

The advantage of the trifunctional BZ and the EP resin combination was evident in the high properties achieved with the copolymer. The two monomers are highly compatibilized with the use of a mixed solvent mixing and drying protocol. Changes in composition of the BZ and EP revealed a shift in reaction kinetics and thermodynamics associated with high miscibility in preparation. The comparison with literature with other BZ monomers and EP showed a distinct advantage. Thus, the structure-composition-property correlation is evident in the near quantitative shift in thermal (DSC) and spectroscopic (IR) characterization of properties with composition. Future work can make use of this pairing to enable high performance in a number of thermoset applications involving high temperature.

Acknowledgements

This work was supported by Coordenação de Aperfeiçoamento de Pessoal de Nível Superior (CAPES), Brasil – Finance Code 001 for Lucio Souza. RC Advincula gratefully acknowledge funding from the Governor's Chair Funds, University of Tennessee system. Technical support from Malvern Panalytical, Frontier Laboratories and Quantum Analytics. Work (or Part of this work) was conducted by RC Advincula with the ORNL's Center for Nanophase Materials Sciences, which is a US Department of Energy Office of Science User Facility.

References

[1] F.-L. Jin, X. Li, S.-J. Park, Synthesis and application of epoxy resins: A review, J. Ind. Eng. Chem. 29 (2015) 1–11.

[2] B. Bilyeu, W. Brostow, K.P. Menard, Epoxy thermosets and their applications I: chemical structures and applications, J. Mater. Educ. 21 (1999) 281–286.

[3] C. May, Epoxy resins: chemistry and technology, Routledge, 2018.

[4] B. Ellis, Chemistry and technology of epoxy resins, Springer, 1993.

[5] E.B. Caldona, D.O. Wipf, D.W. Smith Jr, Characterization of a tetrafunctional epoxy-amine coating for corrosion protection of mild steel, Prog. Org. Coat. 151 (2021) 106045.

[6] J.-P. Pascault, H. Sautereau, J. Verdu, R.J. Williams, Thermosetting polymers, CRC press, 2002.

[7] A.P. Mouritz, Introduction to aerospace materials, Elsevier, 2012.

[8] H. Ishida, T. Agag, Handbook of benzoxazine resins, Elsevier, 2011.

[9] N. Ghosh, B. Kiskan, Y. Yagci, Polybenzoxazines—new high performance thermosetting resins: synthesis and properties, Prog. Polym. Sci. 32 (2007) 1344–1391.

[10] H. Ishida, H.Y. Low, A study on the volumetric expansion of benzoxazine-based phenolic resin, Macromolecules. 30 (1997) 1099–1106.

[11] H. Ishida, D.J. Allen, Physical and mechanical characterization of near-zero shrinkage polybenzoxazines, J. Polym. Sci. Part B Polym. Phys. 34 (1996) 1019–1030.

[12] S. Rimdusit, C. Jubsilp, S. Tiptipakorn, Alloys and composites of polybenzoxazines, Springer, 2013.

[13] B. Kiskan, N.N. Ghosh, Y. Yagci, Polybenzoxazine-based composites as high-performance materials, Polym. Int. 60 (2011) 167–177.

[14] E.B. Caldona, A.C.C. De Leon, P.G. Thomas, D.F. Naylor III, B.B. Pajarito, R.C. Advincula, Superhydrophobic Rubber-Modified Polybenzoxazine/SiO2 Nanocomposite Coating with Anticorrosion, Anti-Ice, and Superoleophilicity Properties, Ind. Eng. Chem. Res. 56 (2017) 1485–1497.

[15] E.B. Caldona, C. Al Christopher, J.D. Mangadlao, K.J.A. Lim, B.B. Pajarito, R.C. Advincula, On the enhanced corrosion resistance of elastomer-modified polybenzoxazine/graphene oxide nanocomposite coatings, React. Funct. Polym. 123 (2018) 10–19.

[16] E.B. Caldona, C. Al Christopher, B.B. Pajarito, R.C. Advincula, Novel anti-corrosion coatings from rubber-modified polybenzoxazine-based polyaniline composites, Appl. Surf. Sci. 422 (2017) 162–171.

[17] E.B. Caldona, A.C.C. De Leon, B.B. Pajarito, R.C. Advincula, A Review on Rubber-Enhanced Polymeric Materials, Polym. Rev. 57 (2017) 311–338.

[18] H. Ishida, D.J. Allen, Mechanical characterization of copolymers based on benzoxazine and epoxy, Polymer. 37 (1996) 4487–4495.

[19] R.P. Parreño, Y.-L. Liu, A.B. Beltran, M.B. Carandang, Effect of a direct sulfonation reaction on the functional properties of thermally-crosslinked electrospun polybenzoxazine (PBz) nanofibers, RSC Adv. 10 (2020) 14198–14207.

[20] L. Puchot, P. Verge, S. Peralta, Y. Habibi, C. Vancaeyzeele, F. Vidal, Elaboration of bio-epoxy/benzoxazine interpenetrating polymer networks: a composition-to-morphology mapping, Polym. Chem. 9 (2018) 472–481.

[21] C. Jubsilp, K. Punson, T. Takeichi, S. Rimdusit, Curing kinetics of benzoxazine–epoxy copolymer investigated by non-isothermal differential scanning calorimetry, Polym. Degrad. Stab. 95 (2010) 918–924.

[22] S. Rimdusit, P. Kunopast, I. Dueramae, Thermomechanical properties of arylamine-based benzoxazine resins alloyed with epoxy resin, Polym. Eng. Sci. 51 (2011) 1797–1807.

[23] B. Rao, K. Rajavardhana Reddy, S.K. Pathak, A. Pasala, Benzoxazine–epoxy copolymers: effect of molecular weight and crosslinking on thermal and viscoelastic properties, Polym. Int. 54 (2005) 1371–1376.

[24] M. Xu, X. Yang, R. Zhao, X. Liu, Copolymerizing behavior and processability of benzoxazine/epoxy systems and their applications for glass fiber composite laminates, J. Appl. Polym. Sci. 128 (2013) 1176–1184.

[25] P. Zhao, Q. Zhou, X. Liu, R. Zhu, Q. Ran, Y. Gu, Phase separation in benzoxazine/epoxy resin blending systems, Polym. J. 45 (2013) 637–644.

[26] S. Rimdusit, H. Ishida, Synergism and multiple mechanical relaxations observed in ternary systems based on benzoxazine, epoxy, and phenolic resins, J. Polym. Sci. Part B Polym. Phys. 38 (2000) 1687–1698.

[27] M.U. Joardder, M. Mourshed, M.H. Masud, Bound Water Measurement Techniques, State Bound Water Meas. Significance Food Process. (2019) 47–82.

[28] J. Huang, X. Nie, A simple and novel method to design flexible and transparent epoxy resin with tunable mechanical properties, Polym. Int. 65 (2016) 835–840.

[29] R. Mehta, R. Kumari, P. Das, A.K. Bhowmick, Synthesis and characterization of a biocompatible monotyrosine-based polymer and its interaction with DNA, J. Mater. Chem. B. 2 (2014) 6236–6248.

[30] I.E. Dell'Erba, R.J.J. Williams, Homopolymerization of epoxy monomers initiated by 4-(dimethylamino) pyridine, Polym. Eng. Sci. 46 (2006) 351–359.

[31] S. Ohashi, K. Zhang, Q. Ran, C. Arza, P. Froimowicz, H. Ishida, Preparation of High Purity Samples, Effect of Purity on Properties, and FT-IR, Raman, 1H and 13C NMR, and DSC Data of Highly Purified Benzoxazine Monomers, in: Adv. Emerg. Polybenzoxazine Sci. Technol., Elsevier, 2017: pp. 1053–1082.

[32] X. Li, Y. Xia, W. Xu, Q. Ran, Y. Gu, The curing procedure for a benzoxazine–cyanate–epoxy system and the properties of the terpolymer, Polym. Chem. 3 (2012) 1629–1633.

[33] B.C. Smith, Distinguishing structural isomers: mono-and disubstituted benzene rings, Spectroscopy. 31 (2016) 36–39.

[34] J.S. Bermejo, C.M. Ugarte, Influence of Cross-Linking Density on the Glass Transition and Structure of Chemically Cross-Linked PVA: A Molecular Dynamics Study, Macromol. Theory Simul. 18 (2009) 317–327.

4. Superhydrophobic Benzoxazine-Epoxy Coatings: Electrochemical and Mechanical Performance

Abstract

Corrosion is a natural phenomenon that affects virtually every material, consumes billions of dollars annually worldwide and may result in catastrophic events. Coating is the most utilized technique to prevent corrosion. In this sense, epoxies are widely applied in all sectors of industry. Despite being high performance polymers, epoxies present issues, such as the use of toxic crosslinkers and long curing time. Benzoxazines are an emerging class of high performance self-curing thermosets. In this work coatings based on benzoxazine, epoxy and silica were developed as a means to produce a fast curing, low toxicity and high performance product with high thermal stability. Results revealed superhydrophobic surfaces with great scratch resistance and adhesion to steel substrate. Electrochemical test proved high effectiveness of the coatings as anti-corrosion barrier, with increasing performance with the incorporation of silica.

4.1. INTRODUCTION

Deterioration by corrosion is an important concern for mostly all metallic equipment, from industrial machinery and civil structures to vehicles and electronics. These materials are often exposed to aggressive environments, such as high temperature and pressure or chemically reactive substances such as O_2, H_2S, CO_2, water and salts[1]. Corrosion is a natural occurring degradation phenomenon which affects virtually every material, consumes billions of dollars annually worldwide and may result in catastrophic events. Metals are a critical class of material, which may undergo corrosion through chemical degradation by the environment. The phenomenon is typically a heterogeneous redox reaction and occurs at the metal-environment interface, causing oxidation of the metal and reduction of the oxygen present in the corrosive media[2]. The U.S. Federal Highway Administration (FHWA) revealed that the direct costs associated with metallic corrosion in nearly every U.S. industry amount a staggering total of $276 billion - approximately 3.1% of the nation's Gross Domestic Product (GDP)[3]. The National Association of Corrosion Engineers (NACE) estimates a global cost of corrosion of US$2.5 trillion, and that it is possible to realize savings between 15

and 35% of that total by applying only available corrosion control practices[4]. Several approaches have been developed to prevent the corrosion phenomenon, such as control of the environment, cathodic protection, corrosion resistant materials, plating and cladding[1]. Nevertheless, organic coatings are considered as one of the most widely used methods to protect metals against corrosion[5].

Coatings inhibit corrosion by isolating, to a certain degree, the substrate from the corrosive environment. Effectiveness of isolation is influenced by intrinsic properties of the coating material, such as crosslink density and hydrophobicity[2,6], and by adhesion between coating and substrate[2]. It is understood that adhesion plays such an important part in corrosion control, that several theories on the mechanism of failure of coating suggest that the loss of adhesion precedes the onset of corrosion. Interestingly, the same features that improve barrier property may reduce adhesion of the coating to the substrate. Polar functional groups, for example, are positively influencers to adhesion and, at the same time, are likely to increase permeability[2]. Performance of coatings are commonly assessed by exposure of a substrate/coating system to an environment capable of simulate an accelerated corrosive condition, such as brine immersion, salt spray and electrochemical experiments. Evaluation of results are typically performed by analysis of the type and extent of corrosion failure.

Industrially, epoxy (EP) resins are largely utilized as coating material due to its high thermal stability, chemical resistance, great adhesion, low shrinkage upon curing, high mechanical properties, and low cost[2,6,7]. In addition to coatings, epoxies also widely applied in several other areas of engineering, such as composites, adhesive, casting and binders. They can be used in compositions that can vary from a single epoxy resin with a hardener to multiple epoxy resins combined with modifiers, fillers, reinforcements and hardeners to tailor specific properties[8]. The main cross-linking occurs through the oxirane group as it is a highly reactive chemical structure. While the presence of this group defines the molecule as an epoxy, the basic molecular structure to which the ring is attached can vary widely, giving rise to various distinct properties. The chemical classes most commonly used as hardeners are the amines and anhydrides[9]. The polar nature of the epoxy macromolecule, due to pendant hydroxyl groups derived from opening of the epoxide ring, accounts for its strong adhesion to a wide variety of surfaces. Polarity of epoxy monomers accounts for its solubility in oxygenated solvents such as ketones, esters, and ether-alcohols and in chlorinated hydrocarbons[7].

Combination of polymers is a traditional and effective technique to make materials viable to demands of industry with respect to properties such as, high temperature resistance, light weight, toughness and low cost. In this regard, alloys of benzoxazines with other polymers such as epoxy and polyurethane have been reported[10,11]. Copolymerization between PBZ and diglycidyl ether of bisphenol-a (DGEBA), the most commonly used epoxy resin in the copolymer, could lead to higher crosslink network density and, consequently, to improvement in properties[11,12]. Benzoxazine molecules are characterized by the presence of an aromatic benzene ring and an oxazine ring where two carbons are shared among the two rings, as highlighted in red in **Fig. S 14** (Supplementary Information). As polyfunctional monomers, benzoxazines form thermosetting resins when cured, and produce a low surface energy polymer, the polybenzoxazine (PBZ). PBZs have shown lower surface energy than that of polytetrafluoroethylene (PTFE). In addition, PBZ shows low water absorption, resistance to chemicals and UV, high thermal and mechanical properties and near-zero shrinkage upon curing[13,14]. One of the most important characteristics of benzoxazine is its great molecular design flexibility[11]. For this work, an innovative tri-functional benzoxazine was synthesized by reaction between phenol, paraformaldehyde, and melamine under solventless condition and purified by means of a simple and efficient solvent-solvent extraction procedure. The fundamental structure of the obtained monomer is presented in **Fig. 1.3**.

A key implication from the copolymerization that can be observed in **Fig. 1.8** is that number of hydroxyl groups formed during copolymerization of benzoxazine and epoxy is the same as that produced from the homopolymerization of either monomers. As a consequence, the resulting copolymer should present a good interaction with the substrate to which it is applied. As stated previously, adhesion is vital to the performance of a coating.

Herein we report the use of the trifunctional benzoxazine and DGEBA copolymer and investigate the effects of incorporation of varying amounts of silica when the material is used as coating for protection of metallic substrate against corrosion.

4.2. EXPERIMENTAL SECTION

4.2.1. Materials

Epoxy resin was supplied by Allnex Belgium SA. Beckopox® EP385w/56WAMP is a dispersion, 56% solids in water and isopropanol. Hydrophobic fumed silica AEROSIL® R 9200 was supplied by Evonik Corporation. Low-Carbon Steel Sheet (CS) (max. 0.10%C) 0.03 inches thick was purchased from McMaster-Carr Supply Company. The trifunctional benzoxazine (BZ) monomer was synthesized by Mannich reaction between phenol, paraformaldehyde, and melamine in a solventless environment and stoichiometric ratio of 6:6:1. The reactant mixture was magnetically stirred at 50-60 °C for 1 h and heated to 95-100 °C for 9.5 h, followed by cooling to room temperature. The resulting crude BZ monomer was then dissolved in chloroform, washed with 1 N NaOH solution for several times, and rinsed with deionized water until neutral. This preparation method is considered an example of green chemistry, with the minimum use of organic solvents and simple purification methods. All chemicals involved were used as received.

4.2.2. Instrumentation

Optical microcopy images were obtained by an Olympus BH-2 microscope. Coating thickness was measure with a magnetic coating thickness gauge - Tongbao CM-8856FN.Static water contact angle was measured by a CAM 200 Optical Contact Angle Meter (KSV Instruments Ltd.). Gloss was measured according to ASTM D-523 by a GM-268 glossmeter. Pencil hardness test was performed according to ASTM D3363 with a Bevs 1301/1000 tester – 1000g at the tip and 45° angle between pencil and film surface, Mitsubishi pencils. Adhesion test was performed according to ASTM D3359 with a BAOSHISHAN QFH-A film adhesion tester. Electrochemical measurements for the evaluation of anticorrosion property were performed with Autolab PGSTAT 12 Potentiostat (MetroOhm, Inc.). Electrochemical cell with platinum as the counter electrode, Ag/Ag+ as the reference electrode and the carbon steel substrates as the working electrodes in 1M NaCl ultrapure Milli-Q water solution. Potentiodynamic polarization scan (PPS) was performed by scanning from −4 to 0V

with respect to the reference electrode. Scanning electron microscopy (SEM) analysis was performed with a JEOL JSM-6510LV.

4.2.3. Substrate Preparation

Two sizes of substrate were prepared to be coated and tested. The AISI 1008 carbon-steel sheets were cut into 0.5x1.0 inches to be used in electrochemical tests and 3.0x6.0 inches, to be used for all other tests performed. All substrates were cleaned under sonication in acetone for 15 minutes and were kept under vacuum prior to use. Samples of bare substrate (no coating applied) were heated to the same temperatures as that used for curing the coated samples in order to be used as control group. These samples are designated “Bare” in this work.

4.2.4. Compositions of Samples

Five distinct compositions with varying benzoxazine to epoxy ratio were produced to investigate the uniformity of the cured coatings as function of the monomers composition. The BZ to EP weight ratios were varied as follows: 100/0, 75/25, 50/50, 25/75, 0/100. Monomers solutions were prepared by first dissolving each monomer separately in a suitable solvent; BZ monomer in DMSO at a concentration of 1 mg μL^{-1} and EP resin in a 50:50 mixture of ethyl acetate and ethanol at 0.32 mg μL^{-1}. The two monomer solutions were then combined and mixed to form a single homogeneous solution. Resulting material was a translucent liquid as shown in **Fig. S 16 a**.

Additionally, six other compositions were produced regarding silica content for tests of performance of coating. These samples are designated S0, S10, S20, S25, S30 and S40, corresponding to 0, 10, 20, 25, 30 and 40 wt% silica content respectively. For these six compositions, monomers ratio was set to 48% benzoxazine and 52% epoxy. Definition of monomers ratio was based on results from Chapter 3 due to its higher performance i.e. thermal stability, Tg, content of benzoxazine-epoxy heteropolymer and low temperature of cure. Monomers and silica solutions were prepared as described previously. Mixture was agitated in a vortex mixer followed by ultrasonic bath for 10 min. Resulting material was a very homogeneous and whitish liquid, as shown in **Fig.**

S 16 b. Final products revealed low enough viscosity in order to enable spray coating process.

4.2.5. Preparation of coating

Coatings were prepared by two distinct procedures. Substrates were either spray coated in a single layer process by airbrush with 1 ml of the coating solution on each of the 0.5x1.0 in sheet and 5 ml of the coating solution on each of the 3.0x6.0 in sheets, or coated by pouring the solution directly to the substrate. After spray coating, all samples were kept in oven at 65°C for 1h to evaporate the solvents to prevent formation of bubbles during curing process and, therefore, produce a high quality, homogeneous coating upon curing. Afterwards, samples were heated in air flow oven at a rate of 10°C/min from RT to 300°C and held at this temperature for 30 minutes to be thermally cured.

4.3. RESULTS AND DISCUSSION

4.3.1. Wettability of Compositions on Substrate

A fundamental approach was used to investigate the behavior of distinct compositions of the monomers in their use as coating. For that, compositions 100/0, 75/25, 50/50, 25/75, 0/100 were applied to 3.0x6.0” steel sheets, dried and cured accordingly. All samples were very homogeneously sprayed and coating remained homogeneous after drying procedure. However, **Fig. 4.1** reveals huge differences in behavior of the coatings upon curing. Pure benzoxazine (sample 100/0) displayed an intense running effect, leaving areas uncoated or with a very thin layer while it agglomerated at other regions. Pure epoxy (sample 0/100) shows a very good homogeneity with very sparse and small uncoated areas. A very clear trend in the behavior of the samples can be observed, being that wetting of the surface increases with increasing epoxy content. These results show that not only epoxy may improve properties such as crosslink density, but it also promotes stabilization of the coating upon curing.

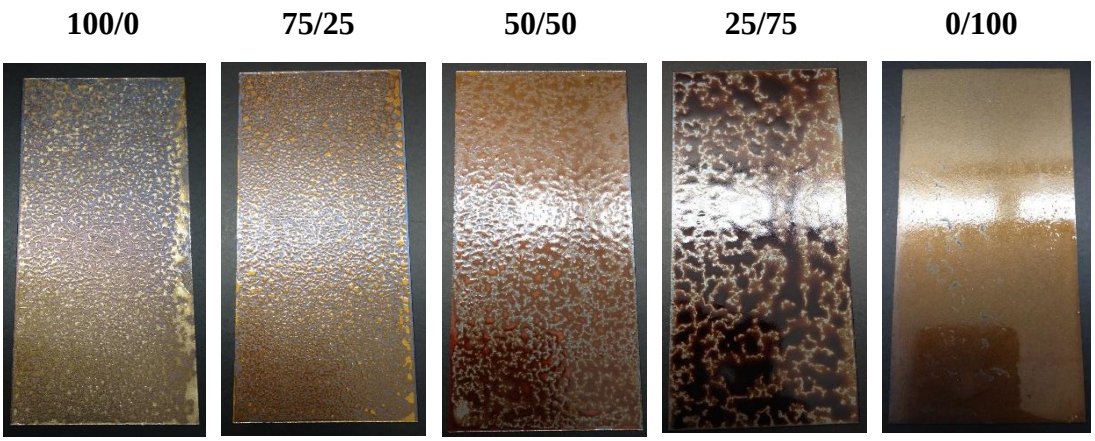

Fig. 4.1. Cured coatings with different benzoxazine to epoxy ratio for investigation of wettability

It is important to emphasize that although, in this particular experiment, no composition covered completely the surface in a uniform manner, this phenomenon is highly influenced by parameters such as material and roughness of substrate and thickness of the coating. Therefore, results obtained in this experiment refer solely to the behavior on the specific substrate and conditions in case. This behavior may be controlled in several ways, which are not object of discussion in this work. As such, these compositions are still likely to be effective as coatings in different conditions. Ratio 48/52 was defined as the composition used for the production of coatings to be further investigated in this work based on the good thermomechanical properties discussed in chapter 3.

- *The following experiments and results refer to samples S0, S10, S20, S30 and S40 as part of the investigation of the effects of different loads of silica particles.*

4.3.2. Surface Morphology - Optical Microscopy

Incorporation of silica particles to the copolymer typically alters the morphology of the coating surface. An analysis procedure of the focus in optical microscopy images was applied in order to assess the implications of the content of particles in the morphology of the coatings. **Fig. 4.2** shows optical microscopy images of samples S0, S20, S25 and S30. Microscope lenses were focused on deepest regions of the surfaces (valleys). As roughness increases, peaks become out of the depth of field range and are, therefore, out of focus. Higher magnifications possess shallower depth of field. The more out of focus the regions are in an image, the higher the distance between valley

and peak, indicating a higher roughness. Therefore, it is possible to notice that varying concentration of SiO_2 changes intensely the surface morphology of the coatings. Sample S0 displays a relatively smooth surface, with all area in focus even at magnifications of 200X, and only slight undulations can be noticed on the surface. Sample S20 reveals higher roughness than that of S0, characterized by very localized and small out-of-focus regions (red arrows) observable in 200X magnification. Sample S25 shows clear out-of-focus regions at 100X magnifications (red arrows). Sample S30 displays large areas further from focus, noticeable in 100X magnification and more evident at 200X.

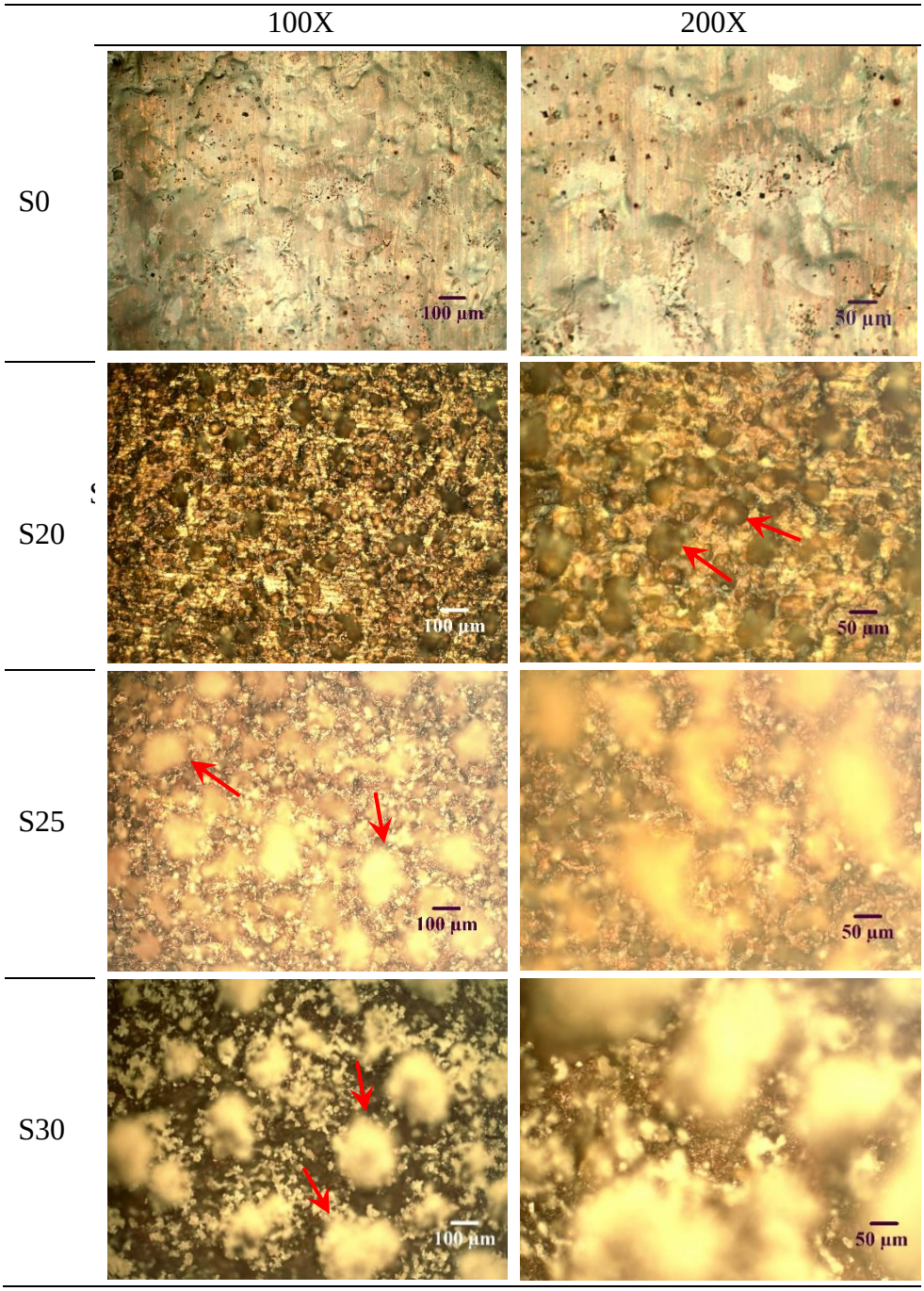

Fig. 4.2. Optical Microscopy Images of Surface of samples S0, S20, S25 and S30 at 100x and 200x magnification

Additionally, images were deliberately obtained with focus on the deepest regions of the surface irregularity (valleys), where thickness of coating is minimal. It is possible to observe that coating is continuous, presenting no cracks or lack of coating material. This result is important and indicates that silica stabilized the coating during cure process, preventing the running phenomenon observed in **Fig. 4.1**. Continuity on

coatings is essential to ensure maximum isolation of substrate from corrosive environment media.

Fig. S 17 shows optical microscopy image of sample S30 at 50X magnification. This image allows a better observation of the surface morphology with a larger depth of field provided by a lower magnification comparatively to those of **Fig. 4.2**. It is possible to notice a highly rough surface, with very well defined protrusions. Texture and translucency of these protrusions suggest high volume fraction of silica, possibly higher than the average of the sample. As discussed in supplementary material, application process is determining to the surface morphology of the coating. Spray coating produced a top layer with high silica concentration in the form of agglomerates. Both, the rough surface morphology with very intense variations in height between the peaks and valleys at a high spatial frequency, and the high concentration of the hydrophobic silica, explain the contact angles observed over 150° discussed further in section 4.3.4.

4.3.3. Thickness of coatings

Thicknesses of compositions S0, S20 and S30 were measured by a magnetic digital coating thickness gauge. Eight samples were measured at five locations each for every composition. Results are depicted in **Fig. 4.3**, where dashed line is the trend of the overall averages. Firstly, it is clear that there is a slight increase in the thickness with the increase in silica content. As could be observed and was discussed previously, incorporation of silica generated a more porous and rough coating. This phenomenon explains the trend of increase in thickness, as the same volume of product was sprayed on all substrates. Roughness on samples containing silica account for the higher volume of the coating after cure. Secondly, it can be observed that standard deviation is highest in sample S0 and lowest in sample S20. As discussed in sections 4.3.1 and 4.3.2, samples with no silica showed defects due to running of the resin, resulting in great variation of thickness, hence, the large deviations. Composition S20 revealed a highly homogenous and smooth surface, as can be observed in **Fig. 4.2**. Interestingly, 20 wt% silica content was able to stabilize the coating during cure procedure to a point where thickness homogeneity is maximum. Sample S30, on the other hand, revealed a slight increase in dimensional variance.

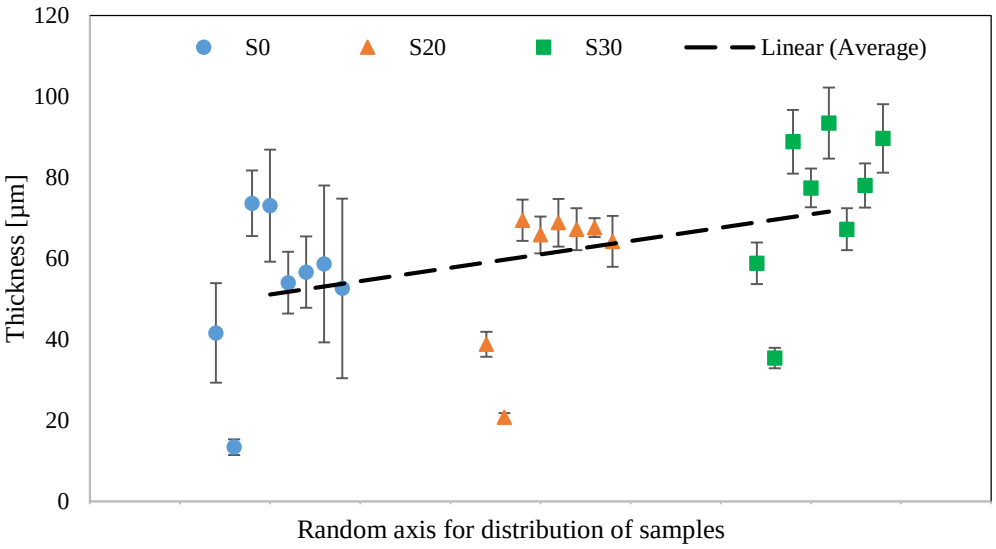

Fig. 4.3. Thickness measurements and standard deviation bars of each sample by composition

4.3.4. Contact Angle on Sprayed Samples

Contact angle (CA) was measured by three droplets on each sample, accounting for the angle at both sides of the droplet, totalizing 6 data points for each sample. **Fig. 4.4** shows the average CA and standard deviation for each sample.

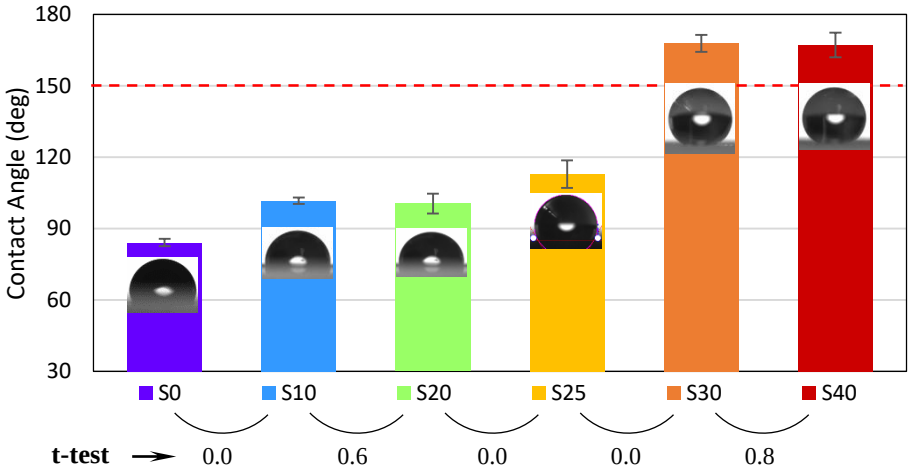

Fig. 4.4. Contact angle of sprayed coatings as function of silica content

Table 4.1. Summary of CA data

Sample	S0	S10	S20	S25	S30	S40
CA (deg)	84.1	101.7	99.2	112.9	167.8	167.1
Std Dev	1.5	1.4	2.4	5.7	3.6	5.2

Sample S0 shows a slightly hydrophilic behavior with a contact angle of 84°. This result can be explained by the smoothness of the surface, which is observable by the shiny aspect of similar samples in section 4.3.1 and in discussion further in section 4.3.5. Additionally, the presence of hydroxyl groups originated from the ring opening polymerization promotes a reduction in solid-liquid free energy[16]. Both these aspects promote a reduction in CA. Sample S10 shows change to hydrophobic behavior, reaching 102° CA. Sample S20 shows 99° CA. It is a similar result to that of sample S10. Evaluation by t-test revealed that data is statistically equivalent. This result indicates that the same mechanism is influencing CA on samples S10 and S20. In addition, the effect of silica on this particular mechanism has reached a plateau. Sample S25 showed slight increase in hydrophobicity. An obvious sudden variation in CA can be observed from the hydrophobic sample S25 to the Superhydrophobic sample S30, as CA surpassed the 150° angle. This phenomenon can be assigned to a transition thru a critical condition of surface morphology. Possibly, the percolation threshold of the particles was reached, producing porosity and bringing the surface to a condition that allows entrapment of air between the water droplet and the coating surface, characterizing the Cassie-Baxter model condition[17]. Sample S40 shows no change in CA when compared to sample S30. Similarity in data is confirmed by t-test as shown in **Fig. 4.4**. Interestingly, another plateau was reached within this hydrophobicity mechanism. Furthermore, standard deviation of contact angle displays an increase trend with increasing content of SiO_2. Meaning surface becomes less homogeneous throughout the sample with the increase in SiO_2 content.

Relationship between contact angle of all spray coated compositions and wettability models, namely Cassie-Baxter's, Wenzel's and Young's was investigated. Cassie-Baxter's equation calculates a higher contact angle than Wenzel's [17–20]. Sample S30 reveals a CA higher than 150°, characterizing superhydrophobic behavior. **Fig. S 18** shows sample S30 submerged in water. It is possible to observe air bubbles on the surface of the coating. This behavior indicates the hydrophobicity and the tendency of the surface to trap air pockets within its asperities. This suggests that during contact angle measurements, droplets were in the Cassie-Baxter state for sample S30. The intense decrease in contact angle observed from S30 to S20, combined with the absence of air bubbles observed in **Fig. S 18**, suggest that during contact angle measurements, droplets were in the Wenzel state for sample S20.

In order to evaluate whether the CA data follows a natural behavior or if the information collected was externally influenced, data points were fitted to a logistic curve given by[21–23]:

$$f(x) = S.\frac{e^{\gamma k(x-x_0)}}{1+e^{\gamma k(x-x_0)}} + f_0 \quad (1)$$

Where,

S - saturation value,

γ - growth rate

x_0 - value of the controlling variable at which ***f*** reaches half of its saturation value

f_0 – initial value of contact angle

Fig. 4.5 shows fitting of the logistic curve to the contact angle experimental data points. It is clear that a very good fitting was obtained, as indicated by the coefficient of determination. Special attention to point S25 reveals a perfect fit to the model. This fitting analysis indicates that the behavior of contact angle as a function of silica content, indeed, follows a natural behavior, suggesting that data obtained experimentally does represent interfacial phenomena, with no external influences. The identified natural sudden change in wettability behavior can be associated with a shift from Wenzel's model to Cassie-Baxter's.

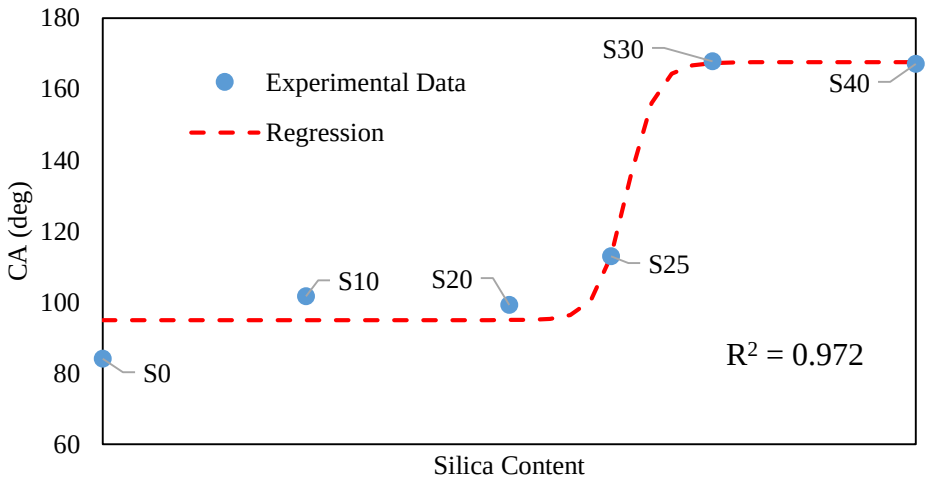

Fig. 4.5. Logistic curve fitting to CA data points

Additionally, in order to assess the influence of the application method of the coating to the substrate on the hydrophobicity, some coating samples were also

produced by directly pouring the solution on the substrate. If, in one hand, spray coating generates high shear strains and turbulence on the fluid, on the other hand, by pouring slowly the solution on the substrate surface, it is possible to induce almost no disturbance on the fluid. Additionally, spray coating tends to promote huge evaporation of the solvents during the travel of the droplets from the spray gun to the surface. In pouring procedure, evaporation of solvents is negligible upon application. For these reasons, it can be understood that these are very distinct processes and, in the mentioned aspects, opposite from each other. Results are discussed in supplementary material.

4.3.5. Gloss

The gloss of the different samples was measured in terms of gloss units (GU). Gloss of a sample is influenced by several factors, including surface texture [24,25] and refractive index [26]. Regarding the surface texture, the higher the surface roughness, the lower the gloss [25]. In addition, considering that for several materials, the refractive index does not vary as much, being close to 1.5, the incorporation of silica particles will cause only a minor influence on the gloss value in comparison to the unfilled polymer [26]. Therefore, it can be considered that the gloss of the samples within this work is strongly dependent and inversely related to their roughness.

The gloss test was, thus, used to investigate the correlation of the roughness to the behavior of water droplets on the surface of the samples, described in terms of contact angle. Initially, gloss of samples S0 and S10 was measured with the glossmeter under geometry 60° and was classified as semi-gloss as per DIN EN13300:2001. Data was converted to geometry 85° per ISO2813:2014 in order to enable comparison with the other samples. Results for samples S0 and S10 show that incorporation of 10 wt% silica did not alter significantly the surface morphology, as indicated by the small reduction of ≈ -12.5% in the gloss value, as shown in **Fig. 4.6**. Furthermore, results from CA and gloss are coherent, as lower gloss indicates higher surface roughness which, in its turn, tends to influences wettability of the surface by increasing CA. Interestingly, 10 wt% silica was sufficient to transition the coating from hydrophilic to hydrophobic, altering CA from 84° to 102°. It is important to highlight that the silica used in this work is functionalized to be hydrophobic, therefore, not only it has an effect on surface morphology, which affects wettability but, intrinsically, it makes the material more hydrophobic due to the chemical groups grafted to the silica particles.

Increasing content of silica to 20 wt% decreased dramatically gloss of the coating, making it necessary to switch the scale of the glossmeter to geometry 85°. Interestingly, this intense decrease in gloss, associated with an increase in surface roughness, did not reflect in an equivalent increase in contact angle (**Fig. 4.4**). In fact, CA is statistically the same as that of sample S10, as revealed by t-test shown in **Fig. 4.4**. This discrepancy between the change in CA and the change in gloss indicates once more that surface roughness is not the only aspect influencing CA. Sample S25 revealed a pronounced decrease in gloss (≈ -65%) when compared to S20. This result agrees with the observed increase in CA (**Fig. 4.4**). Sample S30 displays barely any gloss and is described as dead-matt according to DIN EN13300:2001 standard. The variation in relation to S25 was very intense (≈ -87%), and agrees directly with the variation in CA. As described by the logistic equation (1), it can be presumed that a threshold was reached, such as the maximum volume fraction content of silica or the percolation threshold, at which particles reach a long range influence, creating a macro connectivity, as suggested in literature [27], and possibly, a cumulative effect of the particles. This long range influence may be the origin of the porosity observed by microscopy investigation discussed further in section 4.3.9. Sample S40 displays a similar gloss to that of sample S30, once again agreeing with the values of contact angle measurement. From this result, it can be inferred that roughness reached a maximum.

Gloss results are coherent with that of contact angle (section 4.3.4) in two aspects: they revealed an inverse relationship between gloss and CA, indicating a high influence of the surface roughness on the contact angle, and both experiments reveal plateaus between samples before sample S10 and after sample S30.

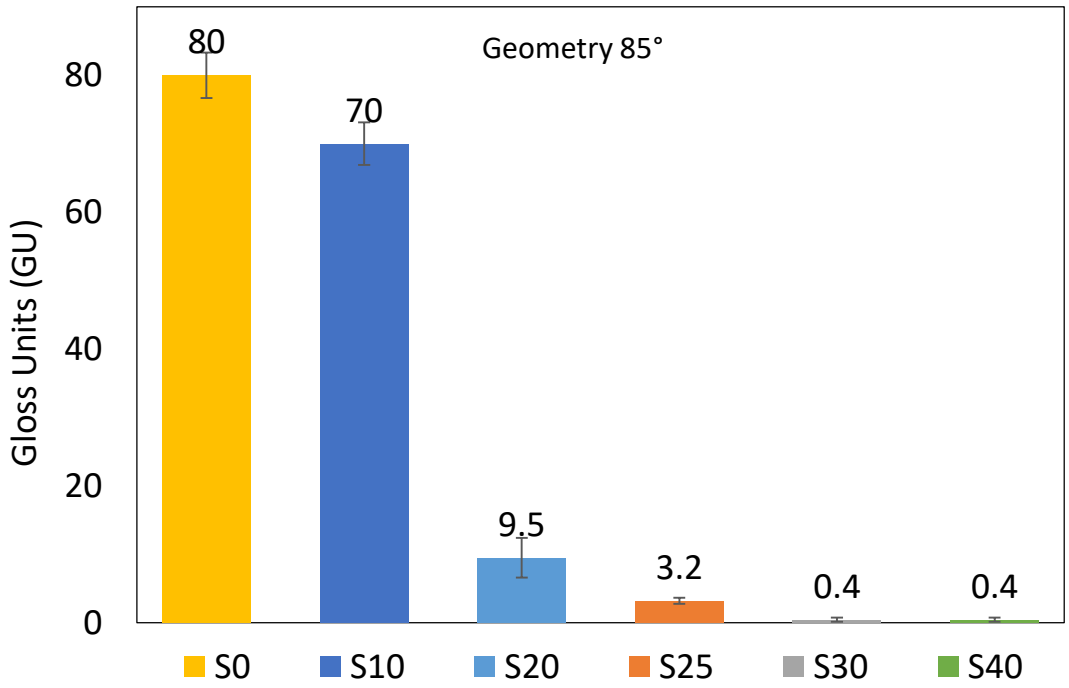

Fig. 4.6. Gloss of sprayed coating as function of silica content - Geometry 85°.

4.3.6. Scratch

Optical microscopy images from scratch tests are depicted in **Fig. 4.7**. Results exhibited were obtained with a 1000g tester and 6H leads, as the most aggressive requirement from the tool set. It is possible to observe that none of the samples were scratched by the lead. In fact, it is noticeable the large amount of graphite deposited on the surface of the coating, meaning that the referred coating materials are harder than the leads. One interesting observation is how the volume of graphite on the surface of each sample increases with increasing concentration of silica. This outcome indicates that the roughness of the surface increases with the increasing concentration of silica, which makes the surface more abrasive to the lead, ratifying the results analyzed in sections 4.3.4 and 4.3.5.

The high hardness observed in these samples can be explained due to the fact that the polymeric matrix of these coatings is composed of domains of polybenzoxazine, epoxy and their copolymer. Polybenzoxazines are known to be hard materials[11,28], the copolymer of benzoxazine and epoxy possesses high crosslinking density[12,14], furthermore, a high degree of conversion upon curing is observed in chapter 3.

Furthermore, the scratch tests were performed at room temperature, that is much lower than Tg of the copolymer (chapter 3). This means that coatings were at glassy state, with very low mobility of the polymeric molecules. The coatings possess, then, intrinsically several features that promote hardness and, therefore, it is evident that the resulting materials are hard, as can be observed in **Fig. 4.7**.

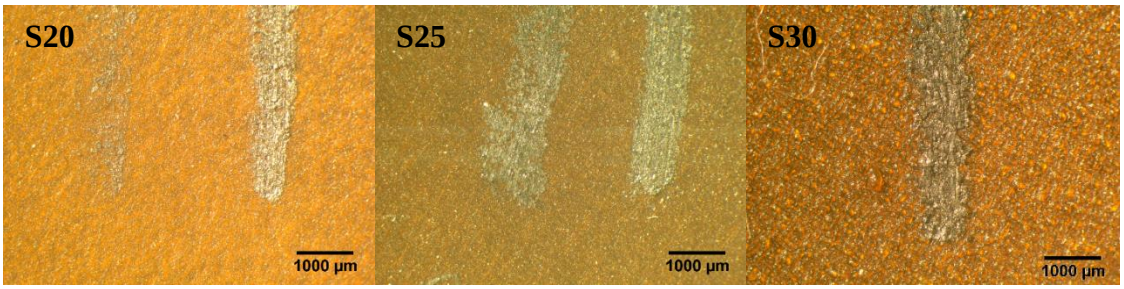

Fig. 4.7. Optical Microscopy Images of Coating Surfaces After Scratch Test – S20, S25 and S30

4.3.7. Adhesion

Adhesion of the coatings to the substrate was assessed by tape test according to ASTM D3359-17. **Fig. 4.8** displays optical microscopy images with 75X magnification of samples S20, S25 and S30 after adhesion test. Sample S20 reveals very fine lines of the cross cuts and no material removed from any of the squares or from the intersections, placing the sample in the best performing classification (5B) according to ASTM D3359-17. Sample S25 shows cracking and consequent detaching of the coating in the proximity of the scratch. This result reveals that S25 is hard and brittle. As the testing tool scratched throughout thickness of the coating, cracks were formed and pieces of coating adjacent to the scratch were removed. Additionally, it is possible to observe regions of the coating in the surroundings of the scratch with a lighter color (red arrow). This region of the coating is detached from the substrate, further indicating that the coating possesses high rigidity, as small deformations caused by the tool in the region of the scratch debonded some areas, indicating that the coating material did not have enough resilience to absorb such deformation. Adhesion test was performed despite the damage caused by scratching and, interestingly, results revealed no further removal of coating material. This sample was not matched to a classification according to ASTM D3359-17 due to this type of damage not being foreseen by the standard. Sample S30 shows similar behavior to that of S25, as material was removed from coating during scratching procedure. However, differences can be observed in the

extent of the damage. A narrower region immediately adjacent to the scratch pattern was affected. No long range detachments can be observed. This difference can be assigned to an increase in brittleness of the material caused by the larger content of particles, causing the coating to break locally. This sample was tested to adhesion despite previous damage and showed no further removal of coating material. Result was not classified according to ASTM D3359-17 due to previous damage.

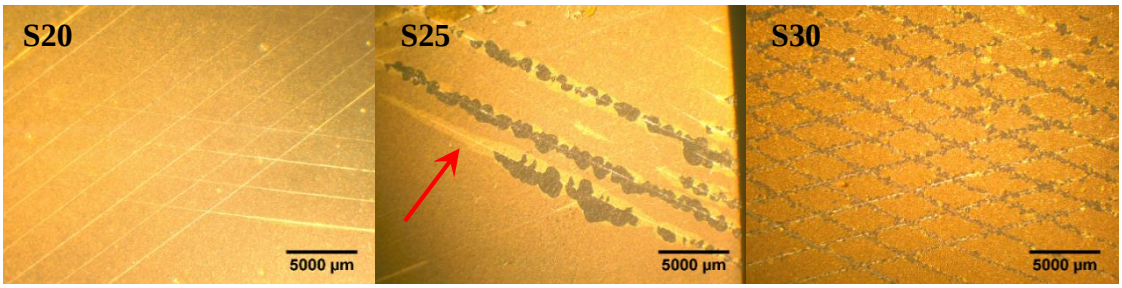

Fig. 4.8. Optical Microscopy Images of Coating Surfaces After Adhesion Test – S20, S25 and S30

Overall, it can be concluded that the three samples showed excellent adhesion performance. Furthermore, taking in consideration scratch tests in section 4.3.6, it can be inferred that samples S25 and S30 show high resistance to scratch due to high hardness of the material however, the increasing hardness caused it to behave in a brittle manner when scratch was effectively achieved.

4.3.8. Electrochemical Corrosion Test

Fig. 4.9 shows potentiodynamic polarization scan (PPS) curves in the near zero-current region for investigation of the Tafel-type behavior, comparison of i_{corr} and analysis of damage to the surface of samples. The sample without any coating (Bare) displays an i_{corr} of 3.0 $\mu A.cm^{-2}$, which was measured at the extrapolation of the cathodic Tafel line (red), where it crosses the zero-current potential[29]. It is also possible to notice that the same procedure, when applied to the anodic Tafel line (green), results in a current of 4.0 $\mu A.cm^{-2}$, different than that of i_{corr}. This phenomenon is explained in literature[29] by changes in the electrode surface, such as roughening, during the test run. This result is coherent, as roughening of the surface typically increases corrosion rate, which is directly proportional to the measured electrical current, as presented further in **equation 2**. Additionally, roughening of the surface could be observed by naked eye and is presented in **Fig. 4.10**, corroborating the results from electrochemical test. **Fig. 4.10** shows images of samples before and after electrochemical test for

investigation of surface degradation. It is possible to observe that the sample without any coating (Bare) reveals an intense corrosion in a circular shape, relative to the region of the samples that was exposed to the electrolyte media during electrochemical test. Result was expected for a low carbon steel in contact with NaCl-water solution and under voltage during test. Sample S0 shows an i_{corr} of 0.22 $\mu A.cm^{-2}$, indicating reduction in corrosion rate when compared to sample Bare. Protection efficiency was calculated to be 92.7%. This result is coherent as the presence of the coating isolates the substrate from the corrosive media. Interestingly, high effectiveness of this coating could be observed despite the presence of defects on the coating, as shown **Fig. 4.10** and discussed in section 4.3.1. This sample shows no visible degradation of the coating after electrochemical test. However, it is possible to notice that on defective regions, color changed from a shiny silver to a matte brown, suggesting corrosion on those spots. This sample is further analyzed in **Fig. S 20**. PPS Analysis of sample S0 reveals a difference between the currents of the cathodic and anodic portions of the curve can also be noticed. However, differently from sample Bare, current displays a decrease from cathodic to anodic (red to green, respectively). This reduction in current is directly related to a decrease in corrosion rate and can be assigned to formation of oxide film on the substrate[29]. Possibly, the size of defects (~ 500 µm) is small enough to keep the oxide film formed during the test attached to the surface working as passivation material. Sample S20 shows an i_{corr} of 0.01 $\mu A.cm^{-2}$, indicating further improvement in protection against corrosion. Protection efficiency was calculated to be 99.7%. It is interesting to observe that both, cathodic and anodic currents, are the same. This result indicates that no change in the surface of the substrate occurred, making it clear that this coating was effective in protecting the substrate against corrosion. Analysis of microscopy images in **Fig. 4.10** reveals highly uniform surface and no observable degradation is present, indicating a great chemical resistance of the coating material to the corrosive condition to which it was expose. Sample S30 shows an i_{corr} of 0.002 $\mu A.cm^{-2}$, revealing huge improvement in protection against corrosion. Protection efficiency was calculated as 99.9% with respect to the sample without any coating. Sample S30 also reveals no changes in surface roughness of the substrate, which is characterized by the same values of cathodic and anodic current. Analysis of microscopy images in **Fig. 4.10** reveals no degradation from electrochemical test.

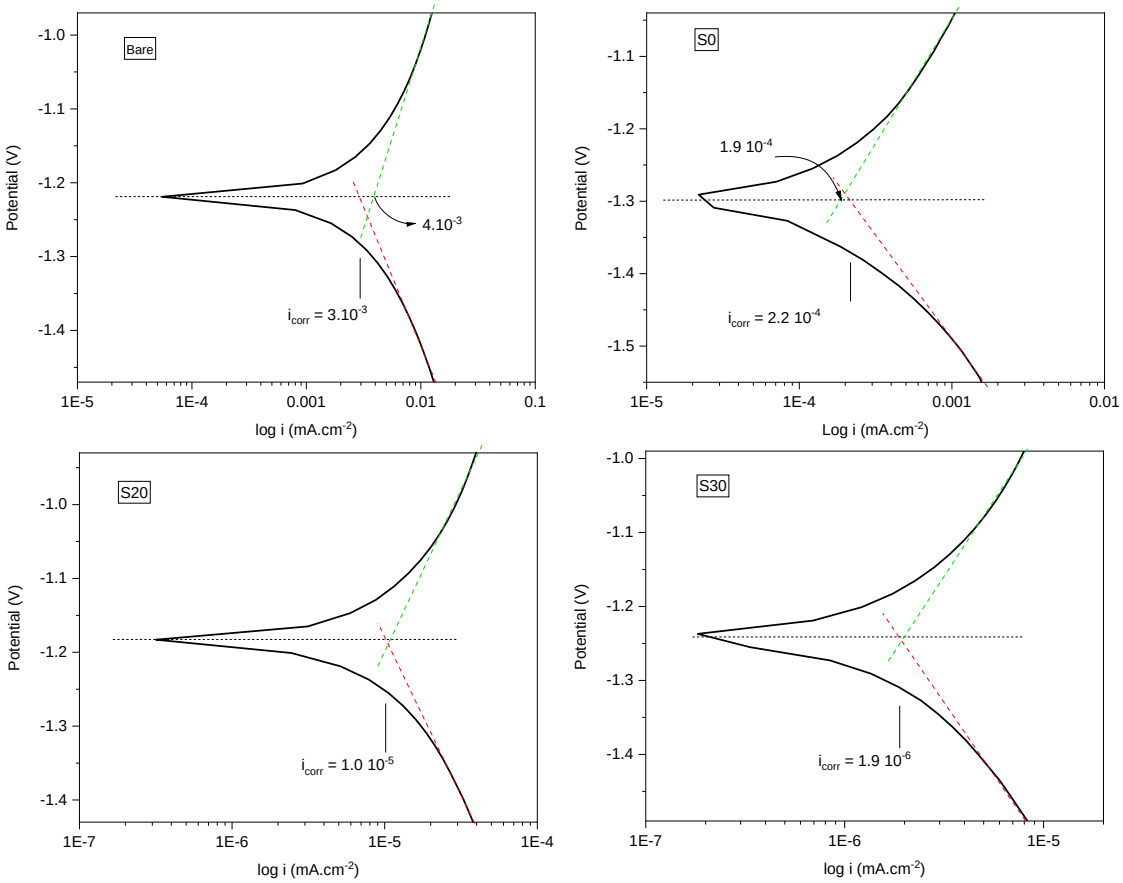

Fig. 4.9. Potentiodynamic polarization curves in the near zero-current region of sample Bare, S0, S20 and S30

Table 4.2 summarizes results from PPS. Corrosion rate (CR) is calculated according to equation 2[33]. Sample Bare, as control group, revealed highest corrosion rate, as anticipated. CR is drastically reduced with the application of coating and, interestingly, addition of silica to the coating material contributes intensely to reduction of corrosion rate. Sample S0 had CR decreased by nearly 14x when compared to sample Bare. The coating was highly effective despite the defects generated during cure procedure. As discussed in sections 4.3.1 and 4.3.2, silica provided stability to the process of cure, resulting in a more continuous coating. As such, sample S20 had its CR further decreased by 300x when compared to sample Bare. Additionally, as discussed previously, silica influenced greatly the hydrophobicity. Hydrophobic coatings repel water and, therefore, hindered absorption of the corrosive media and the diffusion of O_2 and ions. Consequently, sample S30 revealed the best performance against corrosion, with CR 1500x lower than that of sample Bare. Additionally, it has been widely investigated that particles may improve anti-corrosion protection due to a

lengthening of the path for ions to travel from the corrosive media to the surface of the substrate by forcing the ions to deviate from the particles[30–32].

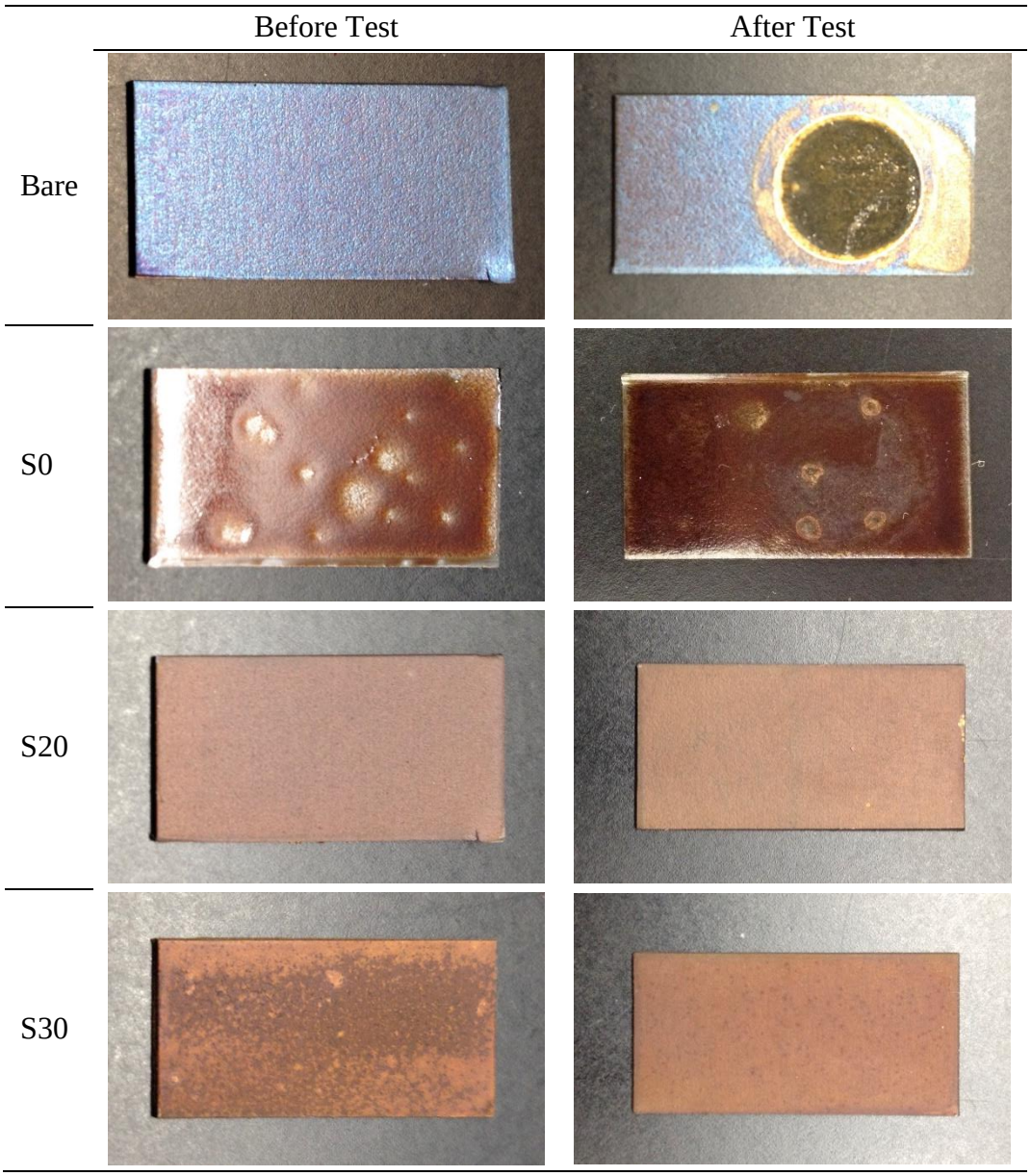

Fig. 4.10. Images of samples Bare, 0%, 20%, 30% before and after electrochemical test for investigation of surface degradation

Table 4.2. Data from PPS experiment of samples Bare, S0, S20 and S30

Sample	I_{corr} ($\mu A.cm^{-2}$)	E_{corr} (V)	CR (mm/year)	R_P (ohm)	PE (%)
Bare	3.0	-1.22	$3.84\ 10^{-2}$	21	-
S0	0.22	-1.30	$2.82\ 10^{-3}$	372	92.7
S20	0.01	-1.18	$1.28\ 10^{-4}$	6498	99.7
S30	0.002	-1.24	$2.56\ 10^{-5}$	35120	99.9

$$\boldsymbol{CR = \frac{i_{corr}.K.EW}{\rho}} \quad (2)$$

Where,

CR – Corrosion Rate

i_{corr} – Corrosion Current Density

K – Constant to adjust units of CR

EW – Equivalent Weight - mass of species that reacts with one Faraday of charge

ρ – Density of Substrate

Similarly, polarization resistance (R_P) was analyzed and it describes the same behavior as that observed by CR for all samples. R_P is defined as the resistance of the sample to oxidation during the application of an external potential[34]. R_P increased with the application of coating and improved even further with the increasing silica content.

4.3.9. Surface Morphology - SEM

Scanning Electron Microscopy (SEM) was performed to further investigate the surface morphology and analyze the effect of the electrochemical test on the different samples. **Fig. 4.11** shows SEM images at 500X and 1000X magnification for comparison of the surfaces of samples before and after electrochemical test. It is possible to observe that the surface of the bare sample is fairly smooth before the electrochemical test. It is intensely degraded by the electrolyte media, as can be identified by subsequent images, which reveal a huge irregularity on the surface. Sample S0 is very smooth prior to electrochemical test. This information is in

agreement with results from gloss measurements, optical microscopy images and naked eye pictures. After testing, surface of S0 sample shows no signs of degradation, revealing a very good resistance to the electrolyte media under testing conditions of voltage and current. Sample S20 reveals roughness prior to testing, characterized by the circular pores in the range of 1 – 25 μm. After testing, no degradation on the surface can be noticed despite the increased roughness, which increases greatly the interface area between coating and corrosive media and, consequently, the potential for an electrochemical reaction. Sample S30 shows even greater porosity when compared to sample S20. Interestingly, size of pores is the same in both samples nevertheless, pores revealed to be much deeper in sample S30. Similar to the other coatings, behavior upon electrochemical testing revealed no observable degradation due to electrolyte media. The level of porosity of all samples and the relationship with contact angle behavior is in perfect agreement with literature[17], which states that when the surface is rough but not porous, it can be modeled by Wenzel's equation, and that porosity should change the model to Cassie-Baxter's.

Overall, it can be observed that increasing amounts of silica produced higher porosity on samples. This result is in agreement with gloss test, which revealed that samples with higher content of silica displayed higher surface roughness. Additionally, it is possible to notice that all coatings were highly resistant to the corrosive media i.e. 1M brine under testing conditions, indicating great possibility of protection of the substrate against salt water.

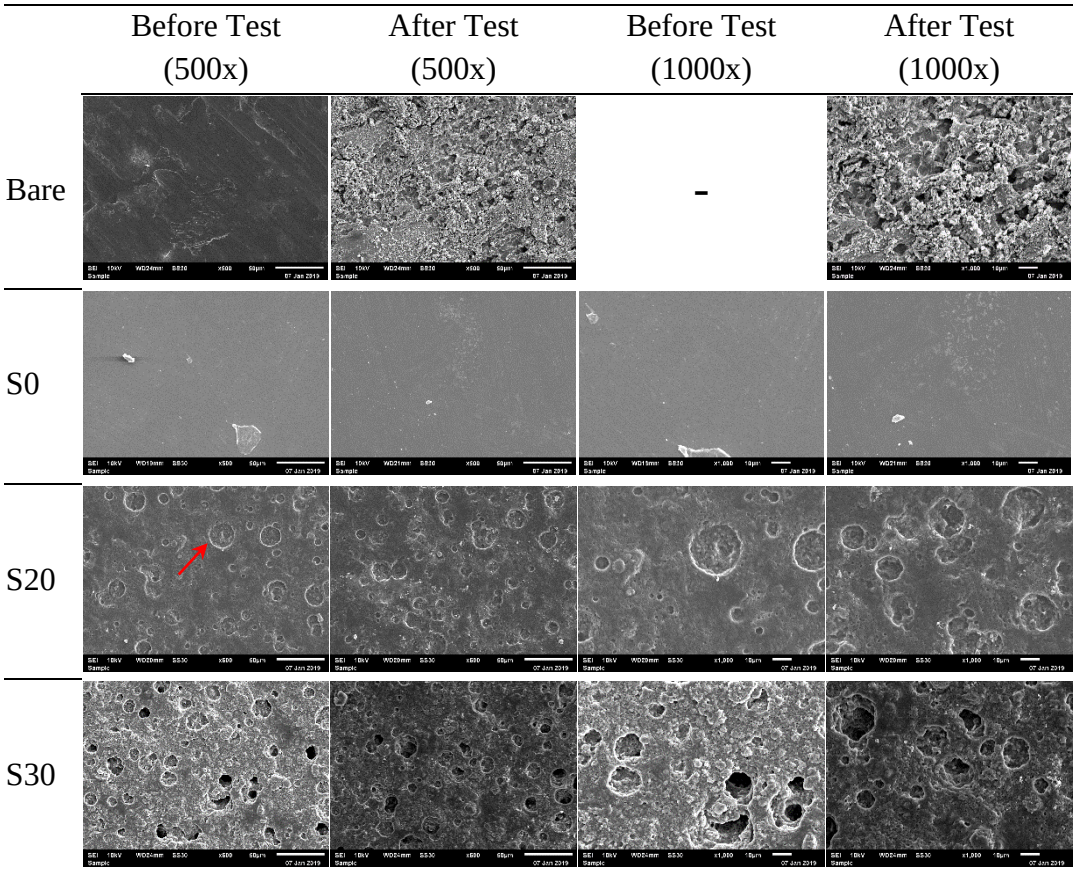

Fig. 4.11. SEM images of samples Bare, 0%, 20%, 30% before and after electrochemical test at 500X and 1000X magnification

4.4. CONCLUSIONS

Trifunctional benzoxazine, epoxy and functionalized fumed silica were successfully used to produce coatings and investigate performance of different compositions. Compositions varying from 100/0 to 0/100 revealed distinct behavior of the coating upon curing. Clear trend shows wettability improvement with increasing content of epoxy. Optical microscopy images showed increasing roughness with the increase in silica content. Thickness of coating S0 revealed high inhomogeneity due to running effect upon curing. Sample S20 showed outstanding homogeneity, both among samples and within the samples. S30 showed a good homogeneity. Furthermore, a slight increase in thickness could be observed and was attributed to the presence of porosity. Contact angle experiment revealed improved hydrophobicity with increasing content of silica for sprayed samples. Loading had unquestionable but small effect on CA up to 25% content. Obvious sudden increase in CA is observed in composition S30 and above. Samples produced by pouring revealed increasing contact angle with the increase in silica content, however, hydrophobicity performance was not as evident as

for sprayed samples. Gloss experiment showed evident decrease in gloss with the increase in silica content, indicating roughening. Gloss does not follow the exact trend as contact angle, indicating that roughness was not the only mechanism influencing contact angle. Results were supported by optical microscopy results. Scratch test revealed high resistance of samples S20, S25 and S30. Adhesion tests showed high adhesion of sample S20, as 5B classification according to ASTM D3359-17. Samples S25 and S30 performed well on adhesion experiment, however, these samples showed cracking and detaching upon cutting. PPS electrochemical test revealed increasing protection against corrosion with increasing silica content. Sample S30 showed best result with corrosion rate 1500x lower than uncoated sample. Additionally, analysis of electrochemical plots revealed that samples Bare and S0 suffered degradations of the substrate, while S20 and S30 showed no damage on the substrate. Visual inspection of samples confirmed degradation of substrate of samples Bare and S0. Additionally, it revealed no degradation of any of the coating compositions during electrochemical test. SEM analysis revealed huge degradation of substrate surface on sample Bare, supporting results from PPS and visual inspection. No coating showed degradation upon electrochemical test. Furthermore, roughness and porosity of samples could be observed increasing with the increase in silica content, once more supporting results from CA and gloss.

Bibliography

[1] P.R. Roberge, Handbook of Corrosion Engineering, McGraw-Hill, 1999. https://linkinghub.elsevier.com/retrieve/pii/S0026057600834455.

[2] A. Overview, R.A. Dickie, F.L. Floyd, Polymeric Materials for Corrosion Control, (1986).

[3] K. Gerhardus, V. Jeff, N. Thopson, O. Moghissi, M. Gould, J. Payer, International Measures of Prevention , Application , and Economics of Corrosion Technologies Study, (2006) 1–216.

[4] L.M. Schmidt, International Measures of Prevention, Application, and Economics of Corrosion Technologies Study, NACE Int. (2016) 1–216. http://impact.nace.org/documents/Nace-International-Report.pdf%0Apapers3://publication/uuid/9784056A-47E3-4988-8D70-B6763CF35EBF.

[5] D.E. Tallman, Æ.G. Spinks, Æ.A. Dominis, G.G. Wallace, Electroactive conducting polymers for corrosion control, (2002) 73–84. https://doi.org/10.1007/s100080100212.

[6] C. Augustsson, Nm Epoxy Handbook, Third Edit, 2004.

[7] A.G. Roberts, Organic Coatings - Properties, Selection and Use, United States Department of Commerce, 1968.

[8] A.P.O. Costa, A.E. Gerbase, C.L. Petzhold, Investigação da Cinética de Cura por Calorimetria Diferencial Exploratória (DSC) de Resinas Epóxi Preparadas a partir de Óleo de Soja Epoxidado com Diferentes Anidridos e Aminas Terciárias, Polímeros. 21 (2011) 146–150. https://doi.org/10.1590/s0104-14282011005000022.

[9] M.A. Boyle, C.J. Martin, J.D. Neuner, ASM HANDBOOK - Composites, ASM International, 2001.

[10] H. Ishida, D.J. Allen, Physical and mechanical characterization of near-zero shrinkage polybenzoxazines, J. Polym. Sci. Part B Polym. Phys. 34 (1996) 1019–1030. https://doi.org/10.1002/(SICI)1099-0488(19960430)34:6<1019::AID-POLB1>3.0.CO;2-T.

[11] S. Rimdusit, C. Jubsilp, S. Tiptipakorn, Alloys and Composites of Polybenzoxazines:Properties and Applications, Springer. (2013). https://doi.org/10.1007/978-981-4451-76-5.

[12] S. Kumar, C.P.R. Nair, Polybenzoxazines: Chemistry and Properties, Smithers Rapra Technology, 2010.

[13] E.B. Caldona, A.C.C. De Leon, P.G. Thomas, D.F. Naylor, B.B. Pajarito, R.C. Advincula, Superhydrophobic Rubber-Modified Polybenzoxazine/SiO2Nanocomposite Coating with Anticorrosion, Anti-Ice, and Superoleophilicity Properties, Ind. Eng. Chem. Res. 56 (2017) 1485–1497. https://doi.org/10.1021/acs.iecr.6b04382.

[14] H. Ishida, Handbook of Benzoxazine Resins, 1st ed., Elsevier B.V., 2011. https://doi.org/10.1016/B978-0-444-53790-4.00046-1.

[15] L.R. de Souza, J.R.M. D'Almeida, R.C. Advincula, Benzoxazine-Epoxy copolymer – Characterization of Thermal Properties and Investigation of Cure, Submitted. (n.d.).

[16] M.A. Butkus, D. Grasso, The nature of surface complexation: A continuum approach, Environ. Geol. 40 (2001) 446–453. https://doi.org/10.1007/s002540000186.

[17] A.B.D. Cassie, S. Baxter, WETTABILITY OF POROUS SURFACES, Trans. Faraday Soc. 40 (1944) 546–551.

[18] K.J. Kubiak, M.C.T. Wilson, T.G. Mathia, P. Carval, Wettability versus roughness of engineering surfaces, Wear. 271 (2011) 523–528. https://doi.org/10.1016/j.wear.2010.03.029.

[19] M.E. Schrader, Young-Dupre Revisited, Langmuir. 11 (1995) 3585–3589. https://doi.org/10.1021/la00009a049.

[20] M.R. Rahimpour, M.A. Esmaeilbeig, Membrane Wetting in Membrane Distillation, Elsevier Inc., 2019. https://doi.org/10.1016/B978-0-12-813551-8.00006-1.

[21] J.R.M. D'Almeida, S.N. Monteiro, The effect of the resin/hardener ratio on the compressive behavior of an epoxy system, Polym. Test. 15 (1996) 329–339. https://doi.org/10.1016/0142-9418(95)00037-2.

[22] W.J. da Silva, L.M. Prioli, A.C.N. Magalhães, A.C. Pereira, H. Vargas, A.M. Mansanares, N. Cella, L.C.M. Miranda, J. Alvarado-Gil, Photosynthetic O2 evolution in maize inbreds and their hybrids can be differentiated by open photoacoustic cell technique, Plant Sci. 104 (1995) 177–181. https://doi.org/10.1016/0168-9452(94)04026-D.

[23] J.R. de S. Passos, S.Z. de Pinho, L.R. de Carvalho, M.M. Mischan, Critical points in logistic growth curves and treatment comparisons, Sci. Agric. 69 (2012) 308–312. https://doi.org/10.1590/S0103-90162012000500004.

[24] Y.X. Ho, M.S. Landy, L.T. Maloney, Conjoint measurement of gloss and surface texture: Research article, Psychol. Sci. 19 (2008) 196–204. https://doi.org/10.1111/j.1467-9280.2008.02067.x.

[25] V. Honson, Q. Huynh-Thu, M. Arnison, D. Monaghan, Z.J. Isherwood, J. Kim, Effects of Shape, Roughness and Gloss on the Perceived Reflectance of Colored Surfaces, Front. Psychol. 11 (2020) 1–17. https://doi.org/10.3389/fpsyg.2020.00485.

[26] F. Faul, The influence of Fresnel effects on gloss perception, J. Vis. 19 (2019) 1–39. https://doi.org/10.1167/19.13.1.

[27] L. Shi, J. Hu, X.D. Lin, L. Fang, F. Wu, J. Xie, F.M. Meng, A robust superhydrophobic PPS-PTFE/SiO2 composite coating on AZ31 Mg alloy with excellent wear and corrosion resistance properties, J. Alloys Compd. 721 (2017) 157–163. https://doi.org/10.1016/j.jallcom.2017.05.333.

[28] S. Rimdusit, W. Bangsen, P. Kasemsiri, Chemorheology and Thermomechanical Characteristics of Benzoxazine-Urethane Copolymers, J. Appl. Polym. Sci. 121 (2011) 3669–3678. https://doi.org/10.1002/app.34170.

[29] G.S. Frankel, M. Rohwerder, Encyclopedia of Electrochemistry vol. 4 - Corrosion and Oxide Films, 2007. https://doi.org/10.1002/9783527610426.bard040007.

[30] A.M. Al-Sabagh, M.I. Abdou, M.A. Migahed, S. Abd-Elwanees, A.M. Fadl, A. Deiab, Investigations using potentiodynamic polarization measurements, cure durability, ultra violet immovability and abrasion resistance of polyamine cured ilmenite epoxy coating for oil and gas storage steel tanks in petroleum sector, Egypt. J. Pet. 27 (2018) 415–425. https://doi.org/10.1016/j.ejpe.2017.07.006.

[31] Z. Qiu, R. Wang, J. Wu, Y. Zhang, Y. Qu, X. Wu, Graphene oxide as a corrosion-inhibitive coating on magnesium alloys, RSC Adv. 5 (2015) 44149–44159. https://doi.org/10.1039/c5ra05974g.

[32] A. Yadav, R. Kumar, H.K. Choudhary, B. Sahoo, Graphene-oxide coating for corrosion protection of iron particles in saline water, Carbon N. Y. 140 (2018) 477–487. https://doi.org/10.1016/j.carbon.2018.08.062.

[33] Gamry, Calculation of Corrosion Rate, (n.d.). https://www.gamry.com/Framework Help/HTML5 - Tripane - Audience A/framework_help.htm#EFM/Introduction/Calculation of Corrosion Rate.htm%3FTocPath%3DElectrochemical%2520Frequency%2520Modulation%7CIntroduction%2520to%2520Electrochemical%2520Frequency%2520Mo (accessed October 19, 2020).

[34] Y. Toshev, V. Mandova, N. Boshkov, D. Stoychev, P. Petrov, N. Tsvetkova, G. Raichevski, C. Tsvetanov, A. Gabev, R. Velev, K. Kostadinov, Protective coating of zinc and zinc alloys for industrial applications, Woodhead Publishing Limited, 2006. https://doi.org/10.1016/B978-008045263-0/50073-8.

5. General Conclusions

This dissertation presented the results on the investigation and development of new compositions for an anti-corrosion coating material. The development of such compositions relied on (i) the synthesis of a novel benzoxazine structure, (ii) the study of its combination with an epoxy resin and (iii) the incorporation of silica particles.

A trifunctional benzoxazine monomer was designed and successfully synthesized from melamine, paraformaldehyde, and phenol in a one-pot, solventless process, with the reaction performed at various times to maximize the product yield. The resulting monomer product was purified using two different, greener chemistry purification procedures and results showed that impurities were indeed present on both procedures, but much less with procedure #1. Procedure #2 showed to be highly promising with interesting results upon investigation of yield. The chemical structure of the synthesized TBZ was characterized by ^{1}H-NMR, which revealed small amounts of oligomers and impurities, and FTIR spectroscopy, which confirmed the presence of signature functional groups of the monomer in all reaction times. The DSC and TGA experiments revealed a thermosetting PBZ product with a T_g of 95 °C, high thermal stability of up to 366 °C, and a high char yield of 37% at 800 °C. Finally, we were able to demonstrate that our TBZ preparation has satisfied a few Principles of Green Chemistry by (1) using safer solid starting materials for easy handling, (2) using solventless synthetic method, which reduces the use of solvents and thus, minimizes waste, (3) using more benign solvents in the purification process, (4) tuning the reactant ratio and reaction times to optimize the product yield, and (5) realizing that the monomer product itself is intrinsically stable and nontoxic.

The synthesized trifunctional BZ was combined with EP resin and the advantage of the copolymer was evident in the high properties achieved. The two monomers are highly compatibilized by mixing with a combination of solvents and a drying protocol. The different BZ/EP compositions revealed shifting in reaction kinetics and thermodynamics associated with high miscibility in preparation. The comparison with literature with other BZ monomers and EP showed a distinct advantage. A procedure was developed to determine the identity of each peak of cure from DSC. Samples with excess of epoxy (5/95 and 25/75) showed favored E-E reaction. Samples in the proximity of the stoichiometric (31/69 and 48/52) revealed maximum amou E

reaction and samples with excess benzoxazine (55/45 and 75/25) showed favored B-B reaction. DSC revealed a synergistic effect on Tg where all compositions with significant amount of both monomers displayed higher Tg than that of samples dominated by one monomer. TGA also revealed a synergistic effect, where most parameters of degradation were improved on sample 48/52 when compared to 5/95 and 100/0, confirming a high thermal stability. Thus, the structure-composition-property correlation is evident in the near quantitative shift in thermal (DSC and TGA) and spectroscopic (IR) characterization of properties with composition.

The BZ/EP copolymer was combined with functionalized fumed silica to produce anticorrosion coatings and investigate performance of different compositions. Contact angle experiment revealed improved hydrophobicity with increasing content of silica for sprayed samples. Superhydrophobic effect was observed on samples S30 and S40. Variation in gloss indicated change in roughness as one of the multiple phenomena influencing CA. Gloss does not follow the exact trend as contact angle, indicating that roughness was not the only mechanism influencing contact angle. PPS electrochemical test revealed increasing protection against corrosion with increasing silica content. Sample S30 showed best result with corrosion rate 1500x lower than uncoated sample. Optical microscopy and SEM analysis supported results from gloss and contact angle. Increase of surface roughness with increasing silica content could be observed. PPS electrochemical test revealed increasing protection against corrosion with increasing silica content. Sample S30 showed best result with corrosion rate 1500x lower than uncoated sample. All coating compositions resisted degradation upon electrochemical test.

6. Future Works

6.1. Investigation of Cure during Drying of Samples

The drying procedure used to eliminate the solvents of benzoxazine-epoxy samples involved elevating the temperature to 190°C. Although 190 °C is lower than the onset of cure for all samples, it is possible that the sample is partially polymerized, due to the time required for the drying process. Therefore, it is suggested that an investigation be conducted in order to identify and quantify if polymerization occurs on the cited samples due to the drying procedure. ^{1}H-NMR and FTIR can be performed on samples after drying to detect reduction of the characteristic oxazine or epoxide signals and the development of oligomer peaks. Other drying methods, such as application of high vacuum under lower temperatures, may also be applied for comparison of DSC peaks of cure.

Additionally, analysis of the evolution of the viscoelastic properties by rheometry at the given drying temperatures could indicate if gelation is occurring.

6.2. Yield under High Pressure

Literature [54] mentions higher yield on synthesis of polyfunctional benzoxazine monomers when the reaction is performed at higher pressure. In this sense, it is worth investigating the influence of pressure on synthesis of the trifunctional benzoxazine studied in this work.

6.3. Purification Process #2

The purification process proposed in this work, named #2, revealed to be highly promising. However, further investigation is still required. The aspect that seemed to be hindering a better performance of the process is the solubility of the monomers and reagents in the specified solvents. Therefore, it is interesting to investigate variations of the process at different temperatures, higher number of washing cycles and lastly using a different solvent, such as ethyl acetate.

6.4. Primer Coat

Primer coats are largely used as the first coat of paint on the substrate to be painted to improve adhesion between the top coat and the substrate, in addition to providing corrosion resistance [3]. For this reason, it is interesting to investigate the influence of a primer for the coatings developed in this work. Suggestions of materials are pure epoxy and pure benzoxazine, for compatibility reasons and other commercially available primers, for specific performance reasons.

6.5. Copolymer Composition Investigation

Composition of the benzoxazine-epoxy copolymers was determined indirectly via DSC analysis. It is interesting to further confirm compositions of the samples by other experiments, such as GC-MS.

6.6. Further Testing of Coatings

Several complementary tests can be executed to investigate the performance of the coatings produced. Aging by UV, electrochemical impedance spectroscopy (EIS), salt spray, pull-off adhesion, microhardness, resistance to other chemical compounds, such as acids and any combination of them.

6.7. DRX Investigation of Crystallinity

Section 3.3.2 suggests crystallinity in the benzoxazine domain after drying procedure. It would be interesting to perform XRD analysis to allow for confirmation of such crystallinity, in addition to calculation of the percentage crystallinity in each sample.

6.8. Kinetics of Cure

Investigation of kinetics of the polymerization of benzoxazine monomers and combination at any rate with epoxy could be performed in order to allow for

determination of the best curing procedure regarding time and temperature. Additionally, results could be compared with calculation discussed in section 2.3.5.

6.9. Coefficient of Thermal Expansion

Protection against corrosion is highly affected by adhesion, which in turn is influenced by the difference of coefficient of thermal expansion between the coating and the substrate. In this sense it would be interesting to measure the coefficient of the several compositions of coatings regarding monomers ratio and the silica content.

6.10. Identification of Hydrophobicity Phenomenon

Sections 4.3.4, 4.3.5 and 4.3.9 indicate that the hydrophobic behavior is influenced by both the hydrophobic nature of the silica particles used and the surface morphology induced by the particles content. Therefore, it would be relevant to understand the influence of each of these parameters. One interesting approach would be to use similar fumed silica particles, except for the hydrophobicity. Using hydrophilic particles that produce comparable surface roughness and porosity could isolate each of the aspects that influence hydrophobicity of the coating.

[54] H. Ishida, PROCESS FOR PREPARATION OF BENZOXAZINE COMPOUNDS IN SOLVENTLESS SYSTEMS, 5,543,516, 1996.

[3] A.G. Roberts, Organic Coatings - Properties, Selection and Use, United States Department of Commerce, 1968.

Appendix I - Figures in high quality

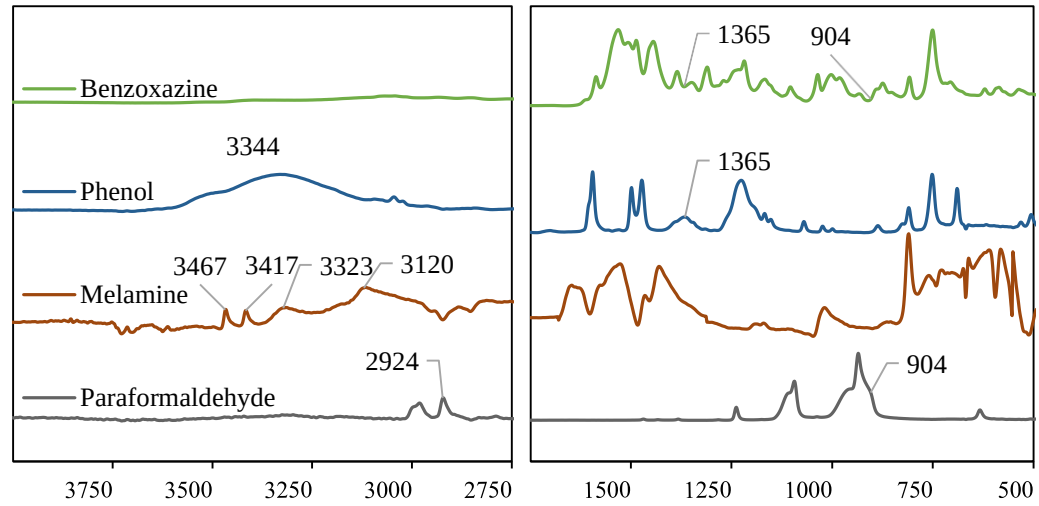

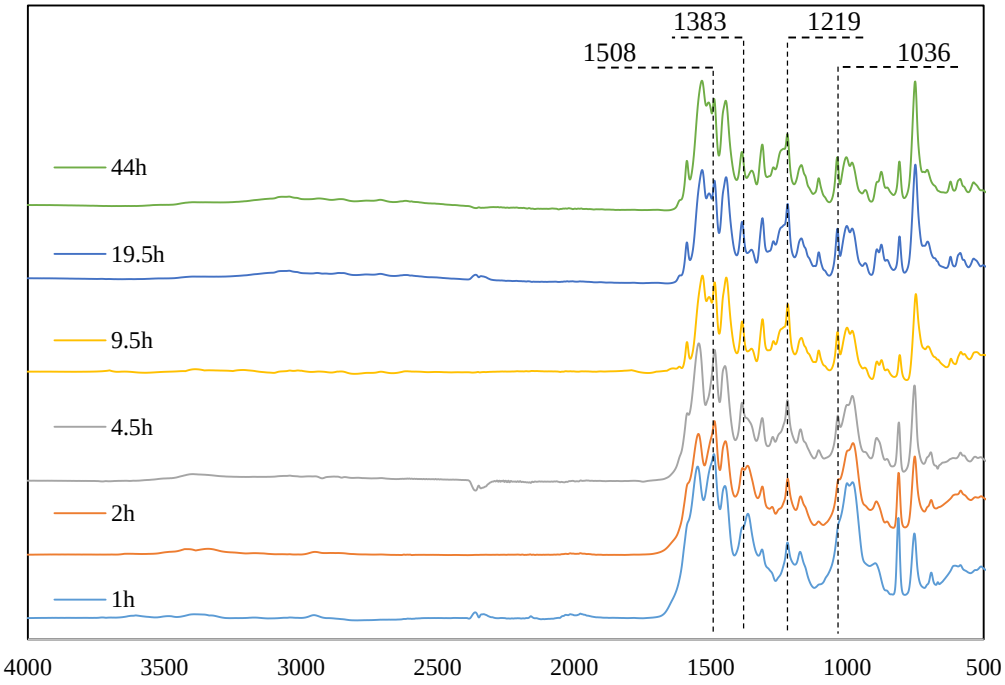

Figure 4.3

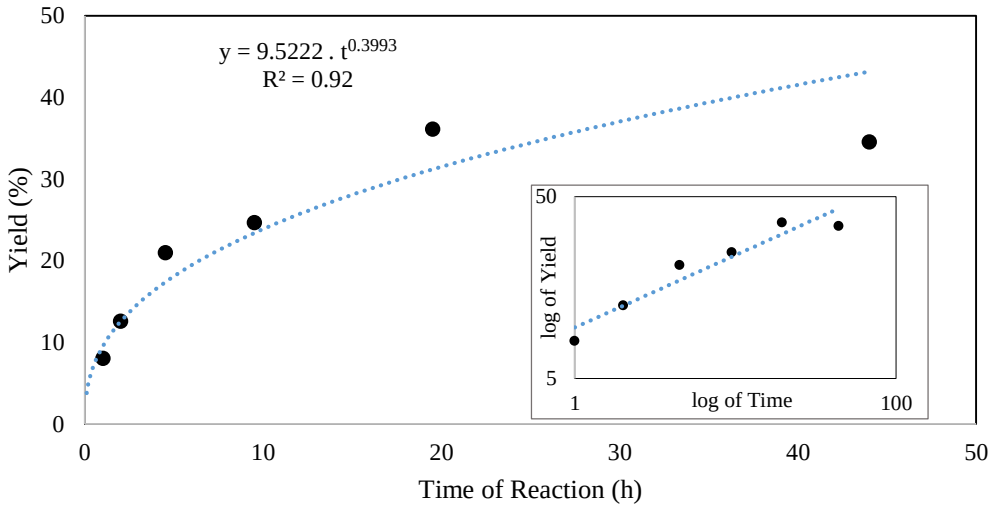

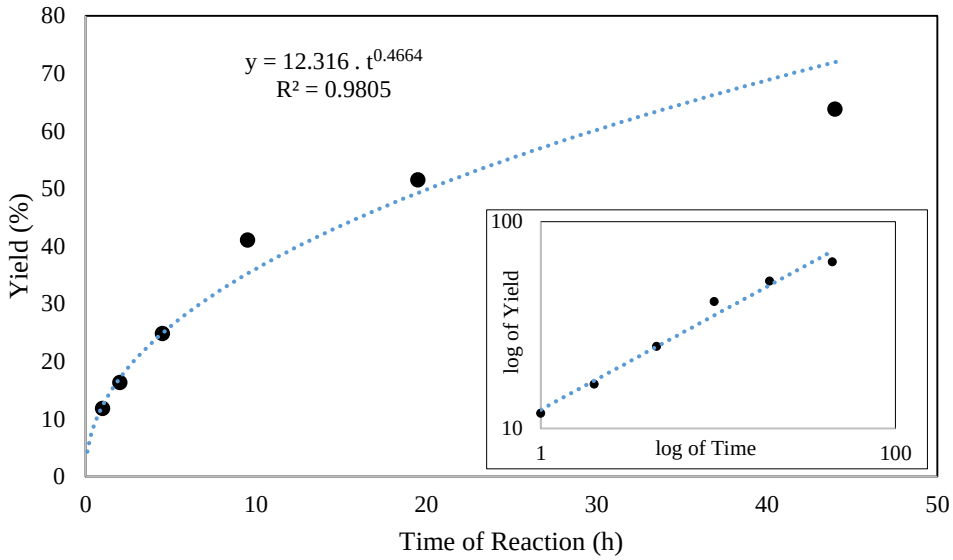

Figure 4.4

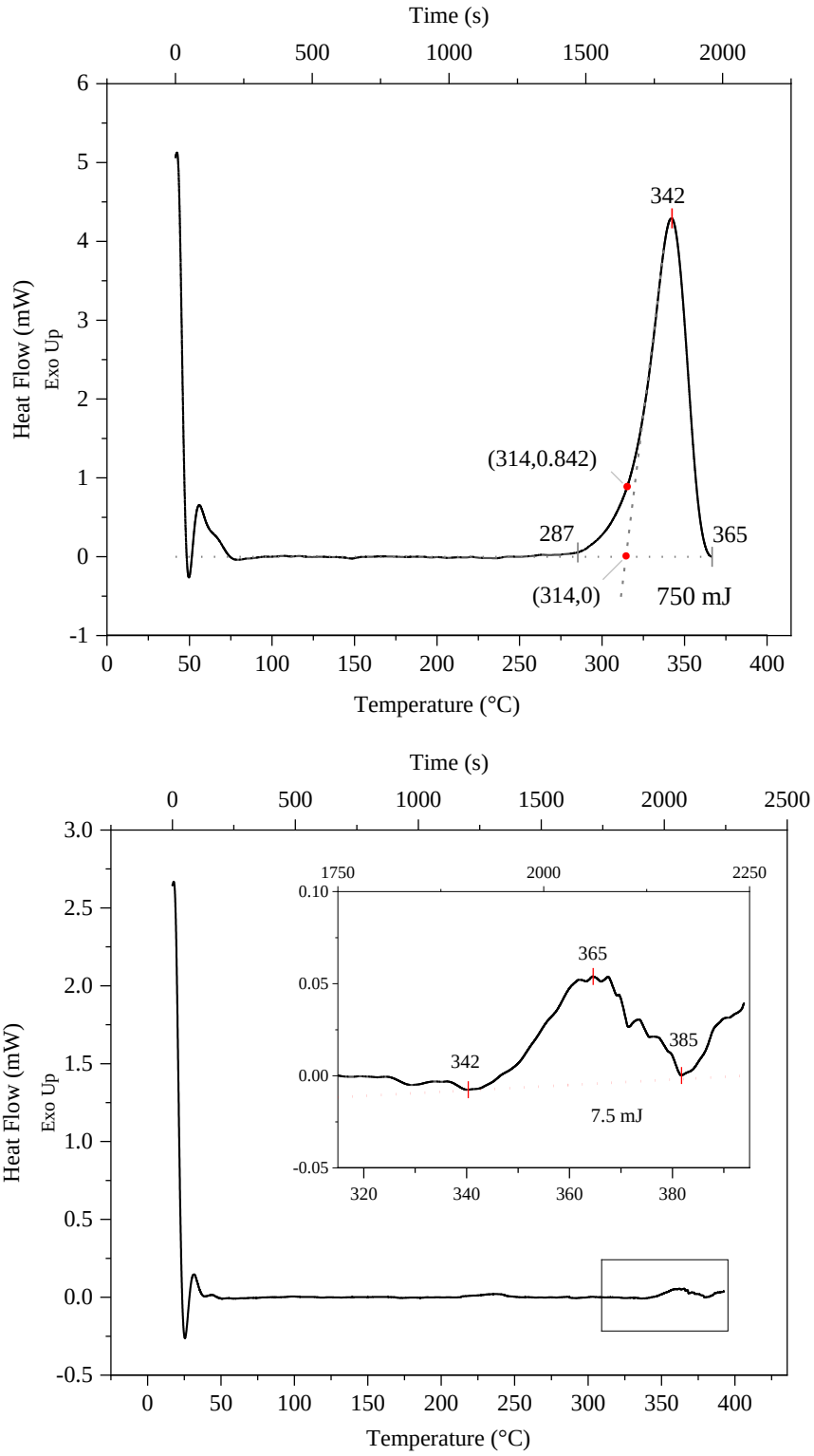

Figure 4.5

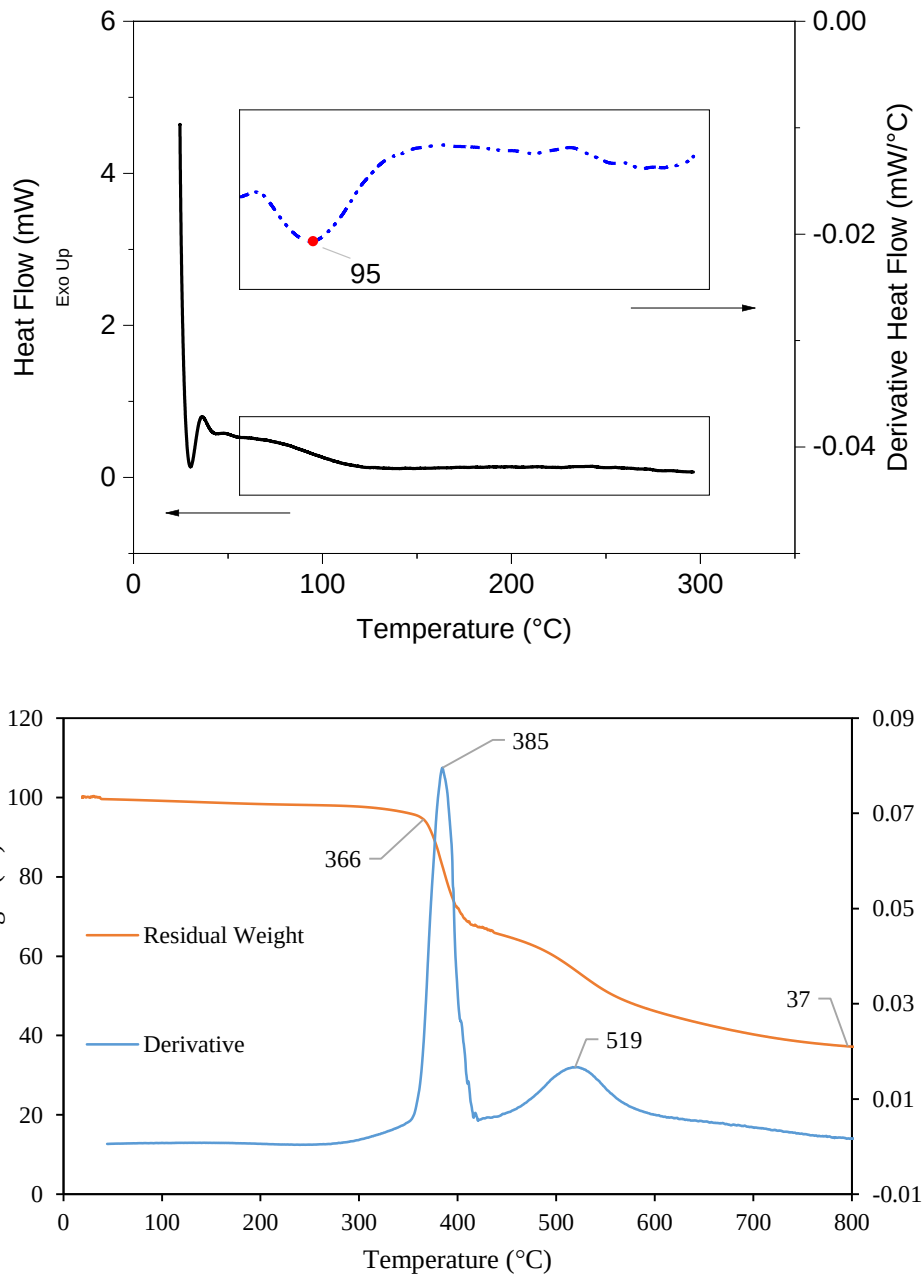

Figure 4.6

Appendix II - Supplementary Information

Chapter 2 - A Greener Approach to Trifunctional Benzoxazine and High Temperature Polybenzoxazine Materials

- Demonstration of rate of reaction as function of variation of concentration of product

Consider the given chemical equation:

$$a.A + b.B \rightarrow p.P \quad \text{(S2)}$$

The rate of reaction (ϑ) is given by:

$$\vartheta = \frac{1}{p} * \frac{d[P]}{dt} \quad \text{(S3)}$$

In our work, Equation (S3) below describes the stoichiometric ratio between all reagents and products.

$$1.M + 3.P + 6F \rightarrow 1.B + 2.H_2O \quad \text{(S4)}$$

Where,

M – Melamine; P – Phenol; F – Formaldehyde; B – Benzoxazine

Therefore, reaction rate is given by:

$$\vartheta = \frac{1}{1} * \frac{d[B]}{dt} = \frac{d[B]}{dt} \quad \text{(S5)}$$

It can be seen that the rate of reaction can be calculated directly by variation of the concentration of product with time.

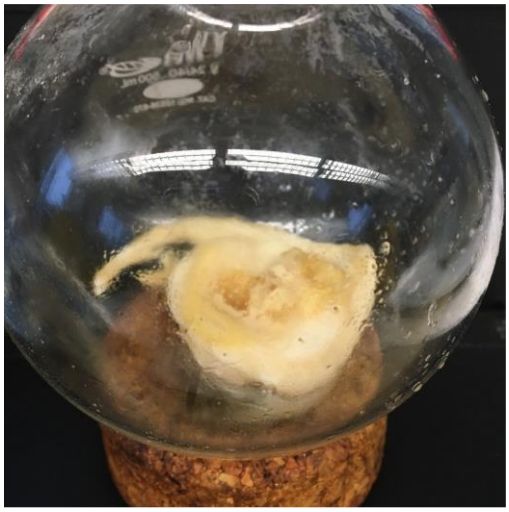

Fig. S 1. Monomer product using stoichiometric ratio of 3:6:1 (i.e. phenol, paraformaldehyde, and melamine, respectively).

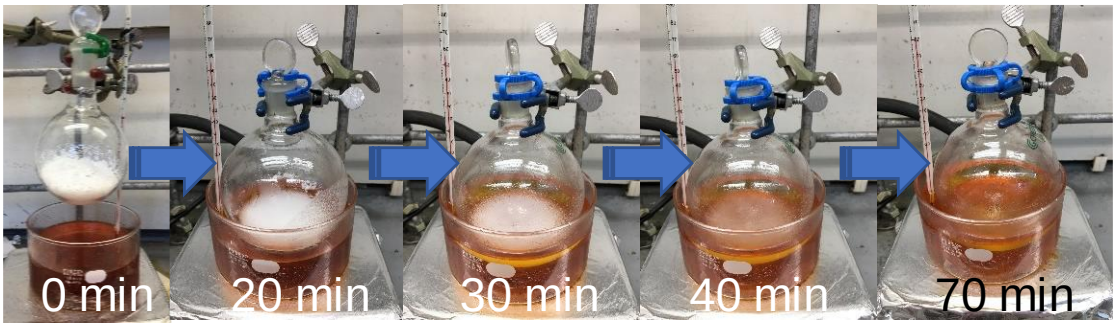

Fig. S 2. Sequence of melting and dissolution of reagents prior to synthesis at 0, 20, 30, 40 and 70 minutes at 50-60 °C.

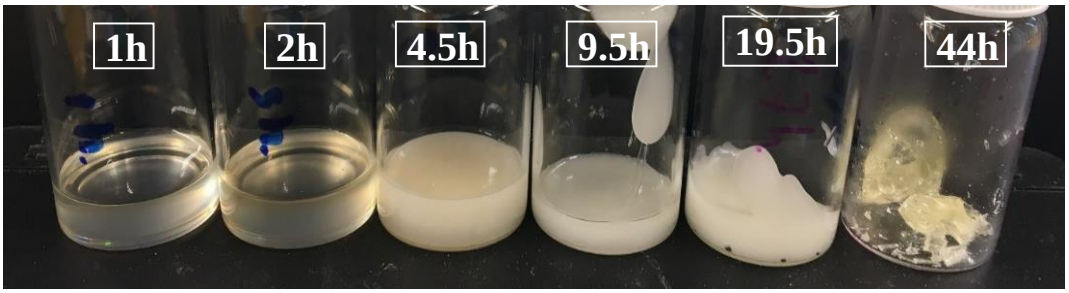

Fig. S 3. TBZ sample products obtained after different reaction times.

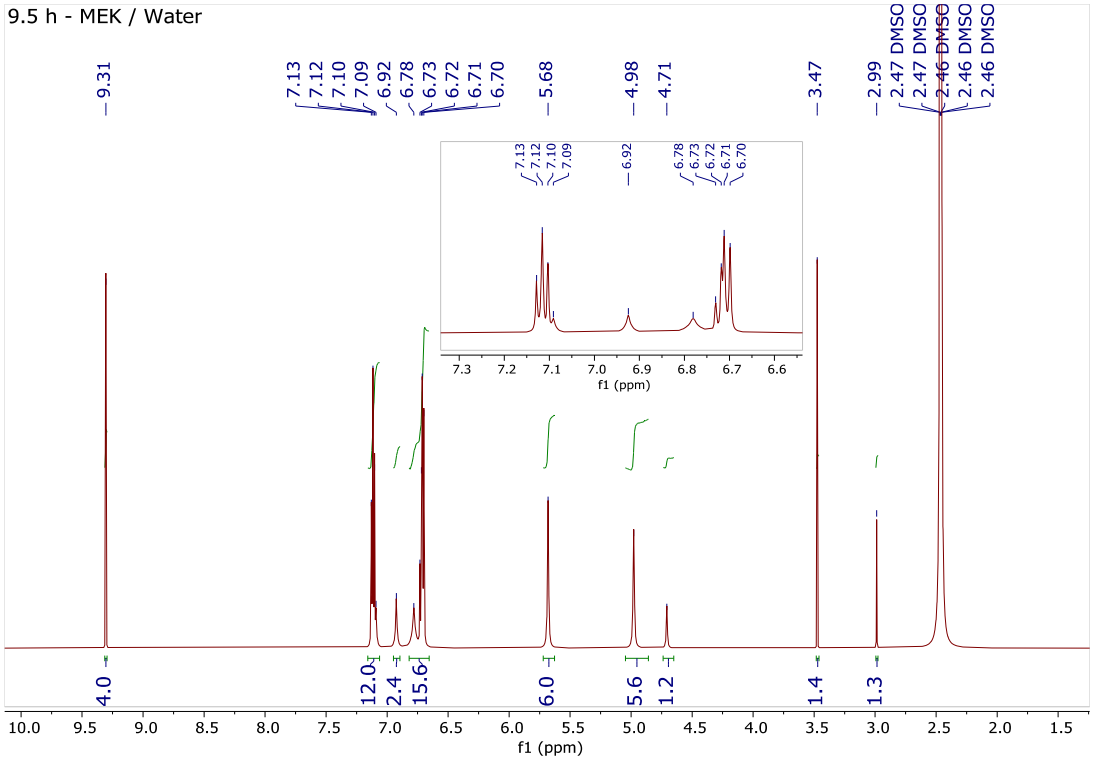

Fig. S 4. ^{1}H-NMR of TBZ (purified by Procedure #2) obtained after 9.5 h reaction time.

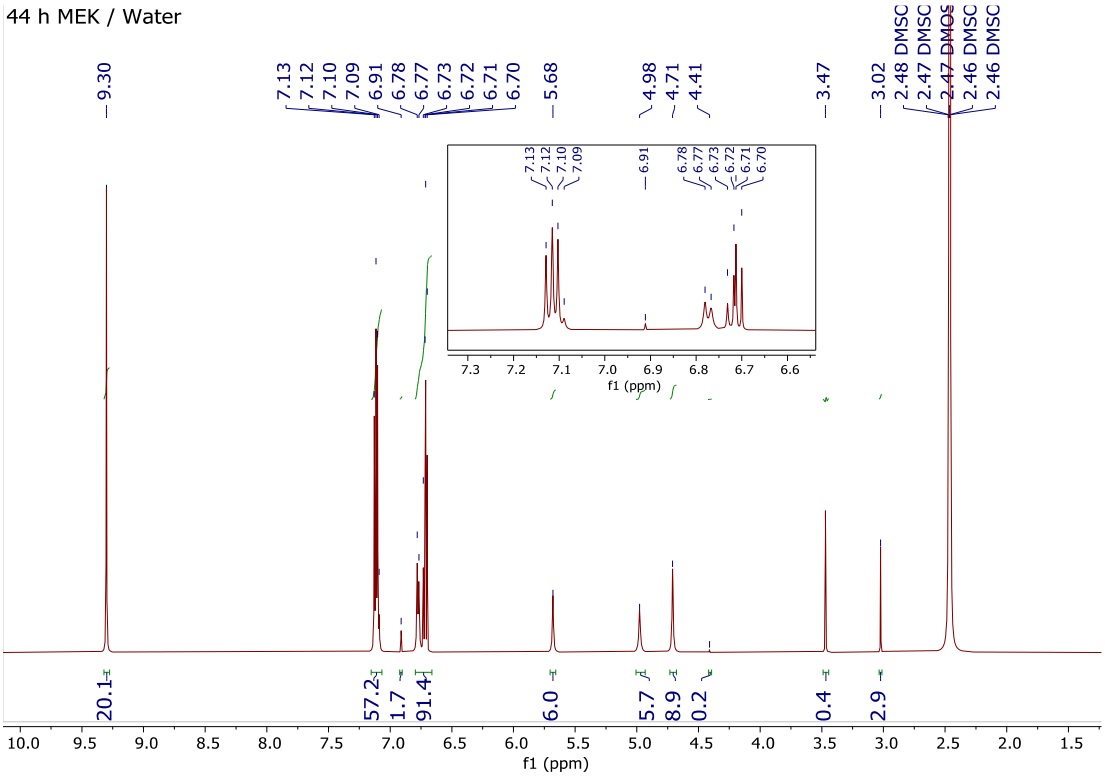

Fig. S 5. ^{1}H-NMR of TBZ (purified by Procedure #2) obtained after 44 h reaction time.

Table S 1. Assignment of peaks of ^{1}H-NMR of TBZ obtained after 9.5 h reaction time and purified by procedure #2

Shift (ppm)	Assignment	Shift (ppm)	Assignment
9.31	Formaldehyde	4.98	Oxazine Ring
7.13 – 7.09	Aromatic Ring	4.71	Oligomer
6.92	Melamine	3.47	Pre-Monomer
6.78 – 6.70	Aromatic Ring	2.99	Open Ring Methyl
5.68	Oxazine Ring	2.48 – 2.47	DMSO

Table S 2. Assignment of peaks of ^{1}H-NMR of TBZ obtained after 44 h of reaction time and purified by procedure #2

Shift (ppm)	Assignment	Shift (ppm)	Assignment
9.30	Formaldehyde	4.71	Oligomer
7.13 - 7.09	Aromatic Ring	4.41	Pre-Monomer 2
6.91	Melamine	3.47	Pre-Monomer 1
6.78 - 6.70	Aromatic Ring	3.02	Open Ring Methyl
5.68	Oxazine Ring	2.48 - 2.46	DMSO
4.98	Oxazine Ring		

Assignment is presented in **Table S 2** and explanations of changes in peaks are as follow:

9.30 ppm (Formaldehyde) – Despite the larger consumption of formaldehyde as reaction takes place for longer times, purification seems to be less effective when compared to samples reacted for 9.5h. Possibly, formation of oligomers decrease solubility of the product and hinders removal of some reagents, in this case, formaldehyde.

7.13 - 7.09 / 6.78 - 6.70 ppm (Phenol) – Integration of peaks reveal an increase of more than 5 times the amount of protons relative to aromatic rings. However, as calculated previously, it is expected an increase of around 2 times due to the higher mass of benzoxazine monomers and oligomers produced in the longer period of time. These extra protons are assigned as phenol in the free form. This deduction can also be verified by the larger peak at 6.78 ppm shift and the presence of the extra peak at 6.77 ppm shift, which are both assigned to proton in the ortho position of the phenol molecule shown in detail of **Fig. S5**. One of the two ortho positions of the phenol has its proton replaced by a carbon that forms the oxazine. This proton on the ortho position signals at around 6.77 ppm. Therefore, it is expected that benzoxazine monomers show less peaks in this region and that total integration is inferior than that of phenol.

6.91 ppm (Melamine) – Integration reduced in 30% when compared to spectrum of 9.5h reaction. This may be explained by the consumption of this reagent during synthesis of the monomers.

4.71 ppm (polymer bridge) – Integration of respective peak shows increase of more than 7X. This indicates that longer times of reaction produce larger amounts of oligomers. This is expected as polymerization is a spontaneous process in benzoxazine and is accelerated by the presence of impurity and temperature. During reaction, monomers are in constant interaction with reagents, such as phenol, in addition to the high temperature required for synthesis, which act as catalyzers to polymerization.

3.47 ppm (Pre-Monomer 1) - Integration reduced in 70% when compared to spectrum of 9.5h reaction. This indicates that component was consumed more than it was produced. First step of reaction to synthesize benzoxazine produces pre-monomer 1. This is a fast reaction (see supplementary material) and, therefore, occurs primarily in the beginning of the process of synthesis. As reaction proceeds, this component is consumed in the production of pre-monomer 2. At the same time, it has its rate of production gradually decreased due to shortage in reagents. These two factors cause concentration of the component to reduce over time, as it is presented in **Fig. S4** and **S5**.

4.41 ppm (Pre-Monomer 2) – Peak is present in 44h reaction spectrum and is not present in 9.5h. Second step of reaction to synthesize benzoxazine produces pre-monomer 2. This is a slow reaction (see **Fig. 1.4**) and is followed by the third step (closure of the oxazine ring), which is a quick reaction. Therefore, pre-monomer 2 tends not to accumulate since it is slowly formed and quickly consumed. However, towards longer periods of time of synthesis, rate of reaction as a whole decreases and pre-monomer 1 accumulated. Therefore, rate of production of pre-monomer 2 is sustained high, while consumption lowers. Consequently, it is expected that there is an increase in the amount of pre-monomer 2.

3.02 ppm (Open Ring) – As monomers reside longer in the presence of high temperature and impurities (reagents), probability of opening of the oxazine ring increases. This process is responsible for the polymerization process explained previously. However, not all monomers that undergo ring opening reach polymerization. It is possible to observe protons of the methyl group generated by the opening of the ring. Interestingly, integration of the respective peak is two times larger

for 44h reaction samples when compared to 9.5h samples. This result is in agreement with the expected increase due to longer exposure to heat and impurities.

It is important to mention that deviations in integration of ^{1}H-NMR peaks are possible due to slight variations in purification process. Therefore, highly precise quantitative analysis is compromised and was not object of this work. Consequently, it was not performed. Instead, the numbers simply provided a reference for a qualitative analysis.

Table S 3. Results and analysis of yield and yield rate with reaction time and using purification procedure #1.

Time (h)	Weight (g)		Yield (%)	Relative Yield (%)	Yield Rate (%/h)
	Collected Sample	Purified Sample			
1	4.505	0.362	8.0	23	8.0
2	5.477	0.69	12.6	36	4.6
4.5	4.89	1.026	21.0	59	3.4
9.5	5.78	1.426	24.7	70	0.7
19.5	6.321	2.282	36.1	102	1.1
44	5.976	2.064	34.5	98	-0.1

Table S 4. Results and analysis of yield and yield rate with times of reaction and purification procedure #2.

Time (h)	Weight (g)		Yield (%)	Relative Yield (%)	Yield Rate (%/h)
	Collected Sample	Purified Sample			
1	5.061	0.599	11.8	19	11.8
2	4.202	0.687	16.3	26	4.5
4.5	4.482	1.114	24.9	39	3.4
9.5	6.145	2.523	41.1	64	3.2
19.5	4.957	2.554	51.5	81	1.0
44	6.880	4.389	63.8	100	0.5

Chapter 3 – (Highly Thermally Stable Copolymers of Polybenzoxazine and Epoxy: The Trifunctionality Advantage)

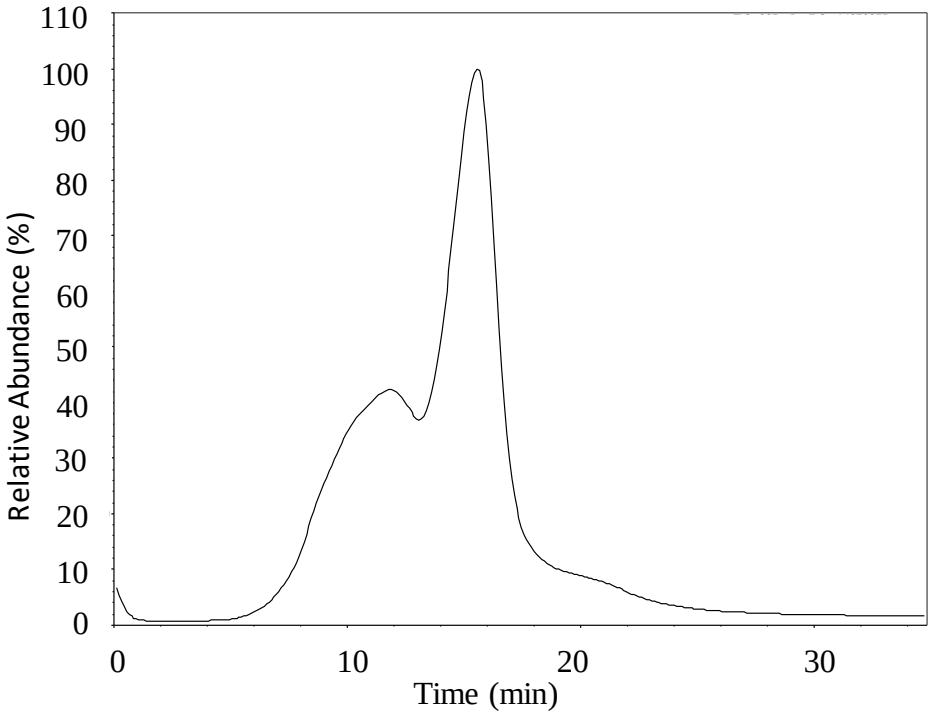

Fig. S 6. EGA curve of the EP resin in this study as a function of time.

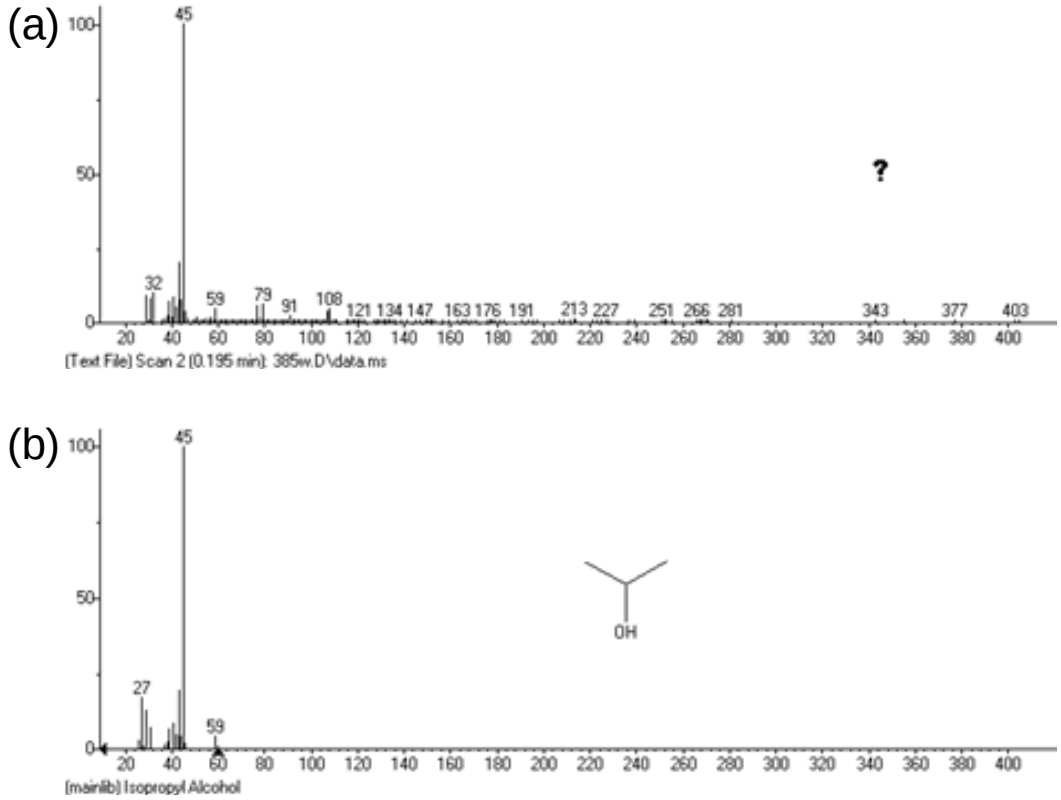

Fig. S 7. Mass spectrum of the EP resin at 0.195 min obtained (a) experimentally) and (b) from mass spectral library for comparison.

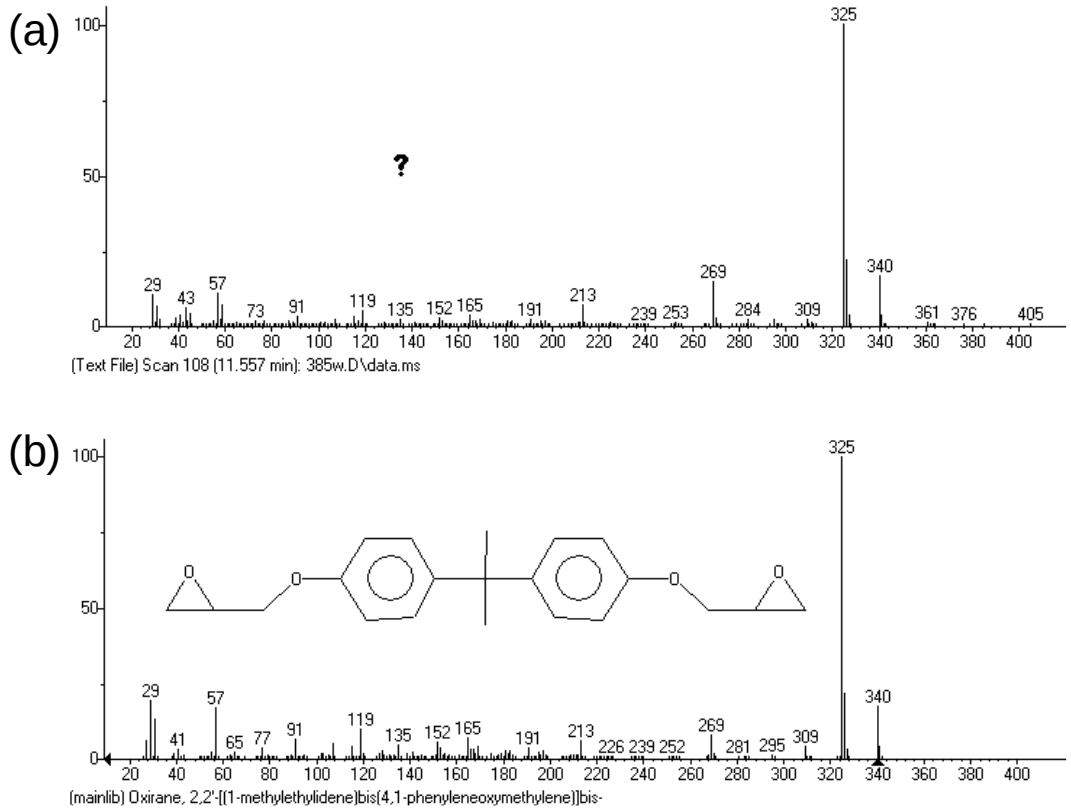

Fig. S 8. Mass spectrum of the EP resin at 11.557 min obtained (a) experimentally) and (b) from mass spectral library for comparison.

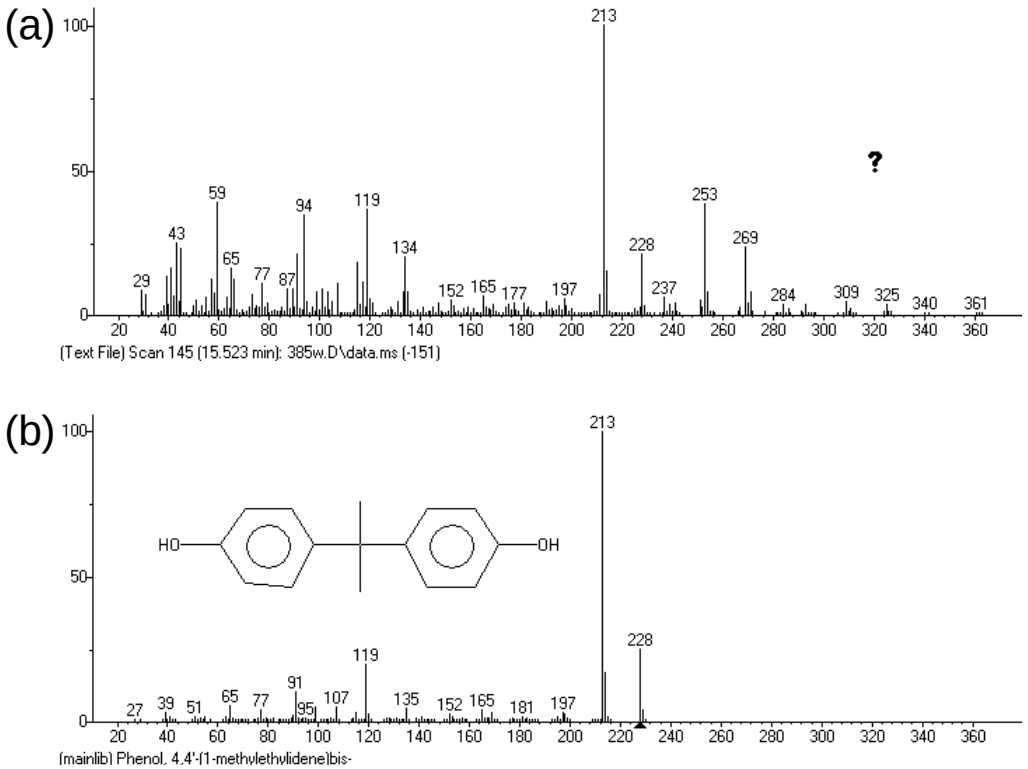

Fig. S 9. Mass spectrum of the EP resin at 15.523 min obtained (a) experimentally) and (b) from mass spectral library for comparison.

Preparation of copolymer – definition of solvents

Solvents were defined to afford the best mixing conditions for BZ and the EP resins. Initially, the synthesized trifunctional BZ was tested for solubility with several solvents. DMSO was the solvent of choice for BZ. The protocol for determining the best mixing conditions for the two resins is as follows: Firstly, 100 mg of BZ was placed in two separate glass vials as shown in **Fig. S 10a**. Increasing amounts of DMSO were added to both vials until complete dissolution was achieved. 100 µL DMSO showed to be effective in dissolving the given amount of BZ as observed in **Fig. S 10b** with a clear solution. Subsequently, 190 mg of the EP resin was added to it, which represented a 48/52 BZ/EP ratio. As shown in **Fig. S 10c**, EP had poor solubility in the DMSO containing BZ, in which white precipitates formed at the bottom.

Next, the two vials were treated differently: vial 1 with increasing amounts of DMSO in an effort to dissolve the EP; and vial 2 with a mixture of ethanol and ethyl-acetate in 50:50 ratio. Ethyl acetate, a less toxic and common solvent, is known to dissolve EP resins very well. However, since ethyl acetate and DMSO are immiscible with each other, ethanol was added as a compatibilizer. **Fig. S 10e** shows the

development of solubility with increasing amounts of the respective solvents ethanol/ethyl acetate. **Fig. S 10f** shows the final result from solvents experiment, where the optimal dispersion was eventually achieved with 600 µL of the 50:50 solvent mixture for vial 2. A very homogeneous and slightly milky product was obtained, suggesting a good solubility (**Fig. S 10f** right). On the other hand, increasing amounts of DMSO up to 600 µL had no perceivable effect on the dissolution of EP resin (**Fig. S 10f** left). One interesting observation in **Fig. S 10f** (right) is a transparent obtained from the DMSO phase in vial 1, indicating that DMSO acted as a good solvent for this particular BZ monomer. Lastly, the final composition of the resins and solvents is summarized in **Table S1**, which includes solvents from the EP product selected for EP suspension composed of 56% solids, 41.5% water, and 2.5% isopropanol, all which are based on the information from the manufacturer. It is important to highlight the benign nature of the solvents used for this preparation.

Table S 5. Composition breakdown for 48/52 BZ/EP sample, including the solvents used and proprietary components from the EP resin.

	Component	Quantity
Monomers	Benzoxazine	100 mg
	Epoxy (solids)	106 mg
Solvents	Water (from epoxy resin)	79 mg
	Isopropanol (from epoxy resin)	5 mg
	DMSO	100 µl
	Ethanol	300 µl
	Ethyl Acetate	300 µl

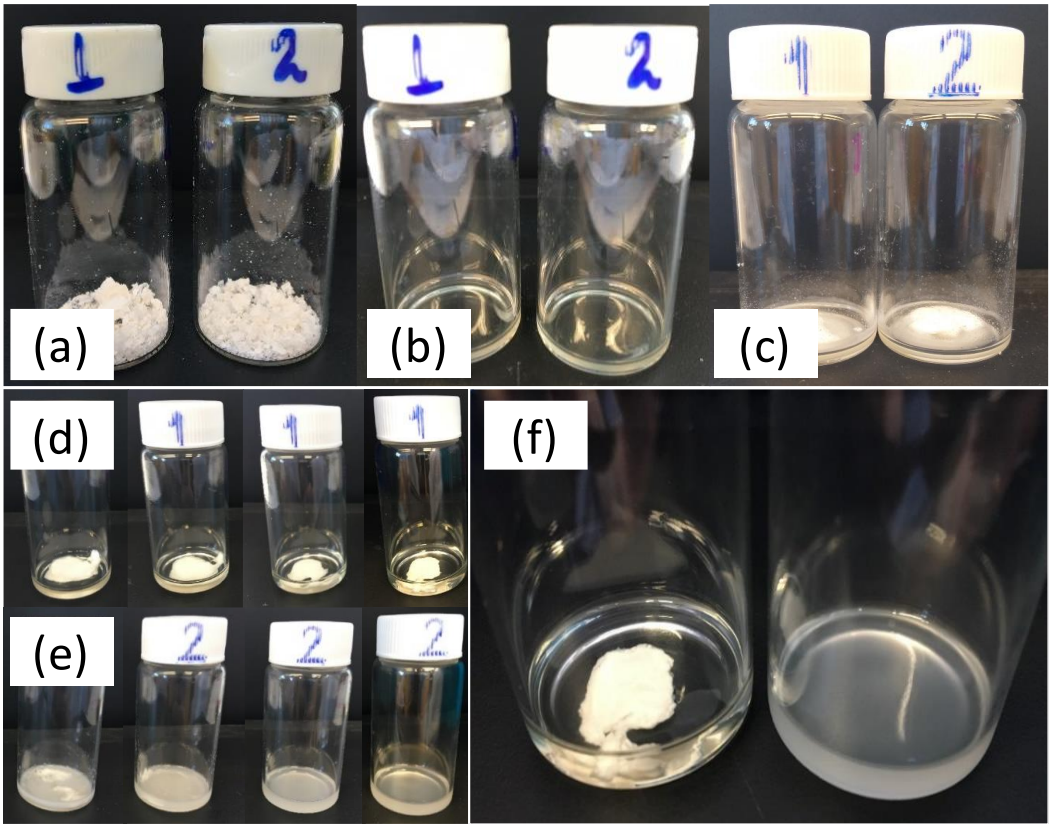

Fig. S 10. Dissolution of BZ monomer and EP resin in suitable solvents. (a) 100 mg BZ monomer. (b) Vials in (a) after adding 100 μL DMSO. (c) Vials in (b) after adding 190 mg EP resin. (d) Vial 1 in (c) after adding more DMSO. (e) Vial 2 in (c) after adding ethyl acetate/ethanol solvent mixture. (f) Final result obtained from (d), left and (e), right

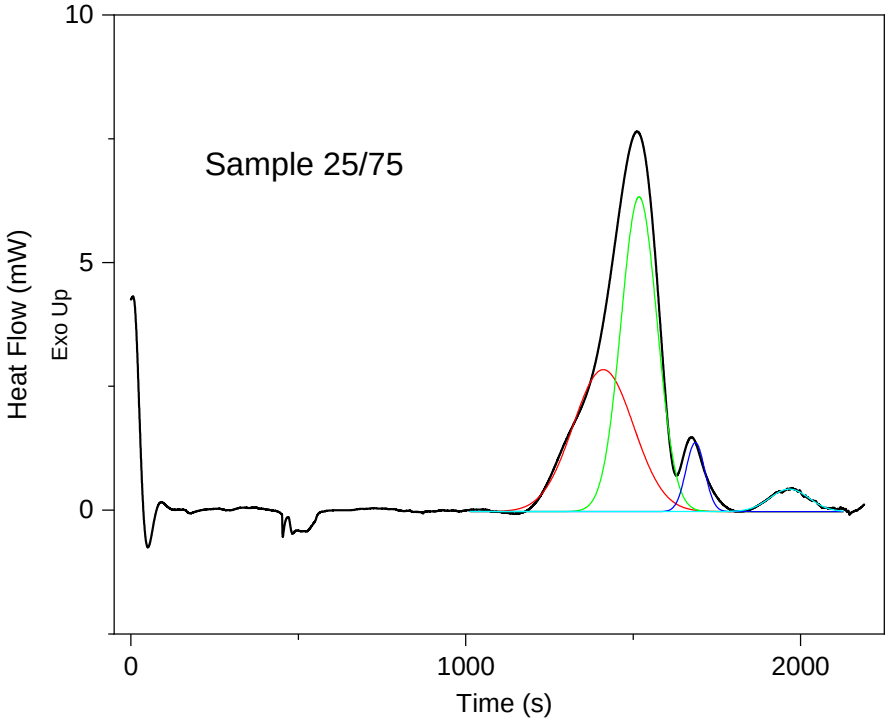

Fig. S 11. Deconvolution of DSC curve for 25/75 copolymer sample.

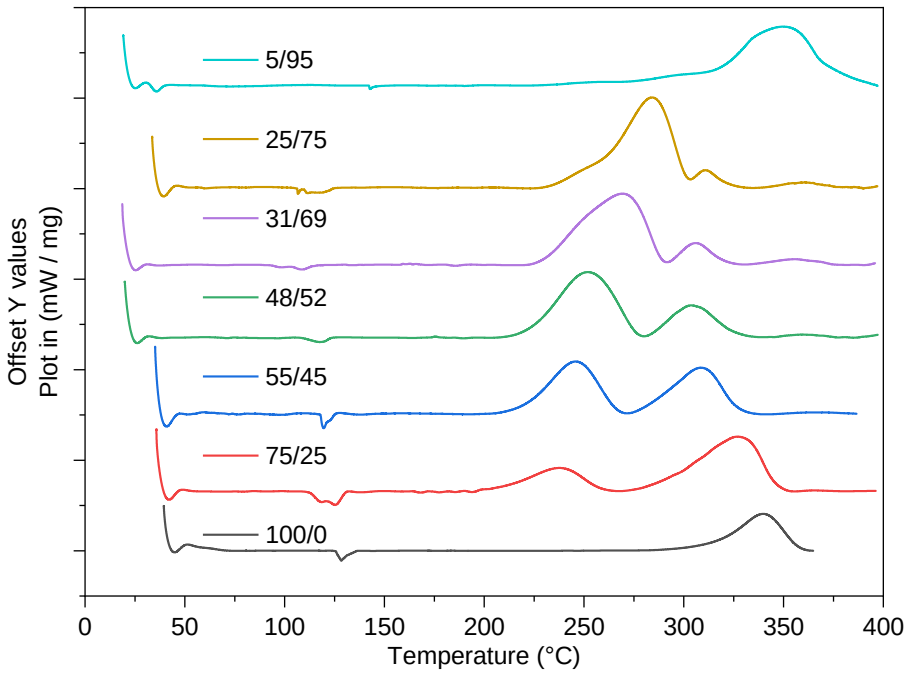

Fig. S 12. DSC thermogram of all compositions for reference (mW/mg x °C).

Peak identification procedure and example

Table S 6. Identification of peaks of cure – sample 25/75

		EP				BZ			
Input	Available mass (mg)	5.76				1.92			
	Peak #	1	2	3	4	1	2	3	4
	Integral (mJ)	647	854	97	66	647	854	97	66
Case 1	Req. mass (mg)	3.57	4.71	0.53	0.36	5.39	7.12	0.81	0.55
	mass cured (mg)	5.07				0.81			
	mass remaining (mg)	0.69				1.11			
	moles of funct. group	1.38E-06				5.78E-06			
	B-E specific energy of reaction (kJ/mol)	470				-			
Case 2	Req. mass (mg)	3.57	4.71	0.53	0.36	5.39	7.12	0.81	0.55
	mass cured (mg)	3.93				0.81			
	mass remaining (mg)	1.83				1.11			
	moles of funct. group	3.66E-06				5.78E-06			
	B-E specific energy of reaction (kJ/mol)	233				-			

The purpose of **Table S 6** is to determine the identity of each peak obtained by deconvolution of the curing curves from DSC.

- First set of lines are input from the system:

- The table presents data for EP (blue) and BZ (yellow) arranged in two columns.

- The second row displays the available mass for each component. This value was calculated based on the total mass of the sample and the percentage of each component in the composition.
- The third row shows the peaks obtained by deconvolution of DSC curves.
- The fourth row shows the energy associated with each peak.
- Two possible scenarios regarding identity of peaks were investigated for each sample composition.

➢ Case 1:

- The first row is the required mass to produce the measured energy on each peak. This calculation considers that every peak is a homopolymerization of each of the two components. For the EP column, calculation was based on data obtained from the literature on energy released per mole of epoxide group reacted. For the BZ column, calculation was based on the data obtained experimentally from the sample 100/0.
- The second row is the sum of all masses associated with the homopolymerization of a particular component.
- The third row is the remaining mass calculated as (available mass) – (mass cured).
- The fourth row is the number of moles of functional groups available for further polymerization based on the remaining mass, molecular mass, and functionality of each component.
- The fifth row is the specific energy associated with the B-E reaction. Calculation is given by the energy associated with the B-E reaction divided by the number of moles of functional groups available for further polymerization.

➢ Case 2:

1. Each peak obtained by deconvolution of curing curves is integrated, providing total energy released on a particular peak.

2. All these peaks are considered possible to be homopolymerization of EP or BZ. For each peak and each component, the mass of that component required to release that given energy is calculated.

3. The obtained required mass is compared to the available mass of that component. If a larger mass is required, the peak is not considered associated to that component. The peaks not considered are in red, for example 5.39 and 7.12, as these required masses are larger than the available mass of BZ This means that there is not enough BZ to produce that particular peak.

4. B-B reaction cannot be assigned to peak #4 because this peak is already taken by E-E reaction. Therefore, B-B can only be assigned to peak #3 (in yellow).

5. These conditions leave only two options for the E-E reaction, peaks #1 and #2. Both these possibilities are evaluated (case 1 vs. case 2). For each of these cases, the total mass of each component is computed and the remaining mass is calculated based on the initial mass. These remaining masses are then converted to the number of functional groups. The smallest number of functional groups is taken as the maximum possible number of B-E reactions.

6. The remaining peak not associated with either B-B or E-E reactions is associated with a B-E reaction and its corresponding energy is used to calculate the specific energy of the B-E reaction. This specific energy is calculated by the energy of the peak divided by the number of available functional groups found in step 5. In this particular example, specific energy was found to be either 470 (case 1) or 233 kJ/mol (case 2).

7. Considering all the results for the other copolymer samples, supported by the data obtained from the literature, it was determined that case 2 is the correct method of identifying the peaks.

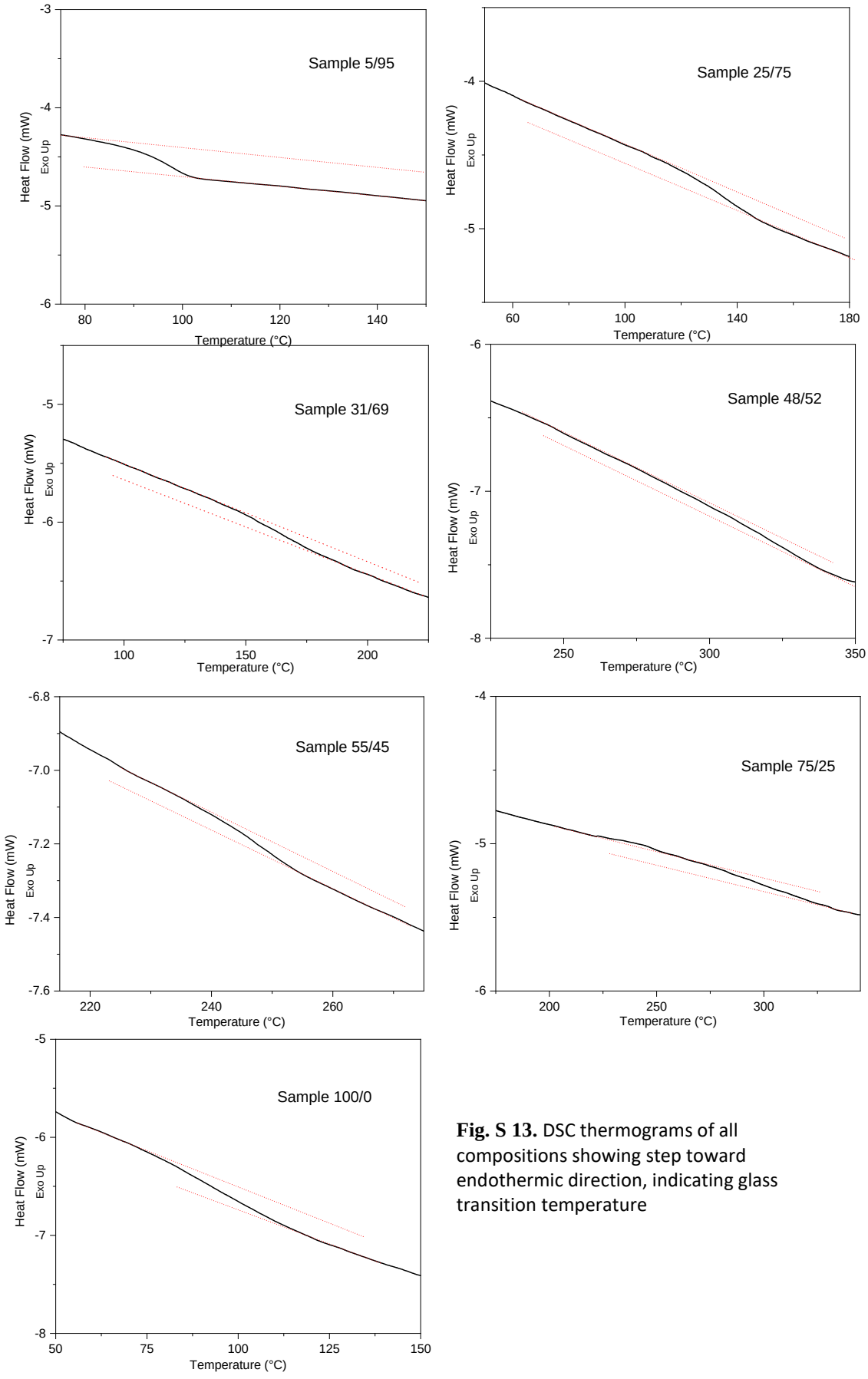

Fig. S 13. DSC thermograms of all compositions showing step toward endothermic direction, indicating glass transition temperature

Chapter 4 - (Superhydrophobic Benzoxazine-Epoxy Coatings: Electrochemical and Mechanical Performance)

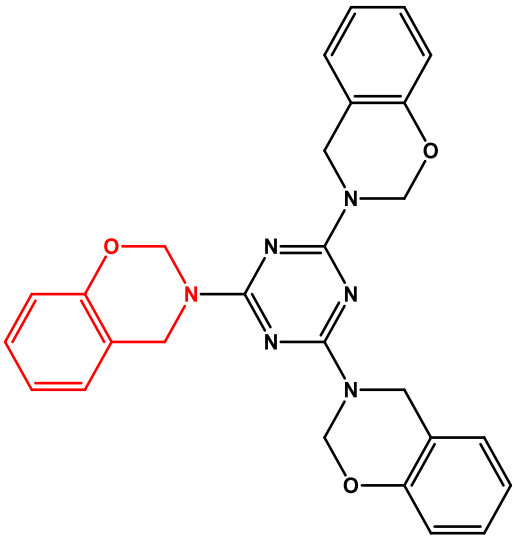

Fig. S 14. Fundamental structure of tri-functional benzoxazine (TBZ) monomer used in this work

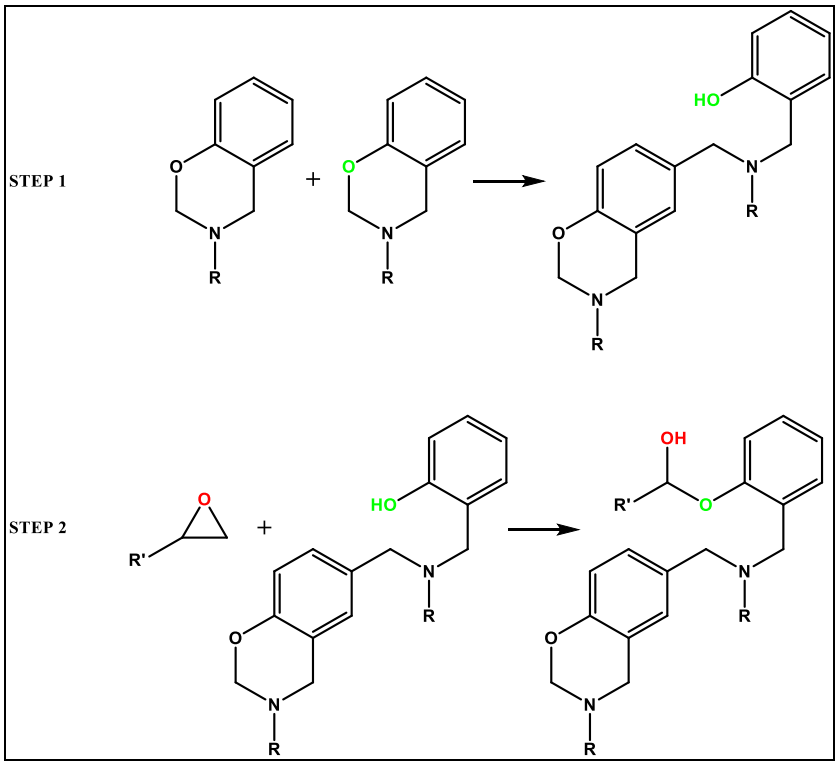

Fig. S 15. Schematic representation of benzoxazine-epoxy copolymerization reaction

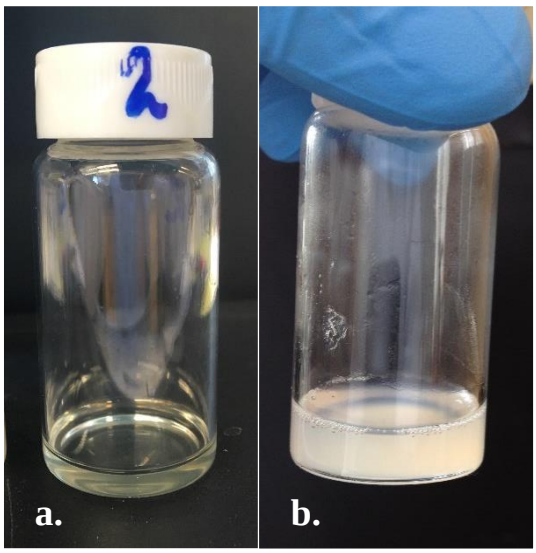

Fig. S 16. a. Benzoxazine + Epoxy + Solvents; **b.** Sample S20 after mixing procedure

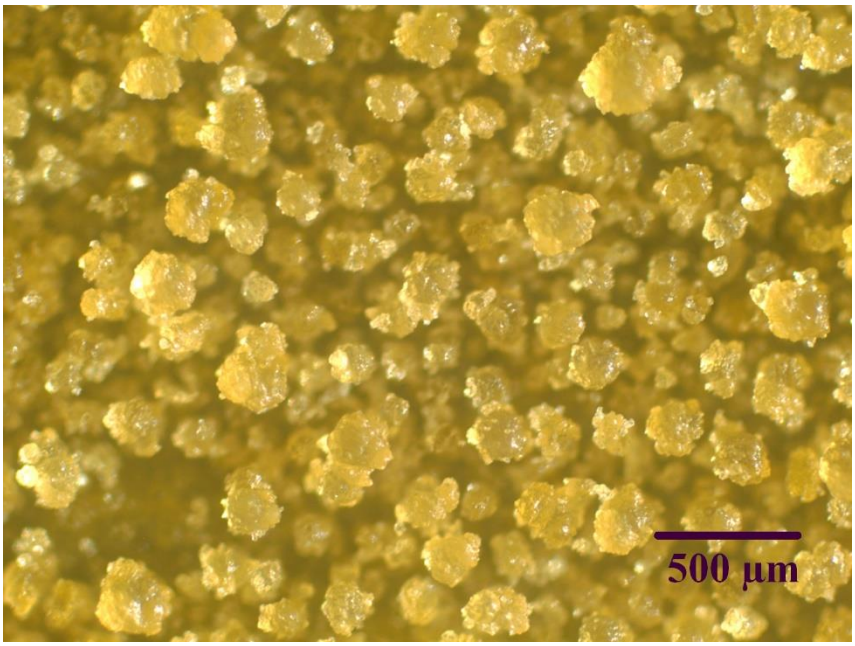

Fig. S 17. Optical Microscopy Image of Sample S30 at 50X Magnification

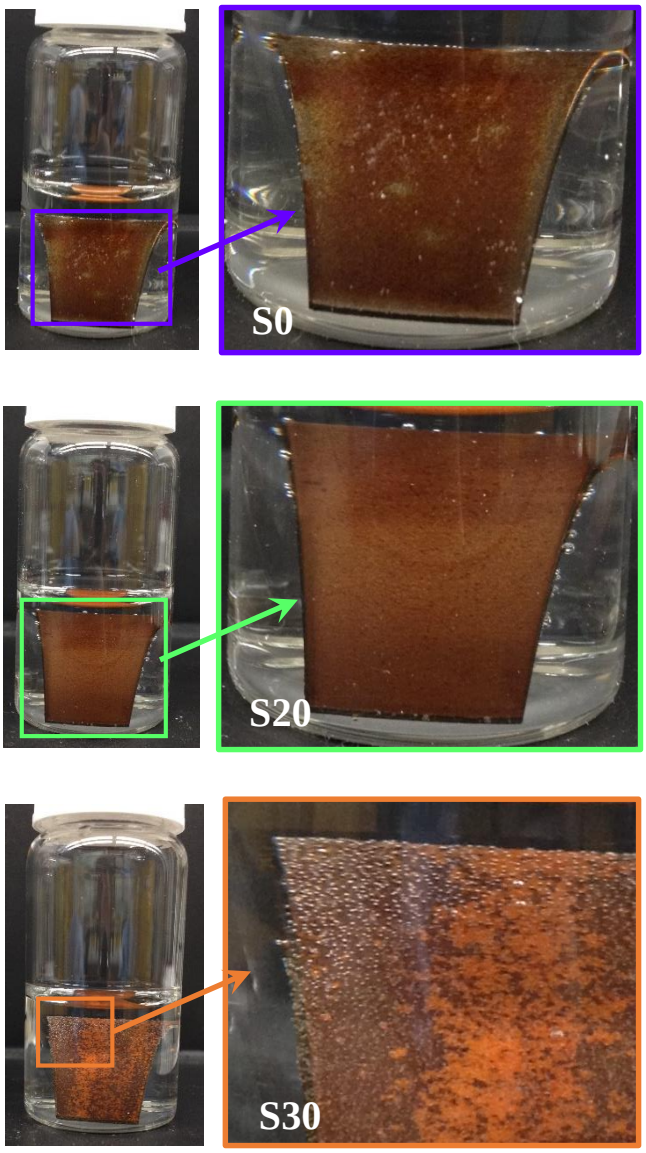

Fig. S 18. Samples S0, S20 and S30 submerged in water

Poured Samples Contact Angle Analysis

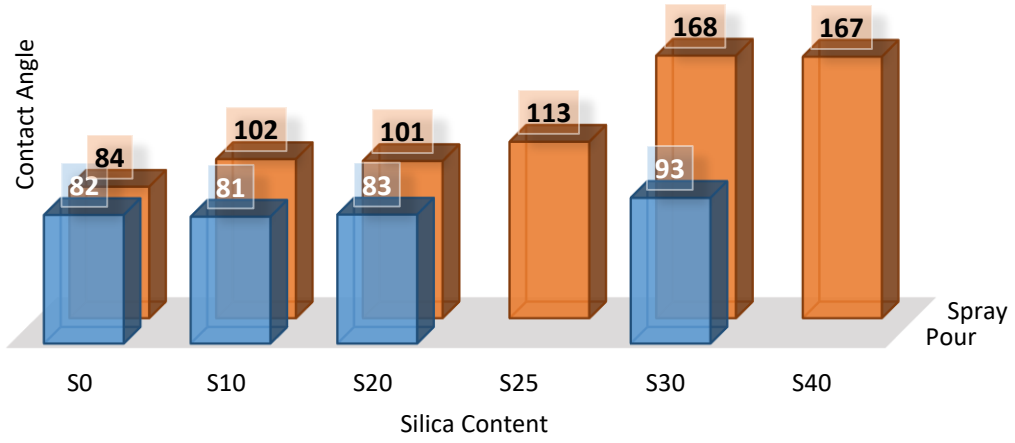

Fig. S 19. Contact Angle comparison between sprayed and poured coatings

The first analysis that can be made is the similarity of results for the two methods on sample S0. Influence of the coating procedure on samples without additive is negligible. This is an interesting result, which shows the intrinsic wetting behavior of the benzoxazine/epoxy blend. In addition, the fact that two very distinct application procedures achieve the same result, implies that it is very likely that any application processes can be used and a consistent result will be obtained. Industrially, this result is of great importance. Not only the most convenient procedure can be selected for production, but also because eventual repairs can be performed without the necessity of clinging to the original procedure.

Another analysis is that all samples prepared by pouring displayed lower contact angle than that of sprayed samples. This result means that the procedure for coating has an important effect on the wettability of the surface, most likely due to changes in surface roughness and to the exposure of the hydrophobic functional groups from the silica. It is possible that in the case of poured samples, part of the particles settled to the bottom of the coating before and during the drying process, since these solutions possessed high concentration of solvents and, therefore, low viscosity. In addition, visually, spray coated samples showed a rougher surface, probably triggered by the coating process itself.

Investigating samples S10 and S20 it can be noticed that the same pattern was achieved with both coating application procedures, as the two concentrations produced similar contact angle result (i.e. 81° ≈ 83° and 102° ≈ 101°).

The most evident difference between application processes is found in samples S30. An increase of 10° in contact angle was obtained with the increase in silica content from 20% to 30% for pouring procedure. However, it is evident that results are nowhere near that obtained by spray coating. It demonstrates that, in this particular case, the application procedure influenced greatly the wettability results. Where just the simple content of silica produced a hydrophobic surface with contact angle of 93°, the same material, when sprayed, generated a superhydrophobic coating with CA of 168°.

Fig. S 17 shows a detail on one of the spots that exhibited lack of thickness of sample S0 after electrochemical test. It is possible to notice a complete absence of coating in the center region (red arrow) possibly caused by the very low thickness of the coating in the area, which resulted in rupture of the coating upon testing. It is possible to see the exposed metallic substrate, showing high roughness, different from that of the virgin metallic substrate. This result supports the assumption that the dark spots were, indeed, corrosion. Furthermore, it indicates that a uniform distribution with a minimum thickness of coating is necessary to perform accordingly and protect the substrate. The image also shows the layer of residual salt from electrochemical test (blue arrow).

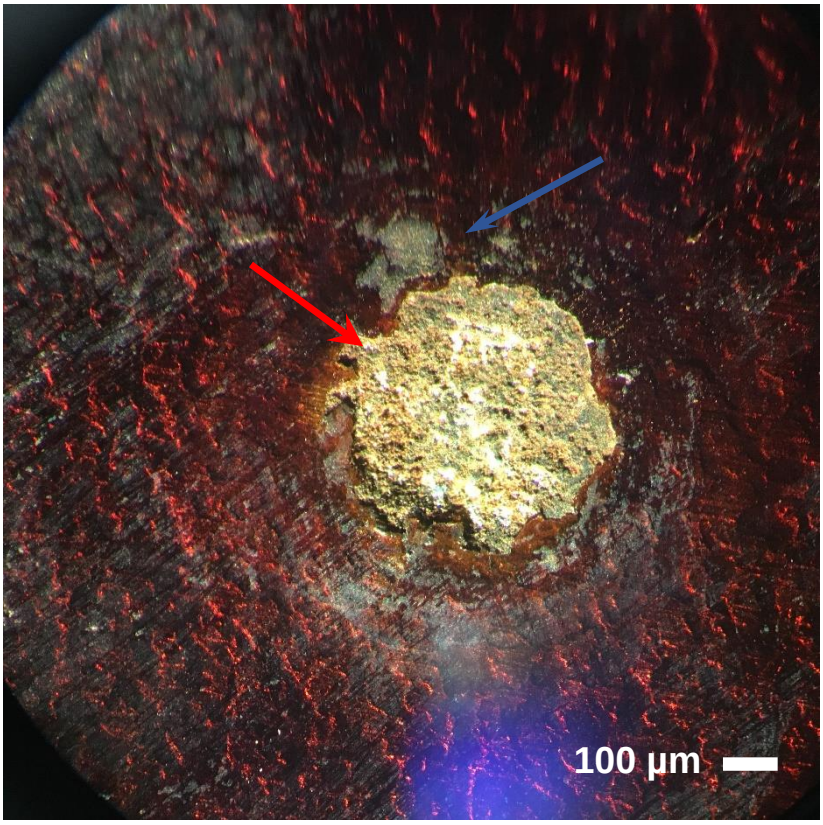

Fig. S 20. Optical Microscopy Image of Samples 0% after electrochemical test

Appendix II – Complementary Elucidations

Section 2.3.4 - Reaction Yield

Analysis of ^{1}H-NMR (**Fig. 2.4** and **Fig. 2.5**) reveal the presence of impurities in the samples purified by procedure #2. Consequently, part of the calculated yield is, in fact, not benzoxazine. Nevertheless, it is important to mention that the behavior of yield as a function time followed the same trend as that of samples purified by procedure #1. It can be concluded that even though impurities were not completely removed by procedure #2, this purification process was effective to the point of allowing observing the same behavior as that of procedure #1, which produced highly pure benzoxazine monomers. As such, the proposed greener procedure #2 revealed to be highly promising, possibly requiring fine adjustments in order to allow for a complete removal of the impurities.

Section 2.3.5 – DSC Study

Posterior to curing the BZ sample according to the calculated procedure (15min. at 314°C), it is interesting to observe that the 2nd run on DSC (**Fig. 2.5**b) display an onset and maximum of residual peak that coincides with maximum and offset of original curing peak respectively (**Fig. 2.5**a). This implies that only the region of higher temperatures was partly not achieved. The cause of this residual curing peak observed may, then, be explained by a massive immobility of the polymeric chains in the system, generated by the vast polymerization attained. Therefore, this residual polymerization would only be possible to achieve at higher temperatures, which would, in its turn, enable greater mobility of the polymeric chains and allow for eventual further crosslinking. As a result, it can be assumed that the proposed procedure for curing was highly effective and that curing was complete.

Section 2.3.6 - Thermal stability study

Additional analysis of thermal degradation of the polybenzoxazine can also be performed as follows. Literature distinguishes polybenzoxazines with and without an observable low-temperature slight weight loss phenomenon in the range of 200–300°C,

which is associated with the loss of the amine group in the case where this group is dangling in the structure. On the other hand, polybenzoxazines that possess the amine group incorporated into the cross-linked structure, do not show this early degradation. The latter is the case of the polybenzoxazine studied in the present work, and results are in agreement with literature. Amine group is part of the crosslinking structure and thermogram does not show early degradation peak. Furthermore, it is expected that the chemical structures initial degraded are the amines which come from the cleavage of the Mannich base, due to the lower energy in the C–N covalent bond (72 kcal/mol) than C-C bond (82.6 kcal/mol), the weaker C–N may be easier to break, and the more stable C–C bond will break at a higher temperature. Breakage of phenolic bonds tend to occur at higher temperatures. In this particular case, first peak at 385 °C is assigned to release of groups due to C-N breakage, while peak at 519 °C is assigned to evaporation of structures due to C-C bond breakages. In addition, it is reported that overlap of the two peaks may occur, and is associated with functionality of the phenolic group. The higher the functionality, the broader and more overlapped the peaks are. Indeed, results are once again in agreement with literature, because the phenolic group of the polybenzoxazine structure presented in this work possesses the lowest functionality possible and thermogram reveals two very distinct peaks with no apparent overlap. This means that degradation of phenolic links started only after degradation of Mannich base finished. These results reveal the excellent thermal stability of the polymerized material produced in this work.